EFFECT OF AGEING HEAT TREATMENT ON THE HARDNESS AND TENSILE PROPERTIES OF ALUMINUM A356.2 CASTING ALLOY

Effect of Ageing Heat Treatment on the Hardness and Tensile Properties of Aluminum A356.2 Casting Alloy

By
George Y. Liu

A Thesis
Submitted to the School of Graduate Studies
in Partial Fulfillment of the Requirements
for the Degree
Master of Applied Science

McMaster University

MASTER OF SCIENCE (2009), Mechanical Engineering
McMaster University Hamilton, Ontario

TITLE: Effect of Ageing Heat Treatment on the Hardness and Tensile Properties of Aluminum A356.2 Casting Alloy

AUTHOR: Ye (George) Liu,
B.Sc. – Material Science & Engineering (Northeastern University, Shenyang, China)

SUPERVISOR: Dr. Sumanth Shankar

NUMBER OF PAGES: xvi, 79

ABSTRACT

The aluminium A356.2 casting alloy is one of most popular alloys for shaped casting of automotive components because of its high strength to weight ratio and the ability to heat treat to attain fairly high toughness. Besides Al, the alloy has Si and Mg as the principal alloying additions to aid in the precipitation of the Mg_2Si phase in the primary Al matrix to strengthen the alloy during heat treatment. Presently, the T6 heat treatment temper is most used on cast components from these alloys. Commercially, in the T6 temper, the component is solution heat treated at around 540 °C for about 10 to 12 hours immediately followed by quenching in water maintained at 80 °C. The component is then left to natural age at room temperature for about 8 to 10 hours followed by artificial ageing at around 155 °C for about 6 to 10 hours. This T6 temper treatment process has been followed for many years and adopted from the 6xxx series Al wrought alloy where the strengthening precipitate is Mg_2Si as well. No significant research has been carried out to evaluate to optimize the T6 heat treatment in A356.2 casting alloys, specifically, the natural ageing phenomenon adopted from the 6xxx series alloy where the Si to Mg ratio is between 1 and 3, has not been optimized in A356.2 alloy, wherein, the ratio Si to Mg is between 4 and 6. Hence, the mechanism of redistribution of Mg and Si atoms during the natural and artificial ageing process would have to be studied for the A356.2 alloy and the process optimized to attain favourable mechanical properties.

In this study, the mechanism of Mg and Si atoms redistribution during the process of natural ageing has been proposed. Additionally, the effect of natural ageing combined with the artificial ageing process on the mechanical properties of the cast component has been quantified. The results of this study propose that the extent of natural ageing in A356.2 alloy depends on the desired combination of strength and elongation in the cast component. A high strength (~230 MPa) and low elongation (~2%) could be achieved if the natural ageing process at room temperature is limited to less than one hour after solution heat treatment and quenching in water at 80 °C, and low strength (~195 MPa) and high elongation (~8%) could be achieved for natural ageing of about 6 hours at room temperature prior to the artificial ageing treatment. The recommendations are valid for solutionizing the components at 540 °C for 12 hours, followed by quenching in water at 80 °C and an artificial ageing at 155 °C for various times.

ACKNOWLEDGEMENTS

Firstly, I want to thank and express my sincere gratitude to my supervisor, Dr. Sumanth Shankar, for his guidance, support, encourage, patience and helpful advices through this project. We had various interesting discussions regarding the present project along the last two years that significantly contributed to removing all the technical road blocks and helped in shaping the path of achieving the goals of the present research activity. Without his encourage and support, this research work and the thesis could not be completed and presented to all.

Many thanks and gratitude to Dr. Manickaraj Jeyakumar for his intensive support and many beneficial technical discussion and suggestion. My many thanks to Doug Culley, Rob Lemmon and Ed McCaffery of the Department of Materials Science and Engineering for their patient assistant in frequent samples Metallography, and evaluating the tensile properties of massive casting samples.

I would also like to thank my colleagues at the Light Metal Casting Research Centre (LMCRC) for all their help and insightful discussions as well as providing a peaceful environment for study and growth. Special thanks go to my colleagues Dr. Xiaochun Zeng and Dr. Peyman Ashtari for their support in theoretical and experimental research. I also wish to thank Mr. Guilhem Casamajou, an exchange student from France, for his help on the tensile testing.

I thank my family members for being patient throughout my research period and supporting me.

TABLE OF CONTENTS

LIST OF FIGURES

LIST OF TABLES

CHAPTER 1 INTRODUCTION AND BACKGROUND

Aluminum alloys have wide applications due to their light weight, high strength, high toughness and easy deformability, high corrosion resistance and excellent machining properties. There are several alloying additions to the Al to form a variety of wrought and casting alloys. A few Al alloys containing Cu and a few containing Mg and Si are heat treatable in the cast condition due to the precipitation strengthening mechanisms. Two of the major families of heat treatable aluminum alloys containing magnesium and silicon are the 6xxx series in wrought aluminum alloys, and 3xx series in casting aluminum alloys.

Aluminum alloys in 6xxx series utilize magnesium and silicon in various proportions to form the Mg_2Si by solid state precipitation reaction in the primary Al phase, making them heat treatable. These alloys are used for various structural and thin walled component applications due to their high strength to weight ratio and high toughness. Typically the 6xxx Al wrought alloys are used for automotive body panels. A representative alloy in this series is the 6061, which is one of the most versatile of the heat-treatable Al alloys. The Al-Si-Mg alloys possess good formability and corrosion resistance as well.

One of the most versatile of 300 series (Al-Si-Mg) casting alloys is the A356.2 alloy. The A356.2 casting alloy is widely used for the casting of high strength components in automotive, aerospace and military applications due to its excellent castability, weldability, high strength, pressure tightness and corrosion resistance [1]. The alloy is generally heat treated to provide various combinations of desired mechanical (strength and toughness) and physical properties. The most common heat treatment is the T6 treatment, wherein the component is solution heat treated at around 540 °C for about 10 to 12 hours immediately followed by quenching in water maintained at 80 °C. The component is then left to natural age in room temperature for about 4 to 12 hours followed by artificial ageing at around 155 °C for about 2 to 12 hours [2]. In the as-cast state the Mg and Si atoms are segregated in the primary Al phase which is mostly dendritic due to the solidification process. The solutionizing treatment dissolves the Mg and Si elements in the primary Al phase. The quenching after solutionizing is to arrest any precipitation reaction during cooling, improve the vacancy fraction to aid mobility of atoms in the ageing process and minimize residual stresses in the component (water at 80 °C) to improve fatigue life. The only disadvantage of the quenching process is the distortion in the part due to the uncontrolled high rate of quenching [3]. The natural ageing process was adopted from the literature for the 6xxx Al wrought alloy series wherein the Mg and Si atoms were found to organize in specific clusters and affect the precipitation mechanism in the artificial ageing stage [4,5,6,7]. The artificial ageing is carried out to result in the precipitation of Mg_2Si phase in the primary Al phase matrix to provide the high strength and toughness to the component [8].
In A356.2 alloy, there has been no research study to methodically investigate mechanisms of atom redistribution in the natural ageing process and the effect of various natural ageing times on the mechanical properties at the end of the artificial ageing process. This study aims to

carry out such an investigation and quantify the effect of natural ageing process on the resultant mechanical properties of the cast component with Al A356.2 alloy. The sequence of precipitation reaction in the primary Al phase during natural ageing would be studied by micro-hardness measurements on the primary Al phase which will reflect any changes to the atom distribution in the phase.

This chapter would address the following topics as found in the technical literature:

- Al-Si casting alloy
- A356.2 alloy
- Heat treatment of Al-Si-Mg alloys
- Solutionizing
- Quenching
- Natural Ageing
- Artificial Ageing
- Mechanical Properties of A356.2 alloy

1.1. Al-Si Casting Alloy

Aluminum casting alloys with silicon as a major alloying element has excellent castability, weldability, pressure tightness, and corrosion resistance [9]. Presently, both the wrought and casting Al alloys containing Si have found extensive use in manufacturing automotive, aerospace, defense and domestic components.

The Al-Si binary phase diagram is shown in Figure 1-1, wherein a simple eutectic reaction takes place at about 577 °C and 12.6 wt% Si [10]. The maximum solubility of Si in the primary Al phase at the eutectic temperature is about 1.62 wt%.

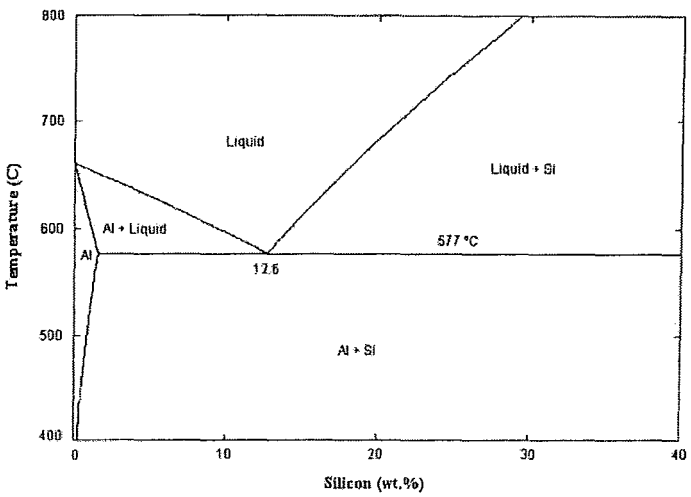

Figure 1-1. Equilibrium binary Al-Si phase diagram

Typically the Al alloys with less than 1.62 wt% Si are termed wrought alloys because of their inability to be shape cast and their ability to attain high strength and toughness values by solid state transformations such as rolling, forging and extrusion. The hypoeutectic Al-Si alloys are the most popular casting alloys and only one composition of hypereutectic alloys has been used for shape casting components [11]. Mg is added to these alloys to enable the precipitation of Mg_2Si phase in the primary Al phase which is predominantly dendritic during the ageing heat treatment process. This precipitation reaction imparts high strength and toughness to the components. Modification of the morphology of the eutectic Al and Si phases by addition of trace levels (about 0.02 wt%) of Sr or Na to the alloy is popular due to the increased tensile and fatigue properties of the cast component [12,13,14,15,16, 17]. Sr additions to the alloy changes the coarse flaky eutectic Si phase to a fibrous morphology and further refines the eutectic Al grains [12].

Hypereutectic Al-Si casting alloys, specifically the 390 alloy find applications where excellent wear resistance and low thermal expansion are required [18, 19, 20]. A typical application for the 390 alloy would be in the manufacturing of engine blocks, piston and cylinder liners [20]. However, the presence of hard primary silicon in the structure makes machining difficult and expensive. It has been found that small additions of phosphorous (0.01wt%) produce fine and more evenly distributed primary silicon crystals, which results in an improved machinability, wear resistance and mechanical properties [18,19].

1.2. A356.2: Al-Si-Mg Casting Alloy

Among the Al-Si-Mg casting alloys, A 356.2 cast alloys is a commercially popular casting alloy. Typical application of the A356.2 alloy in the automotive sector would be the cylinder heads, engine blocks for high priced sports and luxury cars, suspension frames, steering knuckles, parts of support frame in cars and trucks and several other critical components under the hood of a car or a truck. The alloy is heat treatable in the cast condition and exhibits the highest strength to weight ratio coupled with high toughness among the other Al-Si-Mg cast alloys. The typical chemical composition of this alloy is shown in Table 1-1.

Table 1-1 Nominal chemical composition (wt%) of A356.2 Al casting alloy

Si	Mg	Fe	Cu	Mn	Zn	Sr	Ti
6.6 – 7.5	0.30 – 0.45	<0.12	<0.10	<0.05	<0.05	0.01 – 0.025	0.01 - 0.20

A356.2 (ingot) cast alloy, compared with A356.0 (casting) and A356.1 (ingot) castings, has more stringent requirement for the Fe level at < 0.12wt%, compared to <0.15wt% in A356.1 and <0.20wt% in A356.0 alloys, respectively.

The role played by the various alloying elements in a A356.2 Al casting alloy is presented below.

Silicon (Si), after iron, is the highest impurity level in electrolytic commercial Al (0.01 to 0.15%). In 6xxx series Al wrought alloys; silicon is used with magnesium at levels up to 1.5% to produce Mg_2Si precipitates in the primary Al phase during heat treatment. In casting alloys such as A356.2, Si is added to impart additional fluidity in the melt to enable ease of castability.

Magnesium (Mg) is the major alloying element in the 5xxx series of Al wrought alloys. Its maximum solid solubility in Al is 5.5 wt% at about 546 °C. The addition of magnesium markedly increases the strength of aluminum without compromising on the toughness through the precipitation of Mg_2Si phase in primary Al phase. Corrosion resistance and weldability are good with Mg additions. Maximum toughness is achieved after T6 heat treatment of the alloy when the Mg is maintained at less than 0.35 wt%.

Iron (Fe) is the most common impurity found in aluminum. It has a high solubility in molten aluminum and is therefore easily dissolved at all molten stages of production. The solubility of iron in the solid state is very low (~0.004%) [12] and therefore, most of the iron present in aluminum over this amount appears as an intermetallic phase in combination with aluminum and often other elements such as Si. These intermetallic compounds are brittle and act as stress concentration sites for fracture initiation.

Titanium (Ti) is added to the alloy to refine the grain size of the primary Al phase by initiating copious nucleation of the phase at the liquidus temperature.

Strontium (Sr) is added to alloy to effect modification of the eutectic phase morphologies.

1.3. Heat treatment of Al-Si-Mg alloys

Typically, components made with the Al-Si-Mg wrought and casting alloys are heat treated to the T6 temper. The various stages of the T6 heat treatment are discussed in this sub section.

1.3.1. Solution heat treatment of Al-Si-Mg alloys

The typical eutectic reaction (solidus) temperature for the Al-Si-Mg alloy about 555 °C as shown by a typical isopleth from the phase diagram of the Al-Si-Mg ternary system in Figure 1-2. Figure 1-2 was obtained by thermodynamic simulation using the FactSage thermodynamic software [10]. Additionally, the range of composition of Mg between 0.30 and 0.45 wt% is shown in Figure 1-2. Hence, a suitable solution heat treatment temperature for the Al-Si-Mg alloy would be between 540 and 545 °C, to maximize the mobility of the atoms in homogenization and prevent any incipient melting of the eutectic phases [21,22,23]. Figure 1-2 shows that there are four phases formed during the solidification of a typical A356.2 alloy with the given Mg concentration range as shown in Table 1-1. The primary Al followed by Si, β-$Al_{13}Fe_3Si_3$ which is further transformed into the π-$Al_8FeMg_3Si_6$ and lastly the Mg_2Si phase from the trace volume fraction of eutectic liquid at the end of the solidification process. The transformation of β-$Al_{14}Fe_3Si_3$ to the π-$Al_8FeMg_3Si_6$ phase is seldom complete due to the rather

high rate of solidification in a typical shaped casting process of the alloy and hence these two phases co-exist in a typical cast microstructure. The primary Al phase matrix would contain micro-segregation of the alloying elements, primarily, Si and Mg elements during solidification. Hence, the primary Al phase matrix in a typical as-cast microstructure would contain a positive gradient of Si and Mg from the centre of the solidified phase to its periphery. This would not be desirable since the micro-segregation is not favorable to attain high mechanical and performance properties of the cast component.

There are three reasons to carry out the solution heat treatment in the cast component of the A356.2 Al alloy [24]:

- Dissolve the micro-segregation of Mg and Si elements to form a supersaturated solid solution in the primary Al matrix in order to enable the formation of a large number of strengthening precipitates during subsequent natural and artificial ageing processes.
- Homogenize the casting, and attain a globular morphology of the eutectic Si phase to impart improved ductility and fracture toughness to the component.
- Reduce micro-segregation of other alloying elements in the primary Al matrix.

Typically the solution heat treatment is carried out for 12 hours at the isothermal temperature. The homogenization of the alloying elements in the Al matrix takes place within an hour of holding time at the temperature, however, the spherodization of the eutectic Si phase is a slow process [25]. The solutionizing time can be cut to about 6 hours in Sr modified Al-Si-Mg alloys due to the refined fibrous morphology of the eutectic Si phase in the as-cast condition of these alloys.

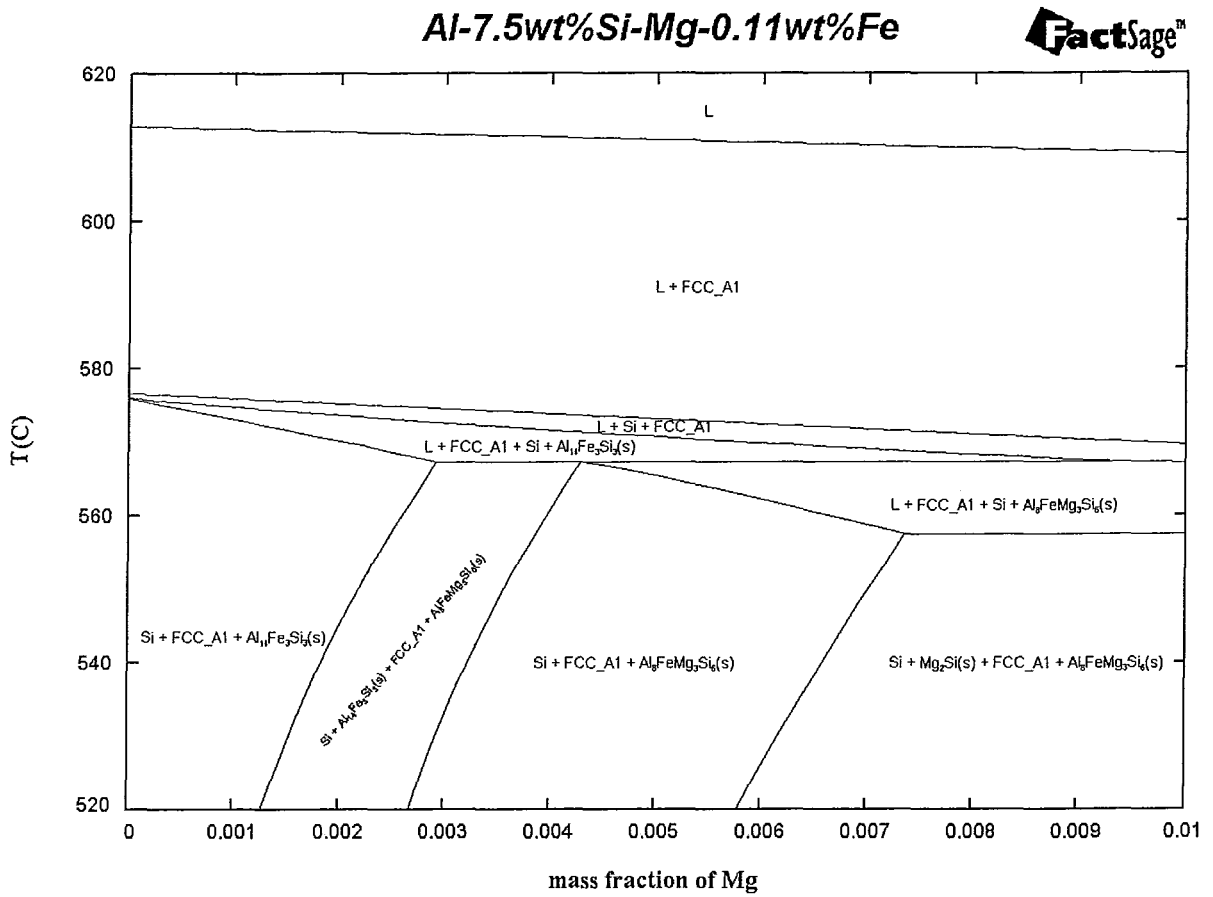

Figure 1-2. A typical isopleth from Al-Si-Mg ternary phase diagram showing the Mg composition range of the A356.2 between 0.3 and 0.45 wt%.

1.3.2. Quenching

Quenching is a critical stage in the T6 heat treatment of Al-Si-Mg alloys. Many researchers and commercial industries do not pay much attention to this stage of the process. Typically the alloy components are quenched immediately after solution heat treatment in a water bath maintained at about 80 °C. A relatively high rate of quenching to retain the homogeneity of the alloying elements in the primary Al phase coupled with requirements of minimum residual stresses in the component (high temperature of the water) are the reasons for the specific quenching medium. One of the detrimental effects of quenching is the distortion of the component at high rates of quenching [3,26].

One of the main effects of the rate of quenching after the solution treatment is the resultant quantity and distribution of vacancies (point defects) in the primary Al matrix which enables and defines the mobility of the Mg and Si atoms during the ageing process. Faster rates of quenching retains a higher vacancy concentration enabling higher mobility of the elements in the primary Al phase during ageing. An optimum rate of quenching is necessary to maximize retained vacancy concentration and minimize part distortion after quenching. A slow rate of

quenching would reduce residual stresses and distortion in the components, however, it causes detrimental effects such as precipitation during quenching, localized over-ageing, reduction in grain boundaries, increase tendencies for corrosion and result in a reduced response to ageing treatment [27,28]. Bates [29] and Zhang [30] have defined the quench sensitivity of the components on the mechanical properties.

The ASTM standard B-917 (B917/B917M2001, 2001) defines the heat treatment for Al casting alloys and the standard specifies that during quenching after solution treatment, it is critical that the cooling proceeds rapidly through the 400°C to 260°C temperature range in order to avoid the premature precipitation which is detrimental to the properties, such as tensile and corrosion resistance. Further, for casting alloys, the quenching delay is recommended to not exceed 45 seconds. In the case of the A356.2 alloy, cast by sand casting or permanent mould, it is recommended to reduce the quench delay time to less than 10 seconds as prescribed by the ASTM standard B-597 (ASTM, 1998).

In Al-Si-Mg alloys, the amount and distribution of the Si and Mg elements in the primary Al matrix would define the resultant precipitation strengthening process (formation of Mg_2Si phase) [31]. Shivkumar et al [22] have reported that in A356 Al casting alloy, about 1.3 wt% Si is retained in the solid solution of the primary Al phase after solution treatment at 540 °C for 12 h and quenched in water at 80 °C and this is about 1wt% excess Si in the solid solution than that dictated by the soichiometry for the formation of the Mg_2Si phase by precipitation reaction.

Recently, Jeyakumar et al [7] carried out experiments on the A356.2 Al casting alloy to investigate the effect of the quench rate and subsequent natural ageing on the mechanical properties of the cast component. They varied the quench rate between about 1 °C/s and 100 °C/s and found that the rate of quenching has a profound effect on the response to the ageing process and the resultant mechanical properties. The faster rates of quenching were achieved by quenching in water at 80 °C and the slower rates by quenching in high velocity compressed air at room temperature. The results show that the quench rate couples with the responses in natural ageing showed more than 150 % variance in the yield strength and nearly 300 % variance in the elongation percentage of the cast component.

1.3.3. Natural Ageing of Al-Si-Mg alloys

Ageing of the alloy is carried out to effect the precipitation reaction of the Mg-Si phases in the matrix of the primary Al phase. Precipitation hardening is a process that involves a particulate dispersion of obstacles to dislocation movements in alloys resulting in strengthening the alloy component. This process is achieved by an intermetallic phase precipitation process in the alloy matrix. The effect of strengthening obtained during the process will depend on the alloy metallic system involved, the volume faction and the size of the particles precipitated, and the nature of the interaction of the particles with dislocations [32].

Most work on the mechanisms of natural ageing were carried out in the 6xxx Al wrought alloys such as a 6061 alloy [33,34,35]. The only work on the effect of natural ageing on the mechanical properties of A356.2 alloy was recently carried out by Jeyakumar et al [7] in which they have studied the effect of quenching rates after solution heat treatment coupled with three condition of natural ageing: no natural ageing, 8 h at room temperature, 72 h at -15 °C. They concluded that the natural ageing process had a profound effect on the final mechanical properties of the alloy component.

Edwards et al [4] summarized the various stages in the ageing process for a 6xxx series Al-Si-Mg wrought alloy for the precipitation of the Mg_2Si phase. The following is the proposed precipitation sequence by Edwards et al [4]:

Super Saturated Solid Solution (SSSS)→ Clusters of Si atoms and Clusters of Mg atoms → Dissolution of Mg clusters → Formation of Mg/Si clusters → Small precipitates of unknown structure (Mg:Si ≅ 1:1)→ β" → β' + B' → β (Stable Mg_2Si precipitate)

The above-mentioned stages occur during the natural ageing process followed by the artificial ageing process. Further, there is a pre-ageing process carried out a few times at 70 °C for a few hours. The above mechanism has been well documented and validated by others [36,37], as well. Vissers et al [38] carried out extensive transmission electron microscopy (TEM) and high-resolution transmission electron microscopy (HRTEM) studies to understand the crystallography of the intermediate phases during the precipitation reaction as proposed by Edwards et al [4]. The summary of this work is presented below where the crystallography of precipitates forming subsequent to the clustering stages was determined.

SSSS → Clusters of Si atoms and Clusters of Mg atoms → Dissolution of Mg clusters → GP Zone (GP-I) → β" (GP-II) → β' + B' + U1 + U2 → β (Stable Mg_2Si phase)

Where,

GP Zones (GP-I)	→	$Mg_xAl_{5-x}Si_6$	→	Primarily Monoclinic
β" (GP-II)	→	Mg_5Si_6	→	Monoclinic
U1 (Type A)	→	$MgAl_2Si_2$	→	Trigonal
U2 (Type B)	→	MgAlSi	→	Orthorhombic
β'	→	$Mg_{1.8}Si$	→	Hexagonal
β' (Type C)	→	$MgSi_{>1}$	→	Hexagonal
β	→	Mg_2Si	→	FCC

Although, the precipitation sequence during ageing of the Al-Si-Mg wrought alloys have been well documented, there is a lack of information about the sequence of precipitation that occur during natural ageing and those during artificial ageing. Further, there is no information about effect of duration of natural ageing on the precipitation response during the artificial ageing process. Additionally, no such work has been carried out in Al-Si-Mg casting alloy where there is at least 1 wt% Si in excess over the soichiometry for the formation of Mg_2Si the primary Al

matrix. It is the aim of this work to understand the specific stages in the precipitation reaction that occur in the natural ageing stage of the T6 heat treatment and further quantify the effect of various times for natural ageing on the responses during artificial ageing and the final mechanical properties of the component.

Self and Co-clusters of Mg and Si atoms in the matrix of the primary Al phase are believed to form by aging treatment of Al-Mg-Si alloys at room and intermediate (70 °C) temperatures. Figure 1-3 shows a differential scanning calorimetry (DSC) curve against the corresponding hardness plot of an as quenched Al-Mg-Si alloy [39]. In this figure, it is believed that the first exothermic peak is associated with formation of self and/or co-clusters of Si and Mg atoms. Murayama et al [40,41] reported that the clusters of Mg atoms are present at as-quenched state, and after a prolong period of ageing at room temperature, clusters of Mg and Si, and their co-clusters are also detected by using atom probe field ion microscopy (APFIM) and high resolution transmission electron microscopy (HRTEM). Some researchers made a distinction between clusters of Si and/or Mg atoms from GP zones. Clusters are zones in the matrix which have higher number of Mg and/or Si solute atoms compared to the random distribution of these atoms in the Al matrix. They are very small (~2nm) with lower solute concentration with undefined morphology and not sufficient enough to give an image contrast in HRTEM. Typically clusters do not have a distinct crystal structure. GP zones are similar to clusters , however, they have a specific crystal structure as defined by Vassar et al [38]. They are ordered solute clusters with the size and the solute content high enough to give an image contrast in the HRTEM. The GP zones typically believed to be generated in preageing stage at 70 °C [42].

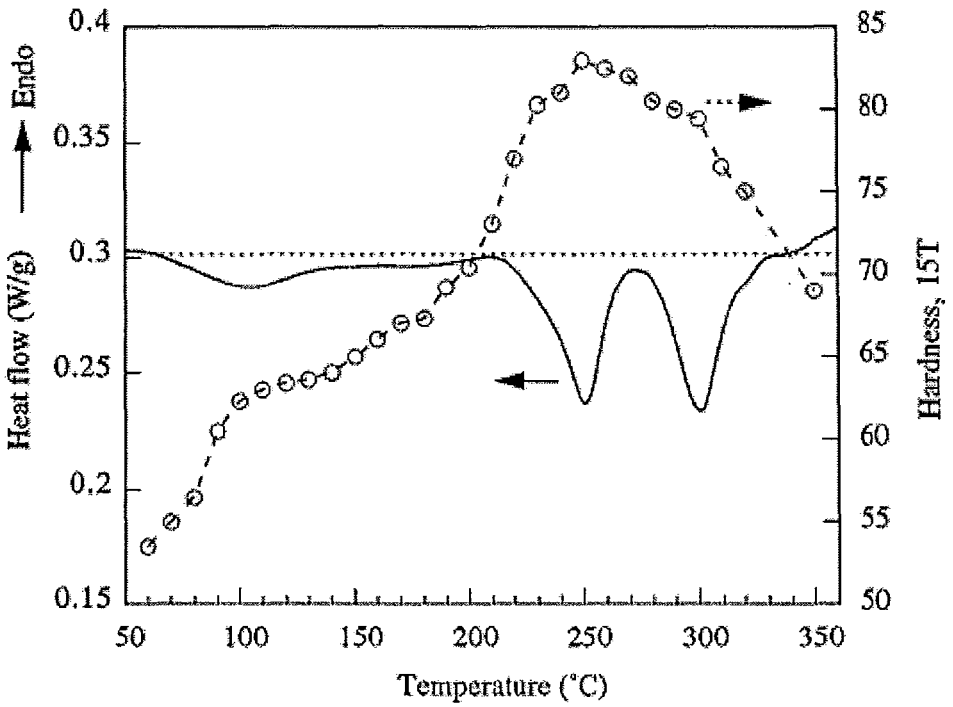

Figure 1-3. DSC and corresponding Hardness plots of an as-quenched AA6111 sample.

The β" precipitates are the most effective strengthening phase in Al-Mg-Si wrought alloys and Al-Si-Mg casting alloys. The exothermic peak drop around 250°C in the DSC curve shown in Figure 1-3 is associated with the formation of these precipitates [39]. β" is a needle-shaped precipitate which has a monoclinic structure and is oriented along <100> of aluminum matrix [38,39]. The β' forms after the β" precipitates as a metastable phase during the ageing treatment. The β' phase reduces the strength of the component when compared to the β" phase as evident in the hardness curve shown in Figure 1-3. The β-Mg_2Si Precipitates are the final stable equilibrium-phase. They are formed during ageing treatment at high temperature and long times.

1.3.4. Artificial Ageing

The stages in this precipitation sequence could occur in the natural ageing process (-30 to 60 °C), pre-ageing at 70 °C and/or artificial ageing at 155 °C [4,7]. However, as mentioned earlier, it is highly unclear about the specific stages occurring in each of the three possible ageing processes. Further, no research has been evident from the literature to validate the sequence of stages during precipitation in a Al-Si-Mg casting alloy such as A356.2. Typically, a person commercially casting with A356.2 alloy in a foundry believes that the artificial ageing process is when the Mg_2Si precipitation occurs and that the natural ageing process is to stabilize the quenched sample after the solution treatment. Typically, cast components after solutionizing and quenching are kept for anywhere between 4 and 12 hours before they are loaded in furnaces for the artificial ageing process. The time for natural ageing mostly depends on the convenience of the foundry such as shifts, production rates and volume of castings required. This project aims to evaluate the validity of this foundry practice.

1.4. Sequence of Precipitation in 6XXX Aluminum Alloys

This section elaborates the details of the stages in a typical precipitation reaction sequence in the primary Al phase of the Al-Si-Mg alloys. Further, experimental and analysis techniques used to verify the various precipitation reaction stages have also been cited and discussed.

1.4.1. Self Clusters and GP zones

Self clusters and GP zones are believed to be the first stages of the precipitation reaction during the natural ageing treatment of the Al-Si-Mg alloys in temperature ranges between -30 °C to 70 °C. The self- and co- clusters are generally in the nanometer size range, and they are too small to be observed in the conventional Transmission Electronic Microscope (TEM). Figure 1-4 shows the bright-field TEM image of a balanced Al-Mg-Si alloy which was naturally aged for 70 days at room temperature. No evidence of any precipitates could be found in this picture [41].

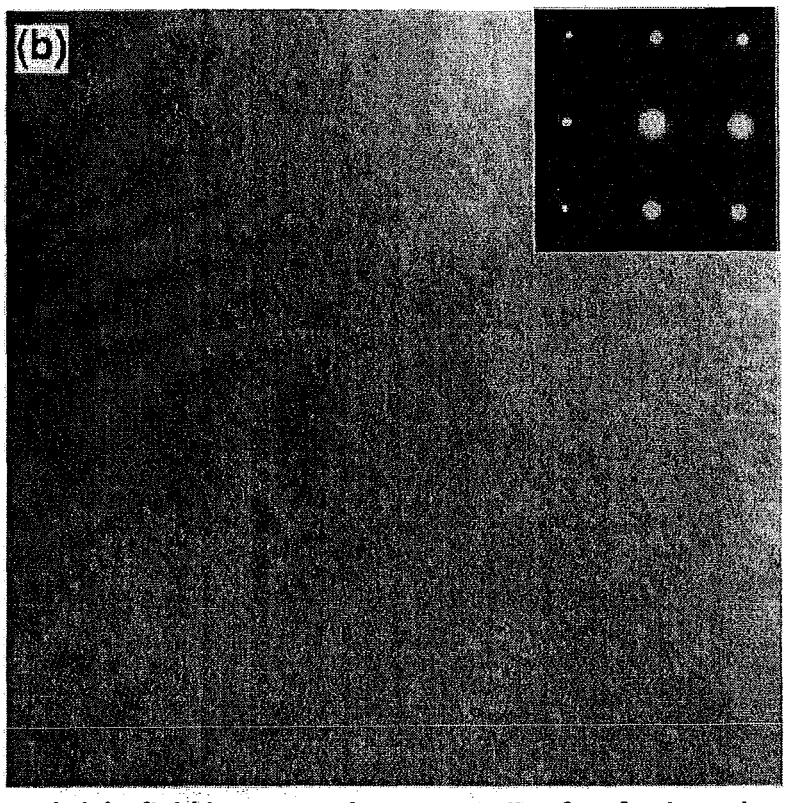

Figure 1-4. TEM bright field images and corresponding [001] selected area diffraction patterns obtained from the Al-0.70Mg-0.33Si alloy after ageing for 70 days at room temperature [41].

Figure 1-5 shows the High Resolution Transmission Electron Microscope (HRTEM) images of Al-0.65Mg—0.33Si alloy sample which was naturally aged for 70 days (Figure 1-5 (a)) and a sample which was artificially aged at 70°C for 16 hours (Figure 1-5 (b)) [41]. As it can be seen, clusters formed during natural ageing at room temperature are still not discernable even in a HRTEM and a few clusters become apparent in a HRTEM for artificial ageing process carried out at 70 °C as indicated by arrows in Figure 1-5(b). The lack of appearance of the clusters or alloys which have been aged in room temperature, in conventional TEM and HRTEM may suggest that the clusters have minimal deviations in coherency with the primary Al matrix and that the number of atoms in these clusters is very few. Further, the clusters in Figure 1-5, could not be specifically identified as being self- clusters or GP zones (GP zones I).

GP zones I is the precursor of the β" phase, while β" was considered as GP zone II [40]. β" is a needle-shaped precipitate which has a monoclinic structure and is oriented along <100> of aluminum matrix. Figure 1-6 shows the typical TEM micrograph of β"-Mg_5Si_6 precipitates (a) bright field image (b) SAD pattern of same area shown in (a) with a $[001]_{Al}$ zone axis [43].

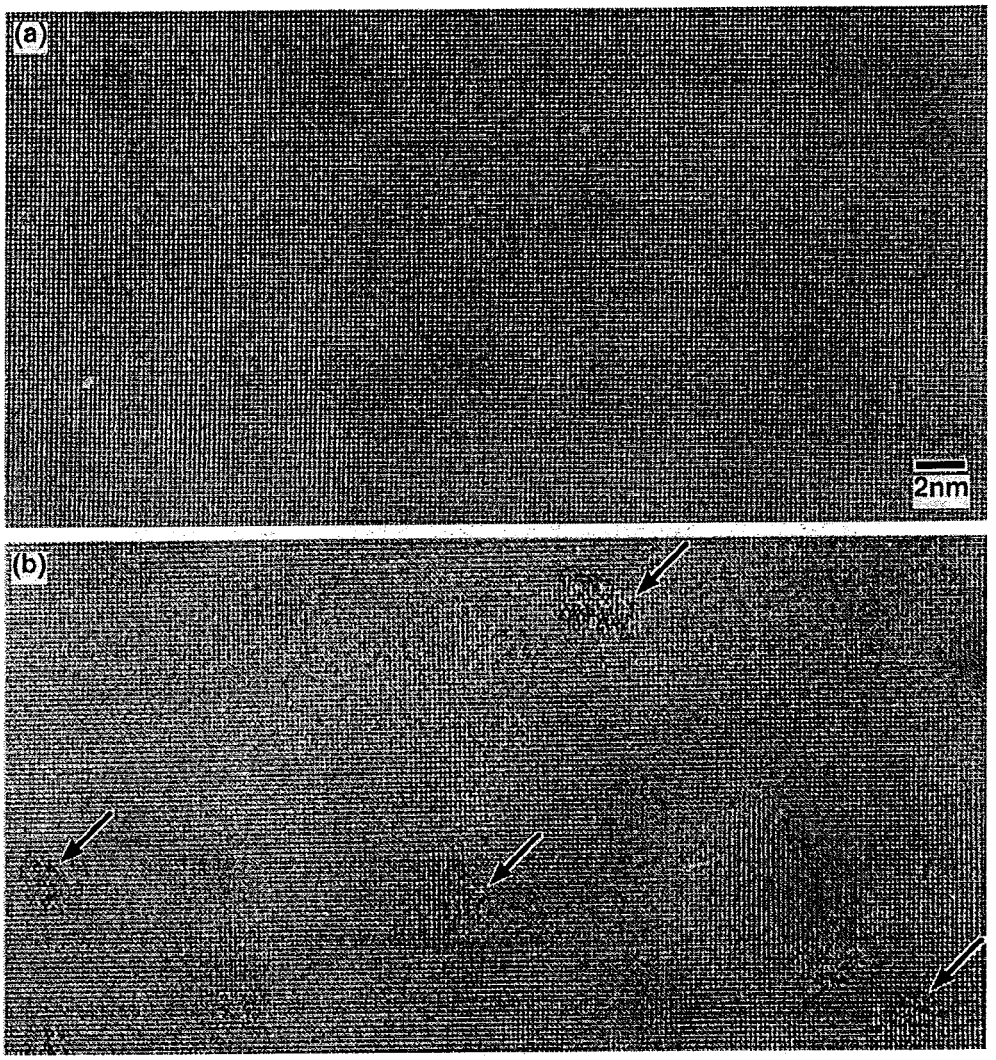

Figure 1-5. HRTEM images taken at the [001]Al zone axis of Al-0.65Mg-0.70 Si (Si-excess) alloy after (a) natural ageing for 70 days at room temperature and (b) 16 hours at 70°C temperature [41].

1.4.2. Precipitation of β' ($Mg_{1.8}Si$)

Formation of β'- $Mg_{1.8}Si$ is the first stage of precipitation reaction in Al-Mg-Si alloys during the artificial ageing treatments at temperatures above 120 °C. In Figure 1-3, the second exothermic peak at around 250°C in the DSC curve shown was proposes to be associated with the formation of these precipitates [39].

There are two known morphologies of β' precipitate: needle-shaped and rod-shaped. It has been shown that the needle-shaped morphology forms first followed by the transition to the rod-shaped morphology [8]. The exact composition of β' precipitates are not unique. The EDS results of Maruyama et al [8] indicates the ratio of Mg:Si can be between 1.75 and 1.78. Vissers et al [38] suggest a ration of 1.8 for Mg to Si atoms. The needle shaped morphology has a

monoclinic structure and is oriented along the <100> direction of the aluminum matrix [37]. The rod-shaped morphology has a hexagonal crystal structure and oriented along the <100> direction of the aluminum matrix [8,38].

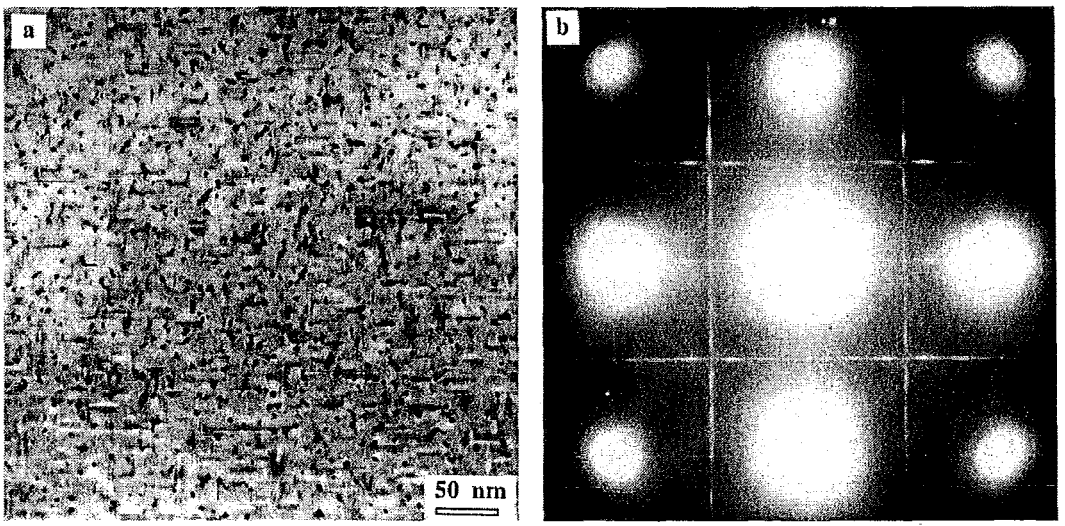

Figure 1-6. Typical TEM micrograph of β"-Mg_5Si_6 precipitates (a) bright field image (b) SAD pattern of same area shown in (a) with a $[001]_{Al}$ zone axis [43].

Figure 1-7 shows a typical TEM bright field image of rod-shaped β' precipitates [44]. They were reported to have a large aspect ratio and therefore they have a prominent shape effect on the strength of the alloy.

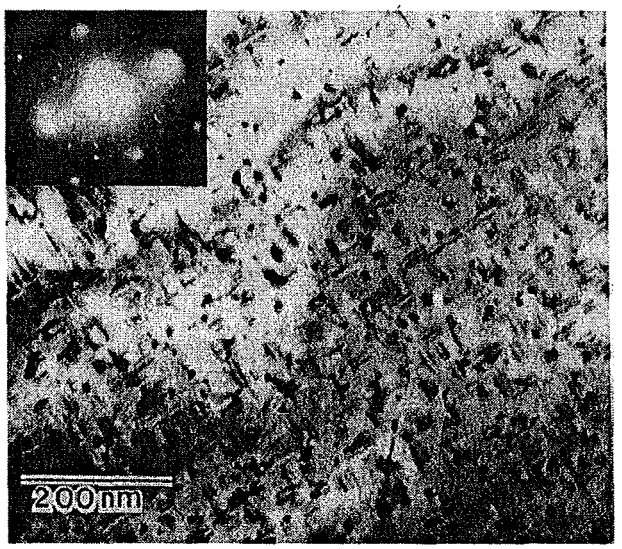

Figure 1-7. Bright-field TEM micrograph showing the rod-shaped β' precipitates and the corresponding SADP [44].

1.4.3. Precipitation of β (Mg_2Si) phase

The β precipitates are the final stable phases in the precipitation reaction sequence of Al-Mg-Si alloys. They are formed subsequent to the β' precipitates during the artificial ageing treatment. β precipitates are in the form of plates which are oriented along the <100> direction of the aluminum matrix. They have the well known crystal structure akin to the CaF_2 structure [37], and according to Maruyama et al [8], the ratio of Mg to Si atoms in β is 2.10.

1.5. Experiment Techniques to Observe Self-Clusters and GP-Zones

As we mentioned in above sections, there are various techniques which can be used to ascertain the nature of precipitates during the various stages of the precipitation reaction in the primary Al phase of Al-Si-Mg alloys. Since, the process of precipitation reaction starts almost instantaneously after quenching the sample from the solution heat treatment temperature by the formation of self clusters of Si and Mg atoms, a viable experiment technique which could capture the in-situ reactions during the natural and artificial ageing process. The precipitates in the reaction at the end of the artificial ageing process could be easily ascertained by popular techniques such as TEM. However, there are not many techniques available to ascertain the precipitates in the reaction during the initial natural ageing process, specifically identify the times during which the self-clusters and GP-Zones form. Understanding the kinetics of the formation of self-clusters and GP zones during the natural ageing and the effect of their formation on the reactions during artificial ageing and hence the mechanical properties of the alloy of these alloys are critical to optimize the duration of the natural ageing process. The extremely small size of the self clusters and GP zones coupled with their rapid precipitation kinetics and the lack of any discernable interface with the Al matrix (clusters are essentially parts of a matrix with coherent or half coherent interfaces with the Al matrix) make the direct observation of the self-clusters and GP zone a difficult challenge to overcome. Indirect techniques wherein measurement of an effect on certain property caused by the formation of self-clusters and GP zones would have to be adopted to observe their formation during natural ageing.

1.5.1. Three Dimensional Atom Probe (3DAP)

Three dimensional Atom Probe is most efficient advanced characterization techniques to detect the formation and development of Si and Mg atom clusters during the precipitation reaction for Al-Mg-Si alloys [40,41]. It can provide the distribution maps of specific atoms during the precipitation reaction. This technique is expensive and there are very few facilities offering time to carry out 3DAP in North America.

1.5.2. Transmission Electronic Microscopy (TEM)

Transmission Electronic Microscopy (TEM) is the most direct and classical technique to study precipitates in the primary Al matrix. However, as discussed in Section 1.4.1. , the self-clusters

and GP zones are not easily observable in conventional and high resolution TEM due to the small size of self-clusters and GP zones, their coherency with the aluminum matrix, and also proximity of the atomic numbers of Mg, Al and Si in the periodic table of elements. Further, TEM and HRTEM are not in-situ processes and demand extensive times for sample preparation which would make these techniques useless to determine the kinetics of the early stages of precipitation reactions in Al-Si-Mg alloys.

1.5.3. Differential Scanning Calorimetry (DSC)

Differential Scanning Calorimetry (DSC) is an indirect technique where the temperatures and heat flows associated with transitions in materials are measured as a function of time and temperature in a controlled atmosphere [4,39,48,44]. DSC has enabled the study of the various transformations such as GP zone formation, and metastable and stable precipitates. However, this technique could not be used to evaluate self-cluster formation and further the technique could not be effectively used for studying isothermal, room temperature transformations in the primary Al matrix. The measurements provide quantitative and qualitative information about physical and chemical changes that involve endothermic or exothermic processes, or changes in heat capacity. It is more common to identify the presence or absence of a given transition but not evaluate the kinetics of the transformation.

1.5.4. Electricity Conductivity Measurement

Electricity resistivity measurement is one of the more popular methods in precipitation reaction studies [23,33,42]. In this technique, the electrical resistivity of a bulk sample is measured continuously to detect and observe any precipitation reaction in the sample which will cause a measurable change in the electrical resistivity. However, the high sensitivity of this technique could also translate into problems caused by high signal to noise ratios in the measurements. In a recent study of the precipitation reactions in the primary Al phase of Al-Si-Mg wrought alloys [42], it was shown that the noise was comparable or higher than the signal during measurements of electrical resistivity during natural ageing process.

1.5.5. Mechanical Properties Testing

There are various mechanical tests available which can be used in the precipitation studies. They include the hardness, tensile properties, stress relaxation, and strain rate sensitivity measurements.

Many researchers use tensile tests to evaluate the effect of natural ageing and/or artificial ageing process on the mechanical properties of Al-Si-Mg alloys [22,23,49]. These studies have elaborated on the effect of various ageing treatments on the final mechanical properties of the alloy but the tensile property evaluation could not be used to study the in-situ kinetics of the precipitation reaction stages.

The hardness test is the simplest and quickest mechanical test available. Despite its simplicity, it can provide a precise overview of the macroscopic/microscopic effects of the precipitation reaction process. The technique is in-situ where in the measurement time of the macro or micro hardness in a sample is comparable to the rate of formation of the precipitates in the primary Al matrix.

There are two methods of hardness measurements for ageing precipitation process from the points of load and indenting area, i.e. Macrohardness measurements (Rockwell hardness, Brinell hardness and Vickers macro-hardness) and microhardness measurement (Vickers micro-hardness). The specifications and applications for these hardness measurements are listed in Table 1-2.

Though these macro hardness measuring techniques are frequently used by some researchers on study of ageing precipitation [23,30,36,39,42,46], but in most case, due to about three orders of size difference between the reaction matrix (in micro meters) and the hardness indentation (in mm), the results provided by these macro hardness measurements are very schematics and descriptive and they are usually employed to couple with other experimental techniques such as DSC. Hence, macrohardness could not reveal the kinetics of formation of self-clusters and GP-zones due to the inability of the technique to detect these reactions.

Microhardness measurements on the primary Al matrix carried out continuously after quenching the Al-Si-Mg alloy samples from the solution heat treatment temperatures would prove to be a viable technique in analyzing the kinetics of the precipitation reactions during the natural ageing process. The size of the indentation in microhardness is in micrometers and is generally smaller than the size of an average grain in the alloy samples solidified at nominal cooling rates akin to those observed in conventional casting processes. The microhardness measurements are very sensitive to subtle changes in the distribution of solute atoms in the primary Al phase and hence, could detect the formation of self-clusters and GP zones during the precipitation reaction.

Given the advantages offered by microhardness measurements in being able to detect the kinetics of the precipitation reaction during natural ageing and the low cost and easy accessibility of microhardness measuring system, this technique was utilized in this study.

Type	Vickers Harness		Brinell Hardness		Rockwell Hardness				
Scales	Macro Vickers	Micro Vickers			**RHA**	**RHB**	**RHC**	**RHD**	**RHF**
Testing Standard	ASTM E92-89	ASTM E384-09	ASTM E10-08		ASTM E18-08				
Features	Indentation hardness		Indentation hardness		Indentation hardness				
Materials indented									
Indenter	136° Diamond Pyramid	136° Diamond Pyramid	hardened steel or carbine balls	hardened steel or carbine balls	120° diamond cone	steel ball	120° diamond cone	120° diamond cone	steel ball
Load	1 to 100 kg	1 to 1000 g	3000 kg	500/1500 kg	60 kg	100 kg	150 kg	100 kg	60 kg
Method	The indented surface area	The indented surface area	The indented surface area	The indented surface area	The depth of impression				
Formula	$HV = 1.854 \times (F/d^2)$	$HV = 1.854 \times 1000 (F/d^2)$	$BHN = 2F/(\pi D(D-(D2-Di2)^{1/2}))$		HR = E-e				
units in formula	*F: kgf; d: mm*	*F: gf; d: μm*	*F: kgf; d: mm*		*F: kgf; d: mm*				
Surface requirement									
Metallography		200X, 400X, 500X and 1000X							

Table 1-2. Summary of Hardness Testing Methods

1.5.6. Tensile Properties of A356.2 alloy

Mechanical properties of as cast components and specifically, the tensile properties such as the yield strength (YS), ultimate tensile strength (UTS), and percentage of elongation (% El) are widely used to evaluate the performance of a cast component.

The tensile properties of A356.2 castings are controlled by the dendrite arm spacing of the primary Al phase, Mg_2Si precipitation reaction in the Al phase matrix, aspect ratio of the eutectic Si phase in the microstructure, nature, morphology and distribution of intermetallic phases evolved during solidification, and inclusions and porosity occurring during the casting process.

The tensile properties can be calculated from the engineering stress-strain curve shown in Figure 1-8 [45]. The stress, or the average longitudinal stress along the axis, in the tensile specimen is given by Equation (2-1).

$$S = P / A_0 \qquad (2\text{-}1)$$

In Equation (2-1), S is stress, P is the longitudinal load on the specimen, and A_0 is the original cross-section area of the specimen.

The yield strength (YS), is the stress when the elongation of the specimen reaches 0.2% offset of the load. The ultimate tensile strength (UTS), or tensile strength in short, is the maximum stress experienced by the sample before failure. Percentage of Elongation (%el) is calculated by Equation (2-2).

$$\%el = \Delta L / L_0 \qquad (2\text{-}2)$$

In Equation (2-2), ΔL is the instantaneous elongation change and L_0 is the original length of the specimen.

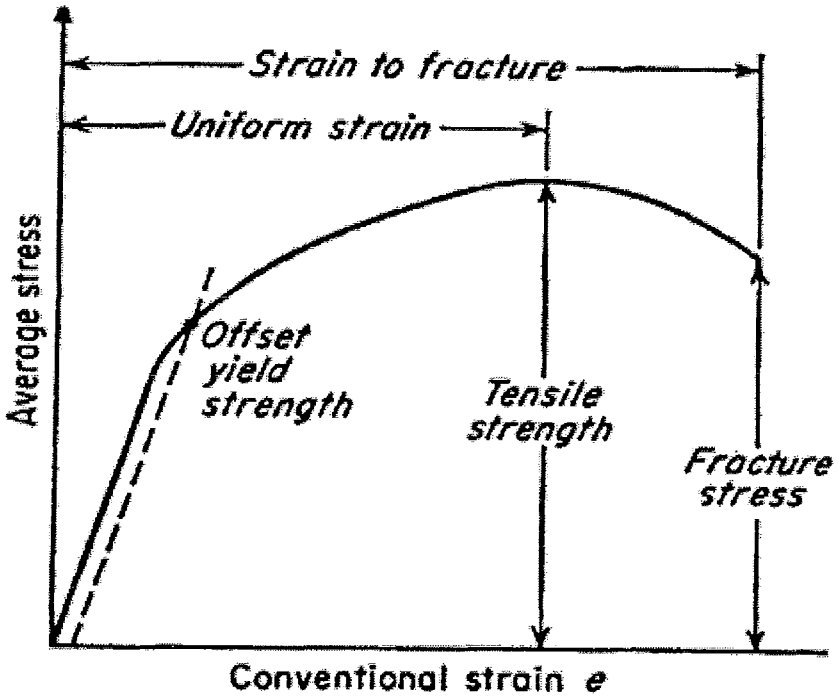

Figure 1-8. The engineering stress-strain curve (G. E. Dieter, 1976)

P.A. Rometsch et al [46] developed an empirical age hardening model for prediction of YS for the A356 and A357 Al casting alloys, wherein they break down the alloys' yield strength into a few contributing factors as shown in Equation (2-3).

$$YS_t = YS_O + \Delta YS_{si} + \Delta YS_{Fe} + \Delta YS_{ss,si} + \Delta YS_{ss,Mg} + \Delta YS_{ppt,Si} + \Delta YS_{ppt,Mg\text{-}Si} \quad (2\text{-}3)$$

In Equation (2-3), Caceres et al [47] considered the total yield strength (YS_t) of a precipitation hardening Al-Si-Mg casting alloy as the sum of the YS of pure aluminum (YS_O) and the contributions to the YS due to eutectic Si particle (ΔYS_{si}), eutectic Fe-phase particles (ΔYS_{Fe}), Si in solid solution ($\Delta YS_{ss,si}$), Mg in solid solution ($\Delta YS_{ss,Mg}$), Si precipitates ($\Delta YS_{ppt,Si}$) and Mg-Si precipitate ($\Delta YS_{ppt,Mg\text{-}Si}$).

The relation in Equation (2-3) could be simplified because the ΔYS_{si}, ΔYS_{Fe} and $\Delta YS_{ss,si}$ are expected to remain relatively unchanged during the ageing process. Although, the $\Delta YS_{ss,si}$ may vary with aging time and temperature, these effects are expected to be minimal since changes in the Si concentration would be from 0.5 to 1.2 wt% in the Al solid solution and expected to increase total YS by only 2 to 3 MPa [48]. Further, albeit a fine-scale Si clusters and Si precipitates are expected to occur in these alloys under some quenching and aging conditions [30], the extent to which these Si cluster and precipitates would influence the total YS of the component remains unknown. For simplcity, it was therefore assumed that the effect of Si precipitation and clustering on total YS is negligible, especially in relation to the very large contribution by the Mg_2Si precipitation reaction. Conquently, Equation (2-3) was simplified to postulate Equation (2-4) [46].

$$YS_t = YS_i + \Delta YS_{ss,Mg} + \Delta YS_{ppt,Mg\text{-}Si} \quad (2\text{-}4)$$

In equation (2-4), YS_i is the intrinsic strength, which may be defined here as being the sum of YS_o and the strengthening contributions which remain constant during the ageing process. The plausible differences in aging hardening characteristics between the matrices of primary Al dendritic and Al eutectic grains were considered negligible since the primary Al phase was homogenized by the solution heat treatment process.

The literature review of the T6 heat treatment of A356.2 alloy components has revealed that very little research work has been carried out to elucidate the mechanism of the Mg and Si atom re-distribution during the natural and artificial ageing processes. Further, in the literature in both the Al-Si-Mg casting and wrought alloys, the specific stages of the precipitation reaction occurring in the natural ageing process and that in the artificial ageing process are not clearly differentiated and explained. Möller et al [49], had concluded that the effect of natural ageing process is profound on the precipitation reaction responses in artificial ageing and the mechanical properties of the cast component with Al 357 alloy. Their study was rudimentary with two levels of natural ageing, 0 and 20 h but the results show that there is a marked difference in the final properties after the respective T6 treatments. Moreover, the quantified effect of natural ageing on the responses during artificial ageing and the subsequent mechanical properties of the component are absent. These lapses in the literature provided the motivation for the present study.

CHAPTER 2 OBJECTIVES AND RESEARCH PLAN

This chapter presents the objectives and the research plan adopted in this study.

2.1. OBJECTIVES

The following are the specific objectives of this study:

- Refine the understanding of the sequence of precipitation reaction of the Mg and/or Si atoms in the primary Al phase of A356.2 casting alloy. Specifically, elaborate on the specific stages occurring in the natural ageing process at room temperature and subsequently, the artificial ageing process at high temperature.

- Quantify the effect of various natural ageing times at room temperature subsequent to quenching the sample in water at 80 °C after the solution heat treatment, on the precipitation reactions during artificial ageing at high temperature and subsequently, the mechanical tensile properties of the component cast with A356.2 alloy.

2.2. RESEARCH PLAN AND PROGRESS

There are two phases of this project to achieve the project objectives and these are elaborated below.

- Phase I
  - Sequence of precipitation reaction sequence during the natural ageing at room temperature for cast component from A356.2 Al alloy.
- Phase II
  - Quantify the effect of natural ageing time on the response during artificial ageing at high temperature, and
  - Quantify the effect of natural ageing time on the mechanical tensile properties of the cast component from A356.2 alloy.

Figure 2-1 presents a schematic flow diagram of the plan for Phase I of the project. Cylindrical samples of about 12.70mm in diameter and 12mm in length were obtained from identical sections of cast components of A356.2 alloy cast in a permanent mould casting process using a P20 tool steel for the metal mould. Solution heat treatment was carried out on all the samples at 540 °C for 12 h at isothermal temperature in a conventional electric resistance furnace. The samples were quenched at three unique cooling rates, respectively as presented below:

- A mixture of anti-freeze solution with dry ice maintained at a constant -40 °C temperature.
- Water at room temperature of about 23 °C.
- Water maintained at 80 °C temperature.

Subsequent to quenching, each sample was maintained at room temperature for natural ageing process. During the natural ageing process, micro-hardness measurements were carried out on the matrix of the primary Al phase from 0 h to 150 h ageing time. The measurements were taken at very small intervals during the first few hours and subsequently, the measurement intervals were increases methodically. The micro-hardness data on the primary Al phase would reveal any subtle precipitation reaction occurring in this phase during the natural ageing process.

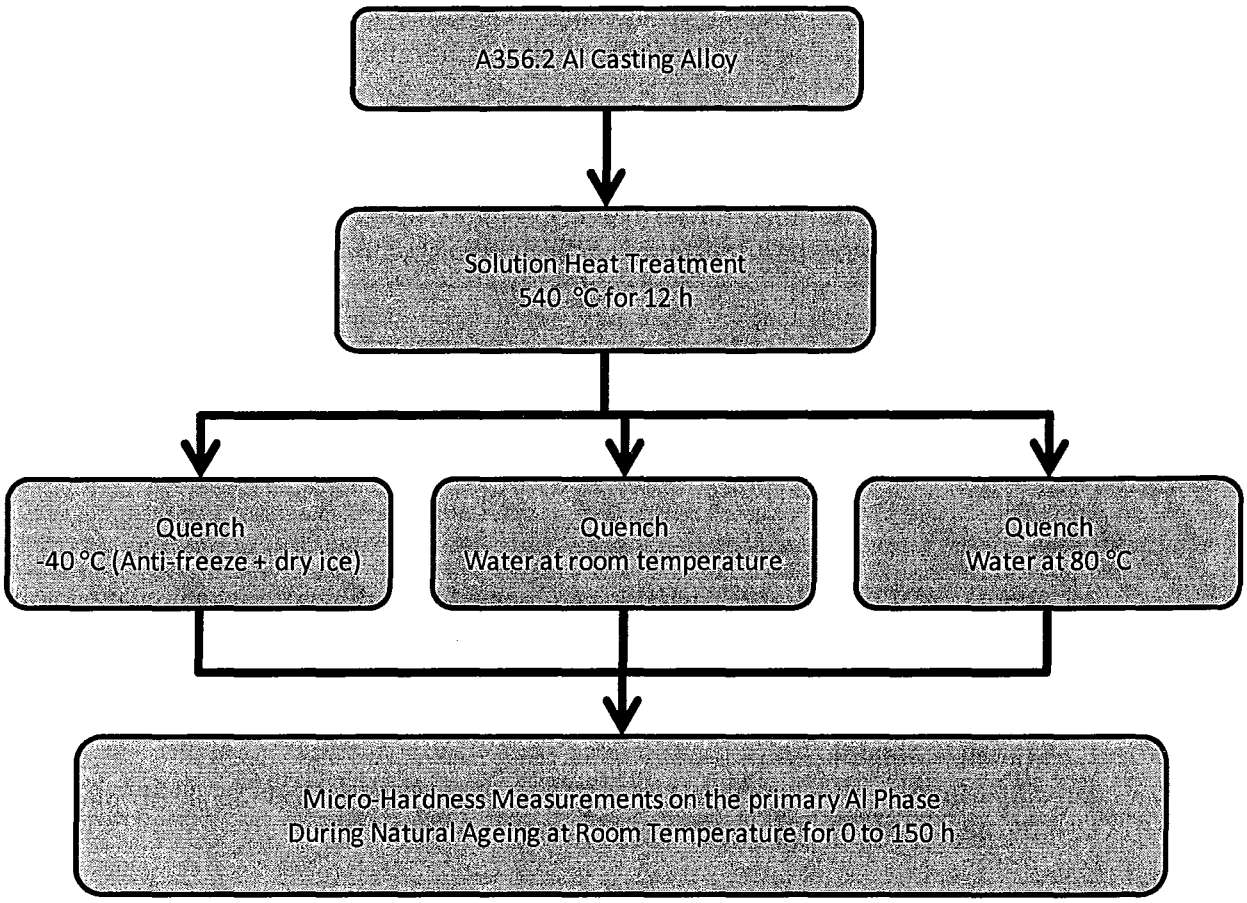

Figure 2-1. Flow chart of the project plan

Figure 2-2 and Figure 2-3 show the schematics of the flow charts elaborating the two tasks in Phase II of the project where in the effect of natural ageing at room temperature on the responses in the high temperature artificial ageing and the tensile properties of the cast component with A356.2 Al alloy were quantified, respectively.

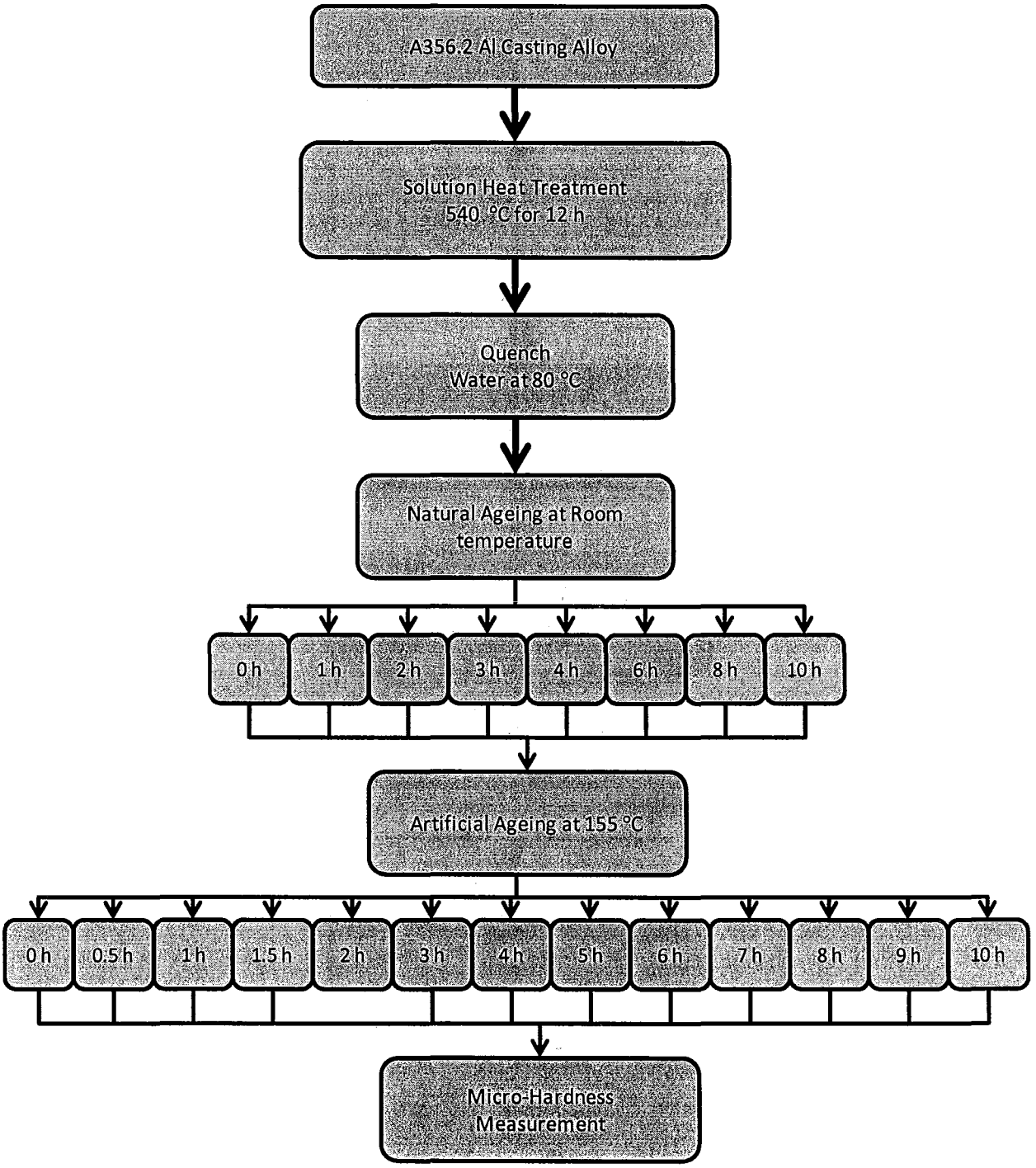

Figure 2-2. Phase II of the project to quantify the effect of natural ageing at room temperature on the responses in high temperature artificial ageing of A356.2 alloy cast component.

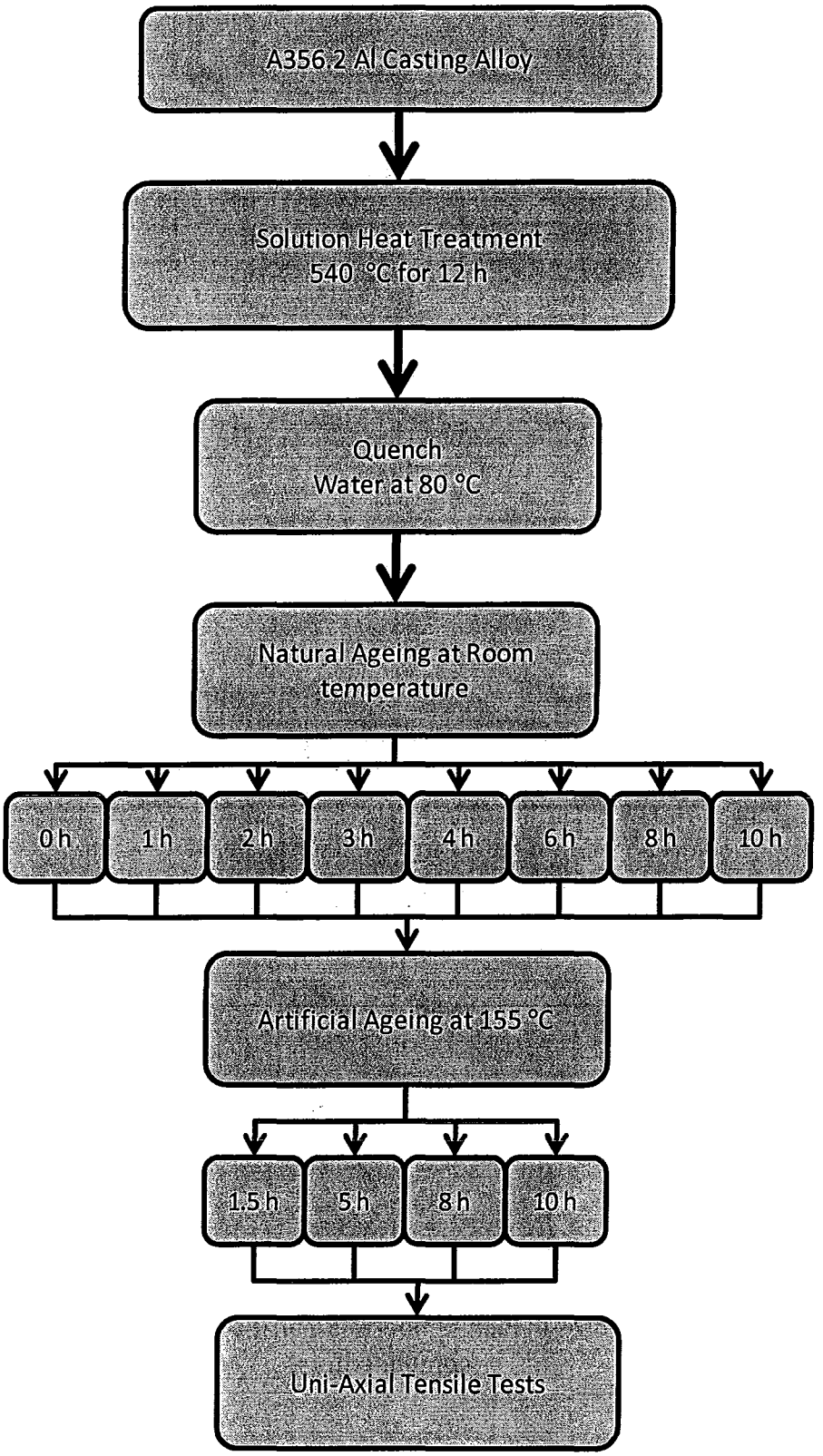

Figure 2-3. Phase II of the project to quantify the effect of natural ageing at room temperature coupled with artificial ageing at high temperature on the tensile properties of A356.2 alloy cast component.

In Figure 2-2, two sets of sample geometry, namely, cast cylindrical samples of about 12.70mm in diameter and 12mm in length and as-cast tensile test bars (ASTM B557-06 standard) manufactured by the casting process specified in the ASTM B108 M-08 Standard. Solution heat treatment was carried out on all the samples at 540 °C for 12 h at isothermal temperature in a conventional electric resistance furnace. The samples were quenched in water maintained at 80 °C. Natural ageing of the samples at room temperature were carried out for various times ranging from 0 to 40 h as shown in Figure 2-2 for the cylindrical samples and Figure 2-3 for the tensile test bar samples. The sample from each natural ageing time was subjected to artificial ageing treatment at 155 °C for various times ranging from 1.5 to 10 h as shown in Figure 2-2 for the cylindrical samples and Figure 2-3 for the tensile test bar samples, respectively. Micro-hardness measurements on the matrix of the primary Al phase in the cylindrical samples and uni-axial tensile test on the tensile test bars were carried out. There were a total of 104 cylindrical coupon samples and 160 tensile test bar samples (5 samples repetition for each condition) in the Phase II of the project.

CHAPTER 3 MATERIALS AND PROCEDURE

In this chapter, elaborate details of the materials and procedures adopted in carrying out the various tasks in this project would be presented.

3.1. ALLOY

The A356.2 was obtained from a commercial vendor and the composition of the alloy as measured by both the Glow Discharge Optical Emission Spectroscopy (GDEOS) and Inductively Coupled Plasma/Mass Spectrometry (ICP/MS) is presented in Table 3-1.

Table 3-1. Average elemental composition (wt %) of the A356.2 Al alloy used in this project.

Si	Mg	Fe	Ti	Sr	Cu	Mn	Zn	Al
7.5	0.46	0.11	0.17	0.02	0.06	0.11	0.04	Balance

3.2. CASTING

The A356.2 alloy was cast in a direct pour gravity casting process in a metal mould. The cast component design and the casting process specified in the ASTM B108M-08 standard were followed. Test bars for tensile test evaluation were cast and the testing procedure prescribed in the ASTM B557M-07 standard were followed wherein a strain rate of 1 mm/min was used in the uni-axial tension mode on a 2 in gauge sample fitted with a digital on-line extensometer. Figure 3-1 shows the design of the standard tensile test bar used in the study. Figure 3-2 shows the design and dimensions of the cast component obtained in the gravity casting process with a metal mould. Two tensile samples are obtained from each casting. The A356.2 alloy is melt and held in an electric resistance furnace for the casting process. Further, the alloy was degassed with ultra high purity Argon gas in a rotary degasser at about 5 l/min and 300 RPM rotation for about 30 min.

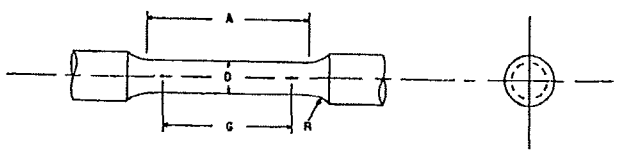

Nominal Diameter	Dimensions, mm			
	Standard Specimen	Small-Size Specimens Proportional to Standard		
	12.5	9	6	4
G—gage length	62.50 ± 0.10	45.00 ± 0.09	30.00 ± 0.06	20.00 ± 0.04
D—Diameter (Note 1)	12.50 ± 0.25	9.00 ± 0.10	6.00 ± 0.10	4.00± 0.05
R—Radius of fillet, min	9	8	6	4
A—Length of reduced section, min (Note 2)	75	54	36	24

Figure 3-1. Dimensions of the tensile test bar. The 'standard specimen' was used.

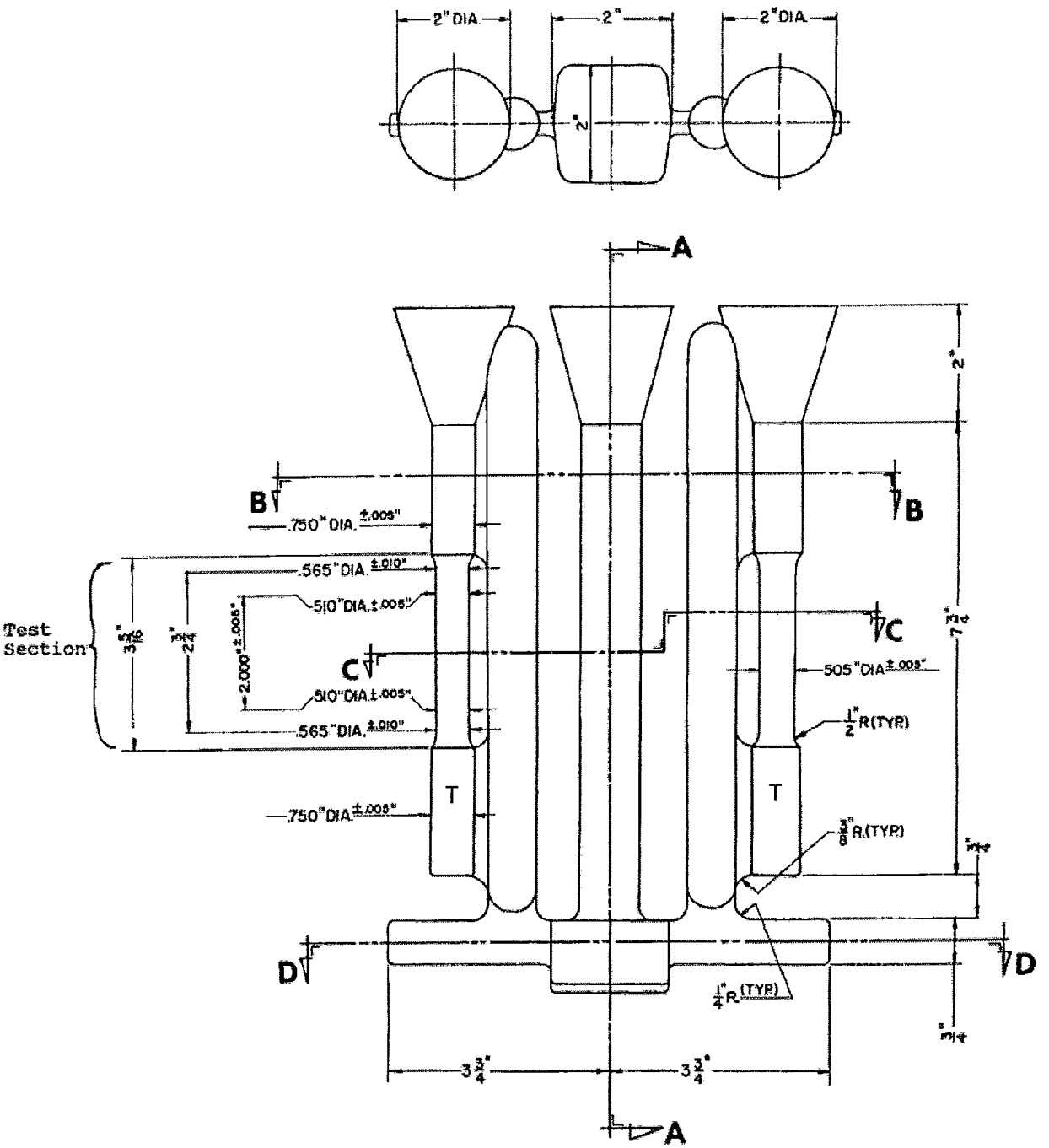

Nominal draft angle to be 20° on all square or rectangular sections in direction transverse to parting line.

NOTE—Test section of test bar: this section to be gradually tapered from the ends towards the center.

Figure 3-2. Design and dimensions of the tensile test bar cast component from the metal mould by direct pour gravity casting process as specified in ASTM B108M-08 standard. The sections marked by letter T are the two tensile samples obtained from the casting.

3.3. METALLOGRAPHY AND MICRO-HARDNESS

The sample preparation for optical microscopy and micro-hardness measurements involved cold mounting the samples with a liquid resin formed by mixing 25 g of Epoxy Resin Solution and 3 g hardener liquid in a plastic mold, followed by grinding with SiC papers ranging from 320 to 4000 grits and polished with alumina suspension ranging from 3 to 1 microns. No chemical etching was carried out on the sample. Samples used for micro-hardness evaluation were further polished using a 0.05 micron alumina suspension. The optical microscopy was carried out on all samples to ensure consistent levels of distribution and morphology of the primary Al and eutectic Si phases. Figure 3-3 shows a typical microstructure of A356.2 alloy in the as-cast condition obtained from the gauge section of a tensile test bar.

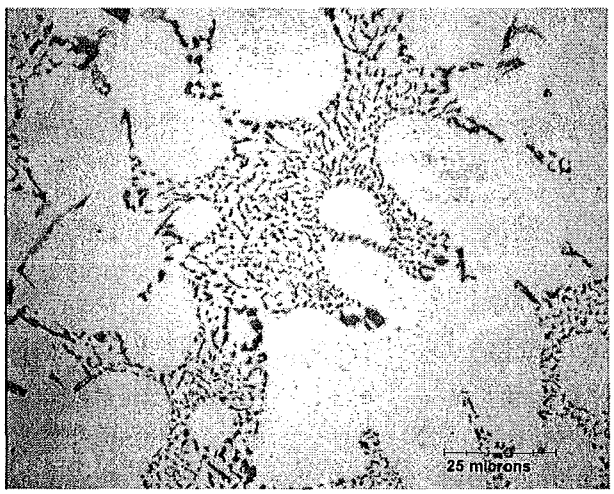

Figure 3-3. Typical microstructure of A356.2 alloy in the as-cast condition. The dark phase is the eutectic Si and the light phase is the primary Al dendrites.

The Vickers micro-indentation hardness measurements were carried out on the samples according to the ASTM Standard E384-09 using a Clemax™ Intelligent micro-hardness system with a load of 25 gf and a dwell time of 10 seconds for each loading. The diamond indenter used was a Vickers indenter in the shape of a square based pyramid with the angle of 136° between the faces. The size of the indention was measured with a micrometer integrated in the microscope at 400X.

A special metallic holder was designed and manufactured to hold the cylindrical samples for the micro-hardness measurements. A typical micro-hardness indentation in the primary Al phase is shown in Figure 3-4. Equation (3-1) was used to evaluate the micro-hardness from the measurements of the indentation on the primary Al phase.

$$\text{Micro-Hardness (HV)} = 1.854 \times 10^3 \, (F/d^2) \qquad (3\text{-}1)$$

In Equation (3-1), F is the applied load in grams and d is the mean of two diagonals in μm.

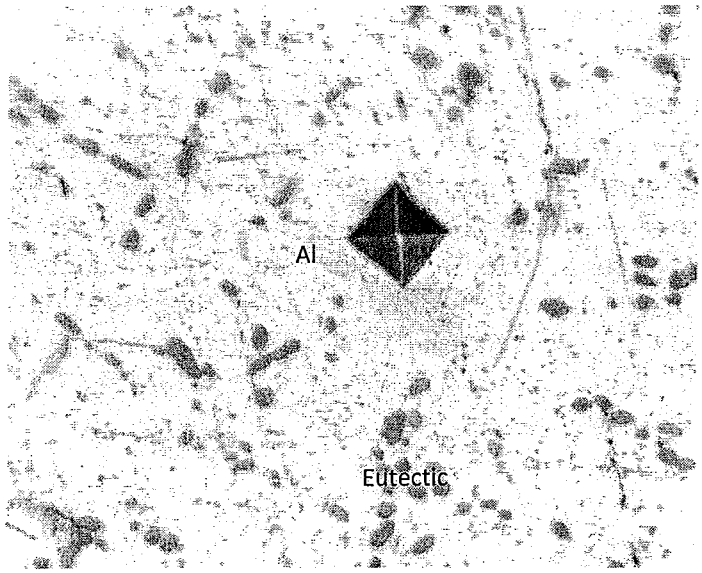

Figure 3-4. Typical indentation in the primary Al phase during the micro hardness measurement process.

3.4. MACRO-HARDNESS

The Rockwell hardness measurements in F scale using a (1/16) inch steel ball indenter and a 60 kgf load was carried out on samples at various intervals of the natural ageing time between 0 and 15 hours. It was an attempt to satisfy an academic curiosity about whether the macro-hardness or bulk hardness data would effectively reflect changes in the precipitation sequence inside the primary dendrite phase of the microstructure. Six indentations were carried out on one sample (12.70 mm diameter cylinders of 12 mm length) every hour on the hour starting from the as quenched state after solution heat treatment. All the samples were quenched in water at 80 °C after solution heat treatment.

3.5. HEAT TREATMENT

All the heat treatment process was carried out in an electric resistance furnace with a maximum temperature deviation of less than 1 °C. Figure 3-5 shows the schematic of a typical commercial T6 heat treatment cycle carried out for cast components made from A356.2 Al alloy. The samples are initially heated in an electric resistance furnace to the isothermal holding temperature of 540 °C. The samples are held at 540 °C for about 12 h and subsequently quenched in water maintained at 80 °C. The samples are then subjected to a natural ageing process in room temperature for anywhere between 6 to 12 h. The artificial ageing is carried out at an isothermal holding time of about 155 °C for 6 to 10 h and subsequently the samples are left to cool down to room temperature in atmospheric conditions. Figure 3-5. Schematic of typical T6 heat treatment cycle for A356.2 Al alloy cast component.

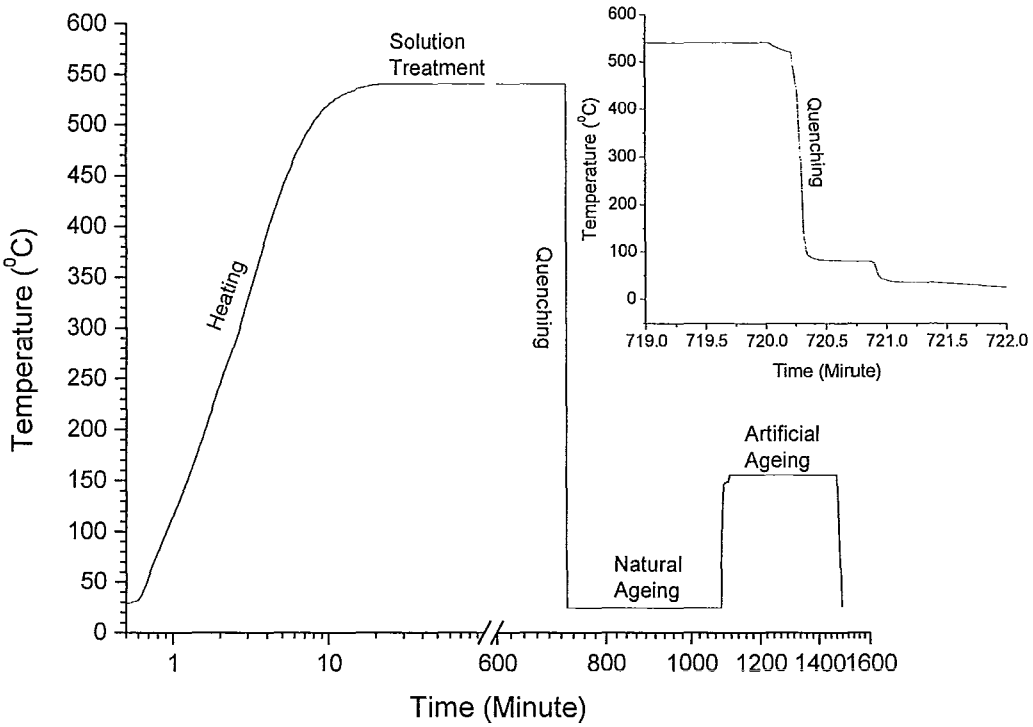

Figure 3-5. Typical T6 heat treatment cycle for A356.2 Al alloy cast component. The inset figure shows the expanded section of the cycle during the quenching after solution treatment.

In Figure 3-5, the quenching process from the solutionizing heat treatment is most critical in determining the kinetics of the precipitation reaction process during the ageing (natural and artificial) processes. In this project, there were three distinctly different quenching rates used as independent variables. Figure 3-6 shows the typical thermal data obtained during the quenching of the component in three different quench mediums after the respective solution heat treatment processes. The three quench mediums were a mixture of anti-freeze and dry ice maintained at -40 °C (Figure 3-6(a)), water at room temperature (~23 °C) (Figure 3-6(b)), and water at 80 °C (Figure 3-6(c)), respectively.

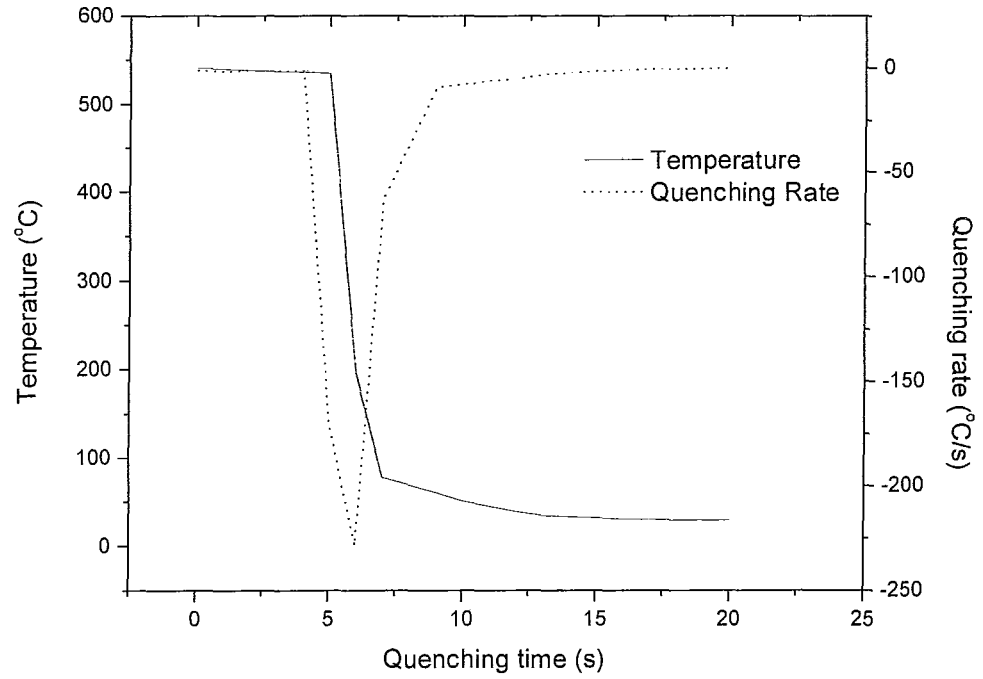
Temperature (°C)
Quenching rate (°C/s)
Quenching time (s)
Temperature
Quenching Rate
600
500
400
300
200
100
0
0
-50
-100
-150
-200
-250
0
5
10
15
20
25

(a)

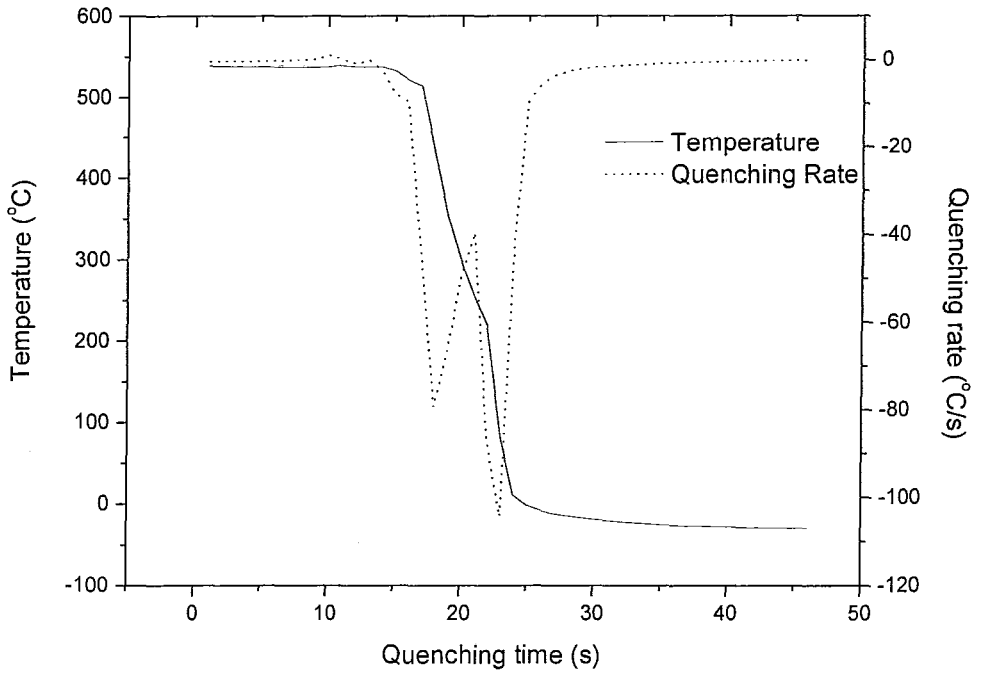
Temperature (°C)
Quenching rate (°C/s)
Quenching time (s)
Temperature
Quenching Rate
600
500
400
300
200
100
0
-100
0
-20
-40
-60
-80
-100
-120
0
10
20
30
40
50

(b)

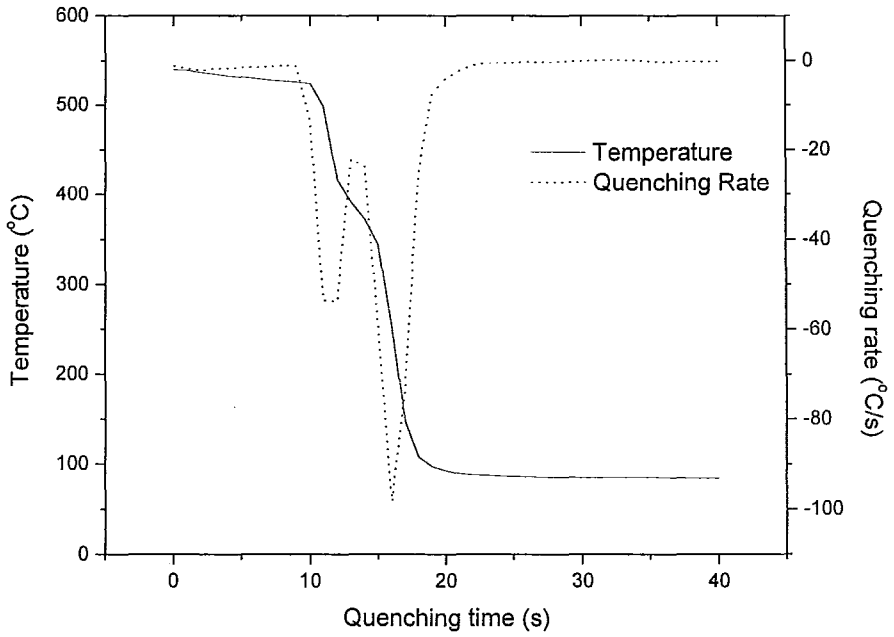

(c)

Figure 3-6. Typical thermal data obtained during the T6 heat treatment of A356.2 alloy samples. (a), (b) and (c) are for a mixture of anti-freeze and dry ice maintained at -40°C, water at room temperature (~23°C), and water at 80°C, respectively.

Figure 3-7 shows typical microstructure of A356.2 cast component after solution heat treatment and quenching in a mixture of anti-freeze and dry ice maintained at -40 °C (Figure 3-7 (a)), water at room temperature (~23 °C) (Figure 3-7(b)), and water at 80 °C (Figure 3-7 (c)), respectively. Figure 3-7(a), (b) and (c) show that the morphology of the dark eutectic Si phase is globular at all the three quenching rates.

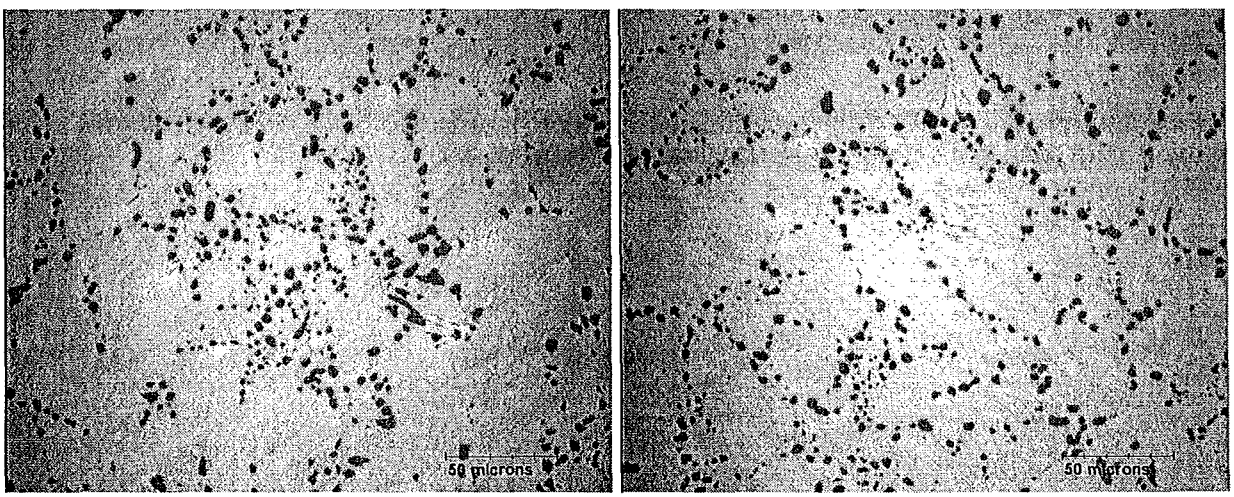

(a) (b)

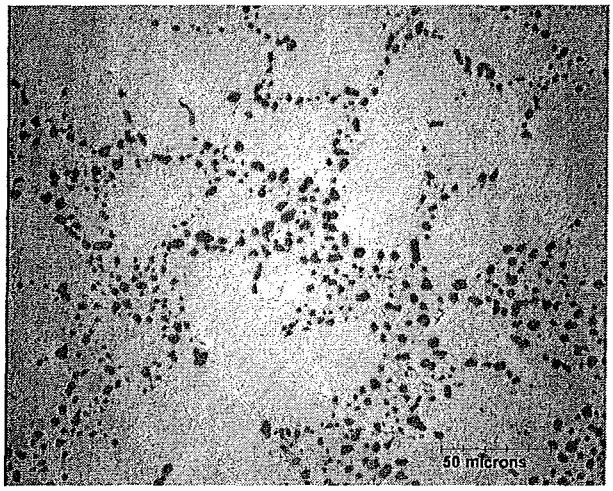

(c)

Figure 3-7. Typical microstructure obtained from optical microscope of A356.2 cast alloy after solution heat treatment at 540 °C for 12 h and (a) quenched in a mixture of anti-freeze and dry ice maintained at -40 °C, (b) water at room temperature (~23 °C), and (c) water at 80 °C. The dark nearly globular phase is the eutectic Si and the light region is the primary Al phase matrix.

Figure 3-8 show typical microstructures of the A356.2 cast alloy samples solution heat treated at 540 °C for various times (2, 4, 6, 8,10 and 12 h) and quenched in water maintained at 80 °C. This figure shows that the Si phase is not fully globular at 2 h of solutionizing and by 6 h the morphology of the eutectic Si phase has attained the minimum aspect ratio (maximum sphericity) possible by the solution heat treatment. It has been proposed [22,49] that the maximum mechanical properties could be attained for this alloy at solution heat treatment times of between 2 and 6 h as well, however, the specifications and the industrial practice dictates a 12 h solution heat treatment at isothermal temperature. To enable minimum influence of solution heat treatment on the microstructure in this study, a 12 h period was chosen.

No discernable difference could be visible in the microstructure of an A356.2 cast sample between the conditions before and after the ageing process.

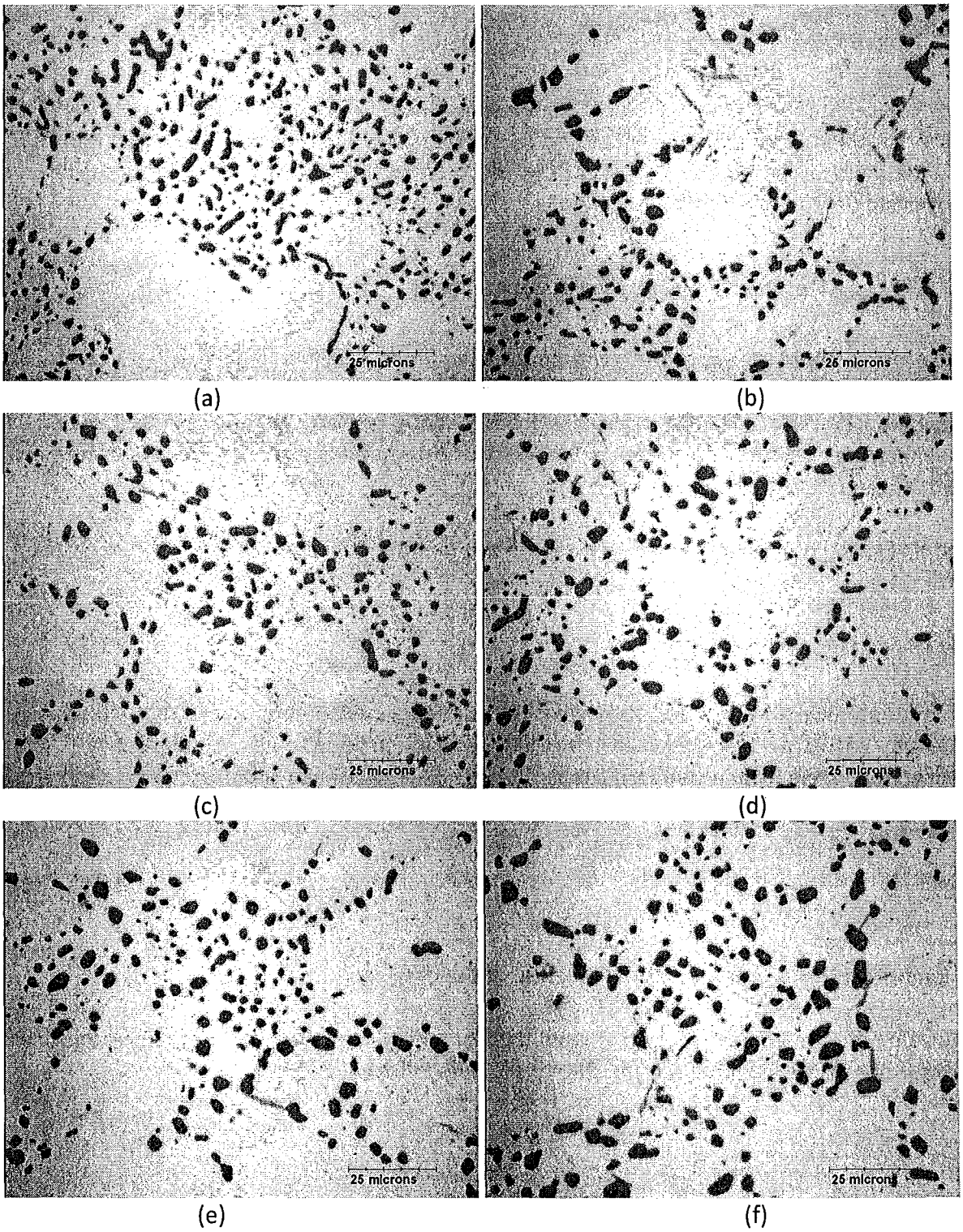

Figure 3-8. Typical microstructure of A356.2 cast alloy samples after solution heat treatment at 540 °C. (a) to (f) are for 2h, 4h, 6h, 8h, 10h and 12h of solutionizing at isothermal temperature, respectively. The dark phase is the eutectic Si, the light grey elongated phases are the Fe rich intermetallic phases (β-$Al_{14}Fe_3Si_3$ or π-$Al_8FeMg_3Si_6$) and the light region is the primary Al phase matrix.

3.6. TENSILE PROPERTY ANALYSIS

Mechanical properties were evaluated under uni-axial tensile loading condition. An INSTRON 8800® testing machine was used and the rate of elongation for each sample was 1 mm/min. No pre-load was applied to the samples at the beginning of the each test. Five samples were evaluated for each condition.

3.7. UNCERTAINTIES IN THE EXPERIMENTAL DATA

The uncertainty in the experiment measurements, micro-hardness, bulk hardness and tensile properties was determined by evaluating the 95% confidence interval. Since, the sample size was 8 and 5 for the hardness and tensile property data, respectively, the standard deviation of the mean was not assumed to be known but, was estimated and the t-value was evaluated from a standard t-table.

Equation (3-2) presents the expression for the 95% confidence interval about the mean of a data set, μ.

$$\left(M - t \cdot s_M\right) \leq \mu \leq \left(M + t \cdot s_M\right) \tag{3-2}$$

In Equation (3-2), M is the mean value of the data set, s_M is an estimate of the standard deviation of the mean and evaluated by the expression in Equation (3-3), and t is the appropriate value from a standard t-table for the 95% confidence and degree of freedom of (n-1), where n is the number of sample in the data set.

$$s_M = \frac{s}{\sqrt{n}} \tag{3-3}$$

In Equation (3-3), s is the standard deviation of the data set.

The value of t for a 5 data set is 2.776 and that for an 8 data set is 2.365. The micro-hardness measurements were 8 data set and the tensile data were a 5 data set.

CHAPTER 4 SEQUENCE OF PRECIPITATION REACTION DURING AGEING OF A356.2 AL ALLOY

One of the contributions of this study is the proposal of a hypothesis to elucidate the sequence of precipitation reaction during the natural ageing and artificial ageing treatments of A356.2 casting alloy, respectively.

In this chapter, the sequence of the precipitation reaction of Mg and Si elements in the Al matrix would be presented. The hypothesis for the sequence of the precipitation reaction during the ageing process was formulated from the analysis of the results in this project as presented in this chapter coupled with the information obtained from the literature as presented in sections 1.3.2. to 1.4.3.

4.1. Precipitation Reactions During Natural Ageing At Room Temperature

In this section a hypothesis for the sequence of precipitation reaction in the primary Al matrix during the natural ageing process at room temperature is presented with results from experiments to support the hypothesis.

4.1.1. Hypothesis for the precipitation reaction during natural ageing

Figure 4-1 shows the schematic of a typical micro-hardness data as a function of natural ageing time at room temperature obtained from the matrix of the primary Al phase in the A356.2 cast cylindrical alloy samples showing the various critical stages of the precipitation reaction during natural ageing.

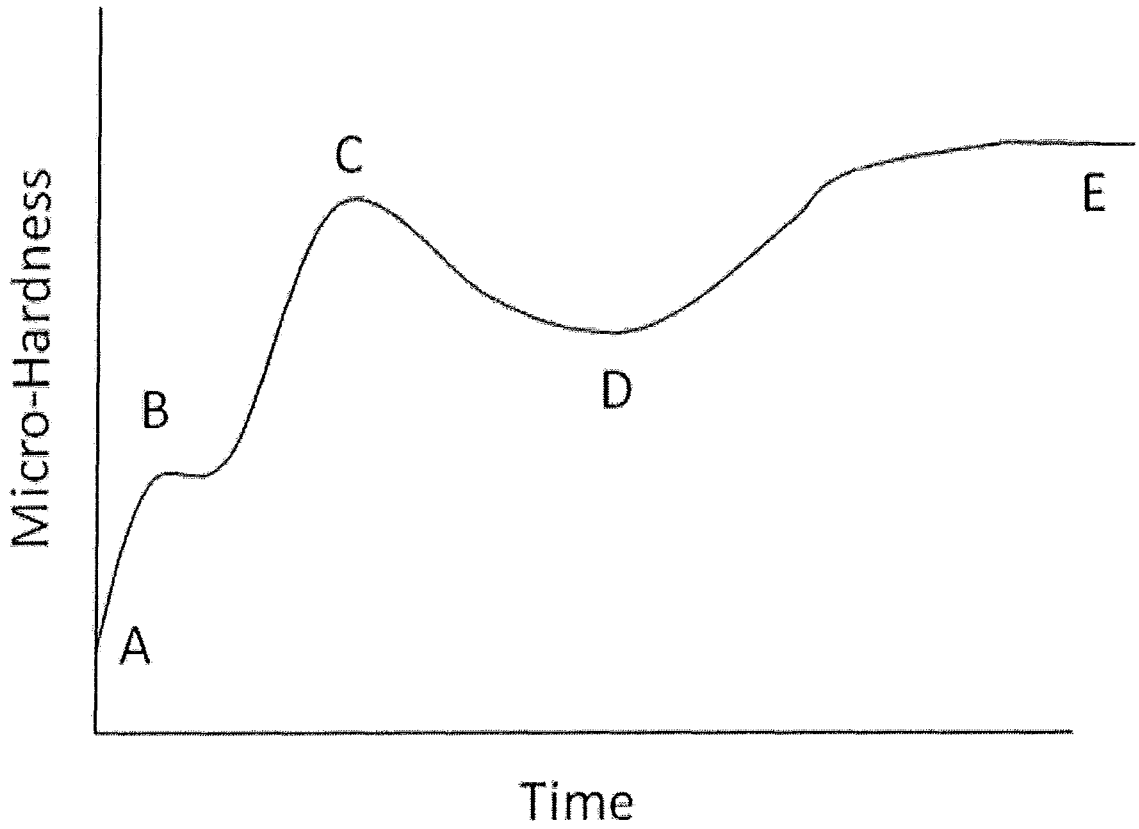

Figure 4-1. Schematic of a typical variation of the micro-hardness data with time during the natural ageing of A356.2 alloy sample at room temperature showing the various critical stages in the precipitation reaction process.

The five stages of the precipitation reaction as shown in Figure 4-1 are elaborated below:

Segment AB

Formation of self-clusters of Si atoms. The rate of formation of these clusters depends on the concentration of vacancies (voids) in the primary Al matrix immediately after the solution heat treatment. Faster quenching rates after solution heat treatment would yield higher concentration of vacancies in the matrix resulting in greater atomic mobility. *GP-I zones*

Segment BC

Formation of self-clusters of Mg atoms. The rate of formation of these clusters depends on the vacancy concentration in the Al matrix and directly proportional to the rate of quenching immediately after the solution heat treatment. *GP-I zones*

Segment CD

Break down and dissolution of the self-clusters of Mg.

Segment DE

Diffusion of Mg atoms to the self-clusters of Si atoms and formation of co-clusters of Mg and Si atoms at nearly equal atomic ratio of both atom types. $\beta'' \rightarrow Mg_5Si_6$ [38].

4.1.2. Experiment Results for Microhardness During Natural Ageing

Figure 4-2 (a), (b) and (c) show the typical micro-hardness measurement data during the natural ageing of the samples quenched in water at 80 °C, water at room temperature (23 °C) and mixture of anti-free with dry ice at -40°C, respectively. The similarities between the micro-hardness data obtained from the primary Al phase matrix for the three quenching rates shown in Figure 4-2 (a), (b) and (c), and the schematic for the proposed mechanism in Figure 4-1 are quite evident suggesting that the proposed mechanism is plausible. Further, Table 4-2 presents the significant observations from the results shown in Figure 4-2 (a), (b) and (c). The uncertainty in the data shown in Figure 4-2 is presented in Section 4.3. of this dissertation.

Figure 4-2 and Table 4-2, coupled with the background information on the phase identities presented in sections 1.3.3. suggest that the proposed sequence of the precipitation reaction during the natural ageing at room temperature of A356.2 alloy cast component may present the salient reaction stages.

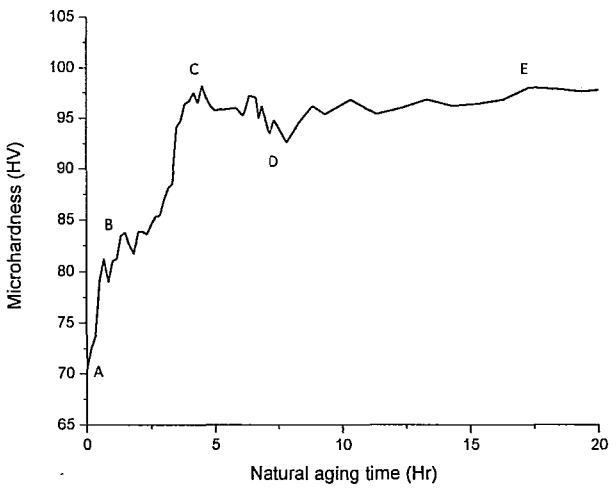

(a)

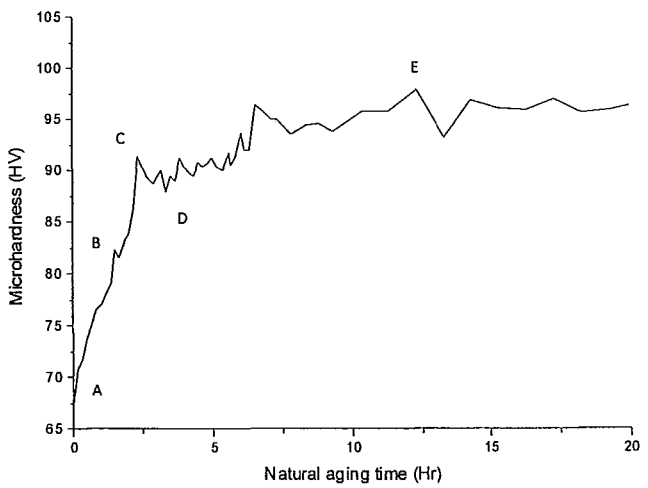

(b)

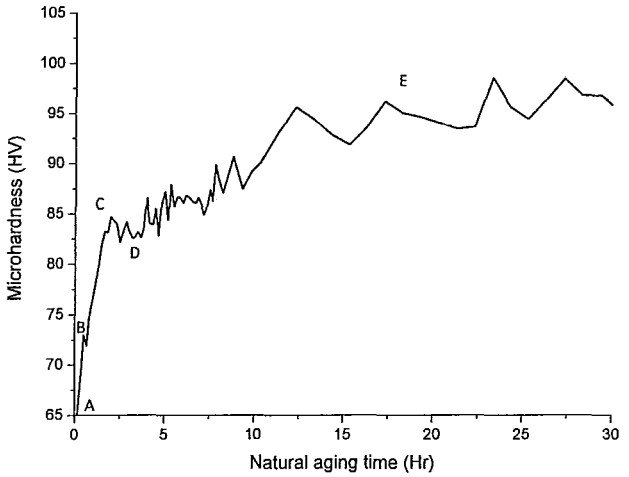

(c)

Figure 4-2. Typical micro-hardness data during natural ageing at room temperature in samples quenched in (a) water at 80 °C, (b) water at room temperature (23 °C), (c) anti-freeze and dry ice at -40 °C, respectively,. immediately after solution heat treatment.

Table 4-1 presents the quantified data for the hardness and time for the significant points A, B, C, D and E shown in Figure 4-2.

Table 4-1. Quantified data for hardness and time of points A, B, C and D of Figure 4-2 shown in Figure 4-2.

Quench Medium	Quench Rate	Feature	Hardness (HV)	Time (h)
Water at 80 °C	Low	Point A	70	0
		Point B	84	2
		Point C	98	5
		Point D	93	8
		Point E	96	12
Water at 23 °C	Medium	Point A	67	0
		Point B	82	2
		Point C	92	2
		Point D	88	3
		Point E	96	12
Mixture of anti-freeze coolant and dry ice at -40 °C	High	Point A	62	0
		Point B	73	1
		Point C	85	2
		Point D	82	3
		Point E	95	12

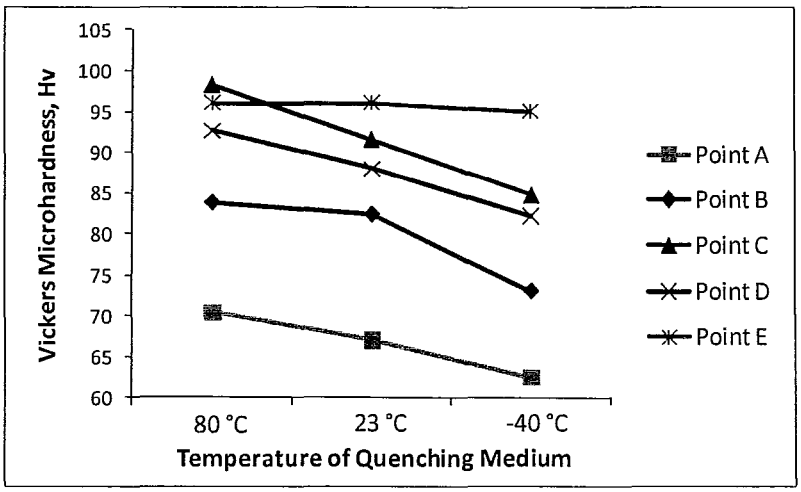

(a)

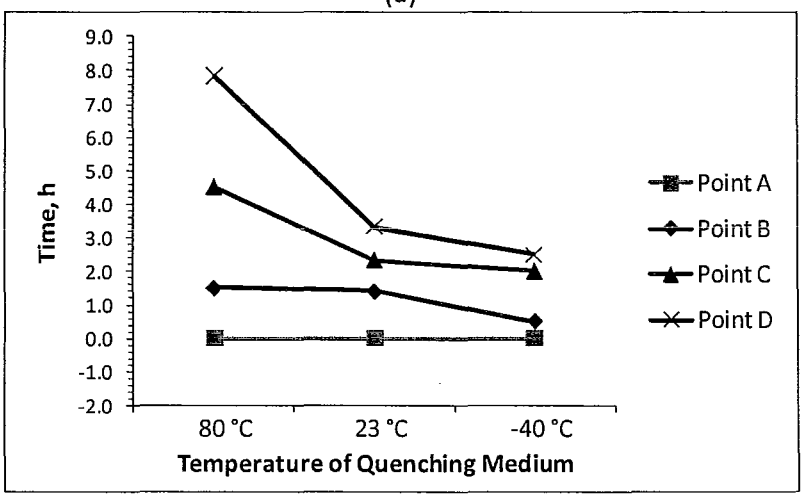

(b)

Figure 4-3. Graphical representation of the hardness and time values at which the points A, B, C, D and E occur in Figure 4-2. (a) Microhardness data, and (b) Time data. The Point E was considered at a constant time of 12 h for all the three rates of quenching.

Table 4-2 presents the salient observations and discussions from the results shown in Figure 4-2, Table 4-1 and Figure 4-3.

Table 4-2. Significant observations in the results of micro-hardness evaluation on the primary phase matrix for the three quenching rates presented in Figure 4-2 (a), (b) and (c).

Observation	Discussion
Location of Point A is at lower hardness data for higher cooling rates during quenching	The concentration of vacancies (voids) in the primary Al phase matrix increase as the rate of quenching increases resulting in lower hardness values.
Location of Point B is at lower time and lower hardness values for higher cooling rates during	Since the vacancy concentration in primary Al matrix increases with increasing quench rates, the mobility of the Si is higher as well resulting in a shorter duration to form

quenching	self-clusters, moreover, the higher vacancy concentration at higher quench rates results in lower hardness values of the primary Al matrix at this point.
Location of Point C is at lower time and lower hardness values for higher cooling rates during quenching	Since the vacancy concentration in primary Al matrix increases with increasing quench rates, the mobility of the Mg is higher as well resulting in a shorter duration to form self-clusters, moreover, the higher vacancy concentration at higher quench rates results in lower hardness values of the primary Al matrix at this point.
Location of Point D is at lower time and lower hardness values for higher cooling rates during quenching	Higher vacancy concentrations at higher quench rates would result in a lower hardness value and higher mobility of Mg atoms in the primary Al phase matrix causing the observed trend in the location of Point D.
Final hardness value at Point E is the same for all quenching rates. However, the change of slope from Point D to E is slower for higher quenching rates.	The final concentration of the β'' (Mg_5Si_6) precipitates and vacancies would be the same for all quenching rates after a long time such as greater than 20 h. However, since the vacancy concentration is higher at Point D for higher quenching rates, the rate of disappearance of vacancies would be slower for higher quenching rates causing a slower increase in slope of the hardness curves for higher quenching rates. The higher vacancy concentration in the primary Al phase matrix would reflect as lower values of micro-hardness.

Figure 4-4 presents the bulk hardness data, Rockwell F Scale (HRF) as a function of natural ageing time between 0 and 15 hours along with the 95% confidence interval. Figure 4-4 shows that the points A, B, C and D shown in Figure 4-2 are not clearly discernable in the bulk hardness data. As expected, bulk hardness would not be a valid measurement tool to study the changes in the precipitation reactions taking place inside the primary phase of the microstructure.

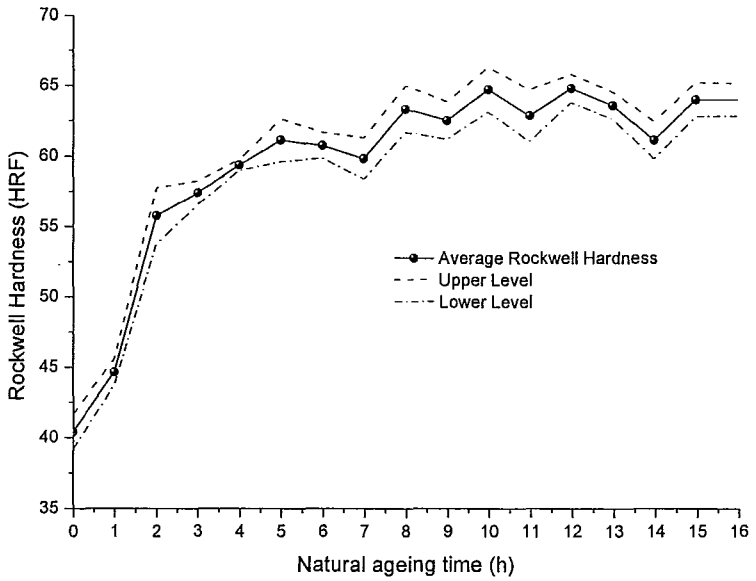

Figure 4-4. Typical macro or bulk hardness data obtained from a Rockwell hardness testing using a (1/16)" steel ball indenter and a 60 kgf force. The data was obtained for various natural ageing times.

The hypothesis presented in section 4.1.1. coupled with the experiment results and discussion from microhardness measurements presented in section 4.1.2. amply demonstrate that the proposed sequence of precipitation reaction during natural ageing of A356.2 alloy is feasible and highlight the salient reaction stages. The proposal is only a hypothesis and would have to be further examined for validity and changed accordingly.

The following is the summary of the proposed hypothesis for the sequence of precipitation reaction during the natural ageing process at room temperature for A356.2 casting alloy

SSSS → Self Clusters of Si atoms and Mg atoms → Dissolution of Mg clusters → β" (GP-II)

4.2. Precipitation Reactions During Artificial Ageing

The transformations in the precipitation reaction during the artificial ageing at high temperature depend on the extent of natural ageing at room temperature carried out prior to increasing the ageing temperature. The artificial ageing process could be initiated at any time during the natural ageing process at room temperature between points A to E in Figure 4-1. In addition to the reactions proposed during the natural ageing process in 4.1. , there are two additional stages of reaction during the artificial ageing process as presented below:

- Dissociation of the co-clusters of Si and Mg atoms ($\beta'' \rightarrow Mg_5Si_6$).

- Formation of $\beta' \rightarrow Mg_{1.8}Si$ precipitates followed by the transformation to $\beta \rightarrow Mg_2Si$ stable precipitates.

In cases, where the artificial ageing is initiated soon after the point D in Figure 4-1, some Mg atoms would be in solid solution and not in the co-clusters and these may diffuse and join exiting co-clusters to form the stable β' and β phases. Hence, dissociation of all co-clusters is not mandatory if Mg exists in solid solution of the primary Al phase matrix.

To provide better clarity, a hypothesis for the sequence of precipitation reaction during artificial ageing process after various durations of natural ageing at room temperature is presented in Table 4-3.

Table 4-3. Hypothesis of Precipitation reactions during artificial ageing for various durations of natural ageing at room temperature.

Duration of Natural Ageing prior to Artificial Ageing (Referenced by sections shown in Figure 4-1)	**Precipitation Reaction in Artificial Ageing**
No Natural Ageing Point A	SSSS → Self-clusters of Si atoms → β' + B' + U1 + U2 → β (Stable Mg_2Si phase)
Segment AB	β' + B' + U1 + U2 → β (Stable Mg_2Si phase)
Segment BC	Dissolution of Mg clusters → β' + B' + U1 + U2 → β (Stable Mg_2Si phase)
Segment CD	Dissolution of some Mg clusters → β' + B' + U1 + U2 → β (Stable Mg_2Si phase)
Segment DE	*Dissolution of β"(GP-II)* → β' + B' + U1 + U2 → β (Stable Mg_2Si phase)

The sequence of reaction in the artificial ageing treatment depends on the extent of natural ageing carried out which dictates the extent of precipitation reaction during natural ageing. The following sub-section presents a pictorial description with discussion for the precipitation sequence during natural ageing combined with artificial ageing, for various significant times intervals of the natural ageing process as show in Figure 4-1.

4.2.1. No Natural Ageing

Figure 4-5 shows the schematic of the precipitation reaction sequence when artificial ageing is carried out immediately after quenching the sample subsequent to solution heat treatment. No natural ageing would be carried out in this case. The precipitation sequence is shown below:

SSSS → Self-clusters of Si atoms → β' + B' + U1 + U2 → β (Stable Mg_2Si phase)

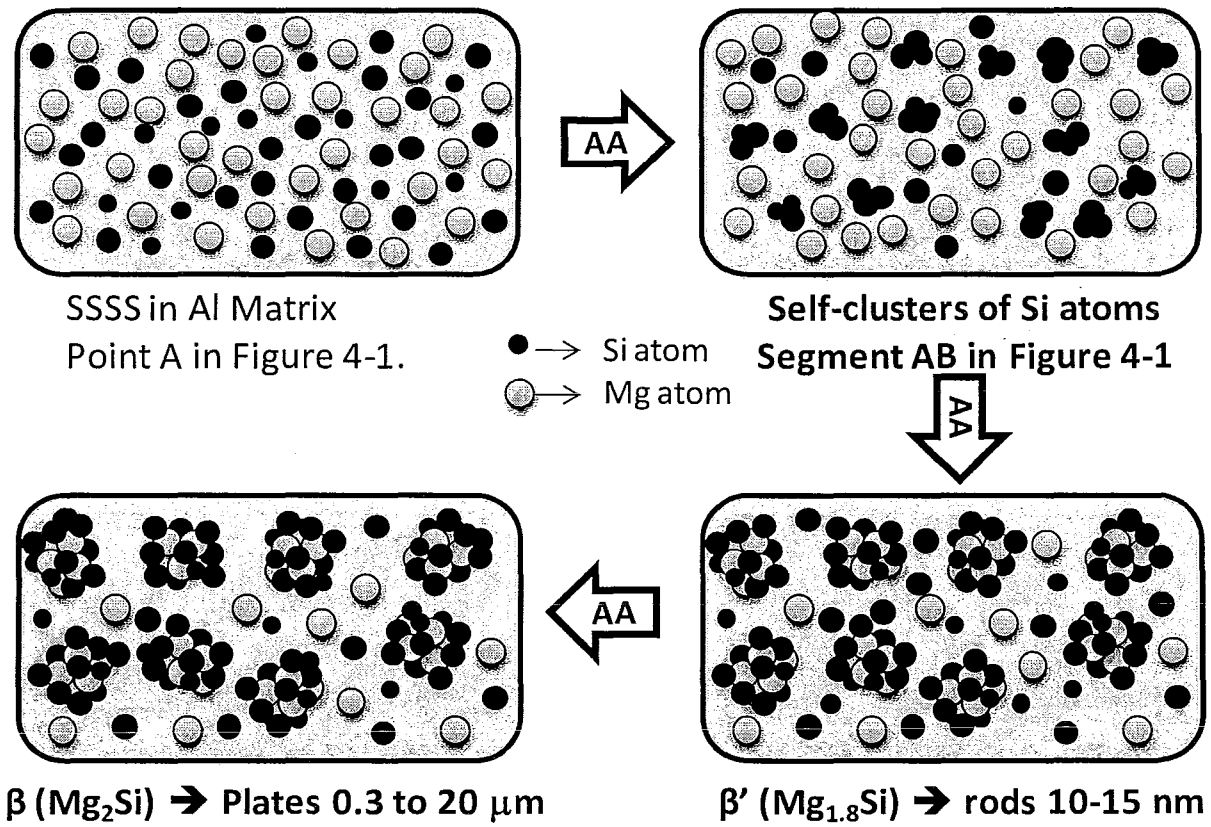

Figure 4-5. Schematic of a typical sequence for the precipitation reaction in the primary Al phase with no natural ageing (NA) and artificial ageing (AA) is carried out immediately after quenching the alloy subsequent to solution heat treatment.

When no natural ageing is carried out, the self clusters of Si atoms forms during the initial stages of artificial ageing and subsequently, the Mg atoms diffuse to these Si self-clusters and form the β'($Mg_{1.8}Si$) phase and subsequently the stable β(Mg_2Si) phase will form as the final stable phase.

4.2.2. Duration of Natural Ageing is in Segment AB

Figure 4-6 shows a schematic of a typical sequence of precipitation reaction when the duration of natural ageing is somewhere in the regions defined by segment AB in Figure 4-1; and subsequently, artificial ageing is carried out. The sequence of the precipitation reaction is given below:

SSSS → Self-clusters of Si atoms → β' + B' + U1 + U2 → β (Stable Mg_2Si phase)

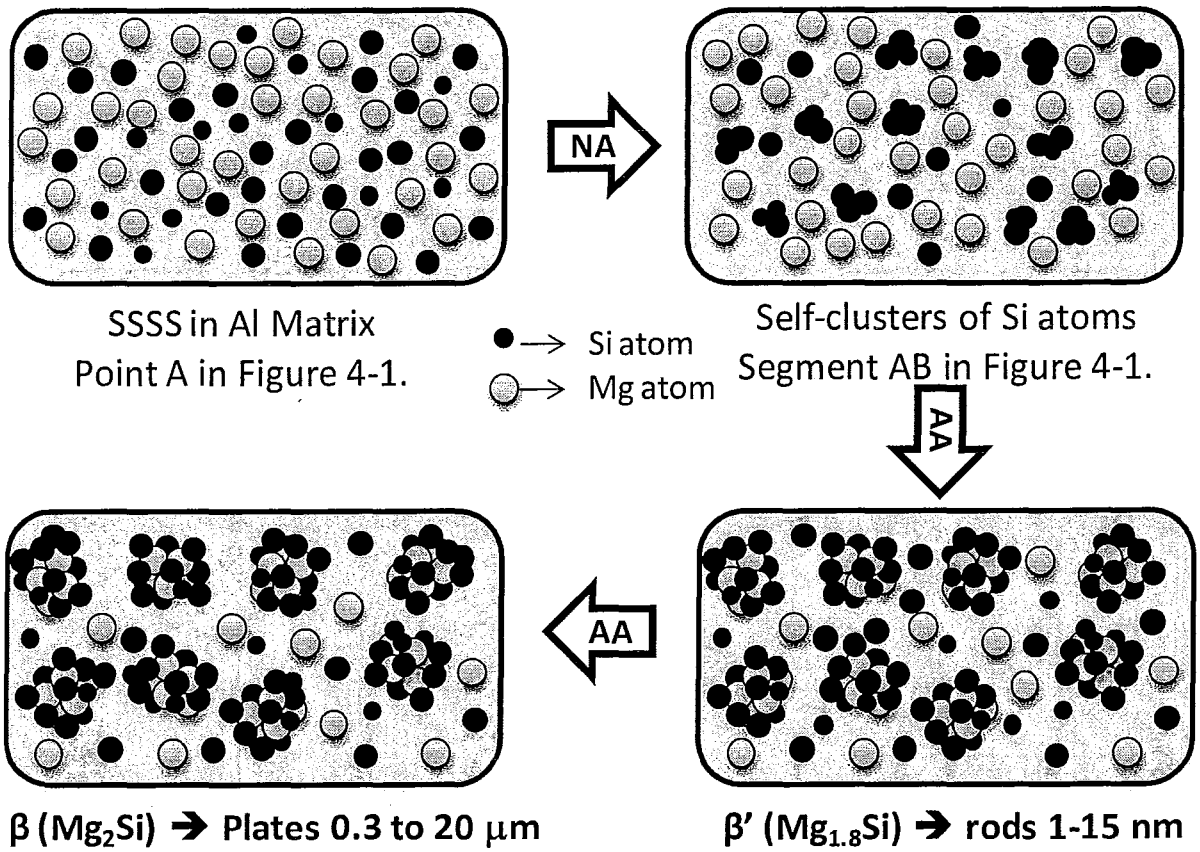

Figure 4-6. Schematic of a typical sequence for the precipitation reaction in the primary Al phase when the natural ageing (NA) is stopped during the reaction in Segment AB of Figure 4-1, and subsequently, artificial ageing (AA) is carried out.

When natural ageing is terminated in a short time interval such that only Si self-clusters and a few Mg self-clusters form during this process, then the Mg atoms will diffuse in the matrix during the initial stages of the artificial ageing to these Si self-clusters and form the β'($Mg_{1.8}Si$) phase and subsequently the stable β(Mg_2Si) phase will form as the final stable phase.

4.2.3. Duration of Natural Ageing is in Segment ABC

Figure 4-7 shows a schematic of a typical sequence of precipitation reaction when the duration of natural ageing is somewhere in the regions defined by segment BC in Figure 4-1; and subsequently, artificial ageing is carried out. The sequence of the precipitation reaction is given below:

SSSS → Self-clusters of Si atoms and a few self-clusters of Mg atoms → Dissolution of Mg clusters → β' + B' + U1 + U2 → β (Stable Mg_2Si phase)

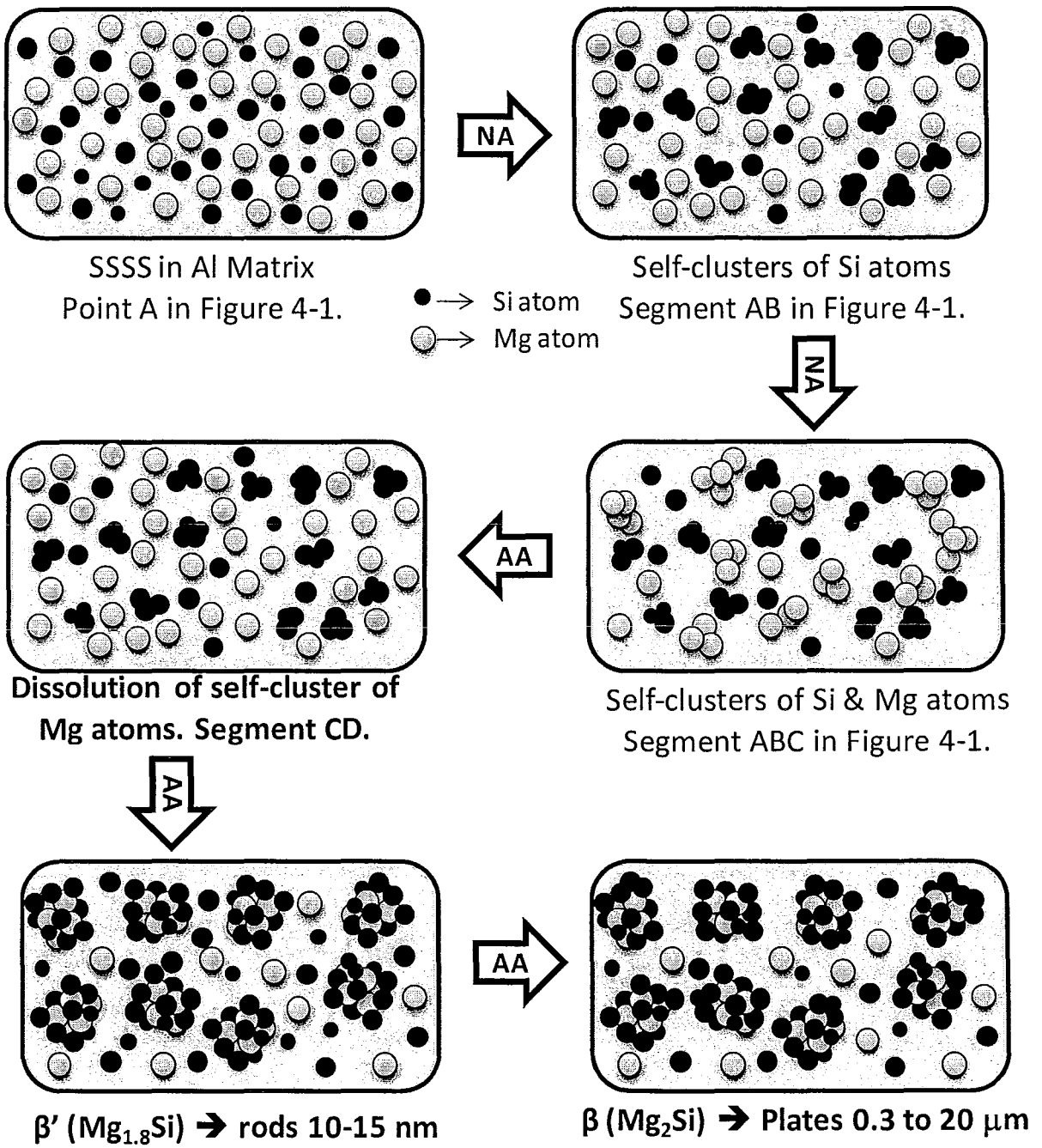

Figure 4-7. Schematic of a typical sequence for the precipitation reaction in the primary Al phase when the natural ageing (NA) is stopped during the reaction in Segment ABC of Figure 4-1, and subsequently, artificial ageing (AA) is carried out.

If the natural ageing process at room temperature is stopped somewhere in the segment BC shown in Figure 4-1, the primary Al matrix would have self-clusters of Si and a few self-clusters of Mg. During artificial ageing process, some dissolution of the Mg self-clusters would take place with simultaneous diffusion of Mg in solid solution to the Si self-clusters to form the $\beta'(Mg_{1.8}Si)$ phase followed by the formation of the terminal stable phase, $\beta'(Mg_{1.8}Si)$. The dissolution of Mg self-clusters during artificial ageing would result in annihilation of certain

amount of vacancies in the Al matrix phase resulting in lower kinetics of the precipitation reaction during the artificial ageing process and a lower final hardness of the primary Al matrix.

4.2.4. Duration of Natural Ageing is in Segment ABCD

Figure 4-8 shows a schematic of a typical sequence of precipitation reaction when the duration of natural ageing is somewhere in the regions defined by segment CD in Figure 4-1; and subsequently, artificial ageing is carried out. The sequence of the precipitation reaction is given below:

SSSS → Self-clusters of Si and Mg atoms → Dissolution of Mg clusters → β' + B' + U1 + U2 → β (Stable Mg_2Si phase)

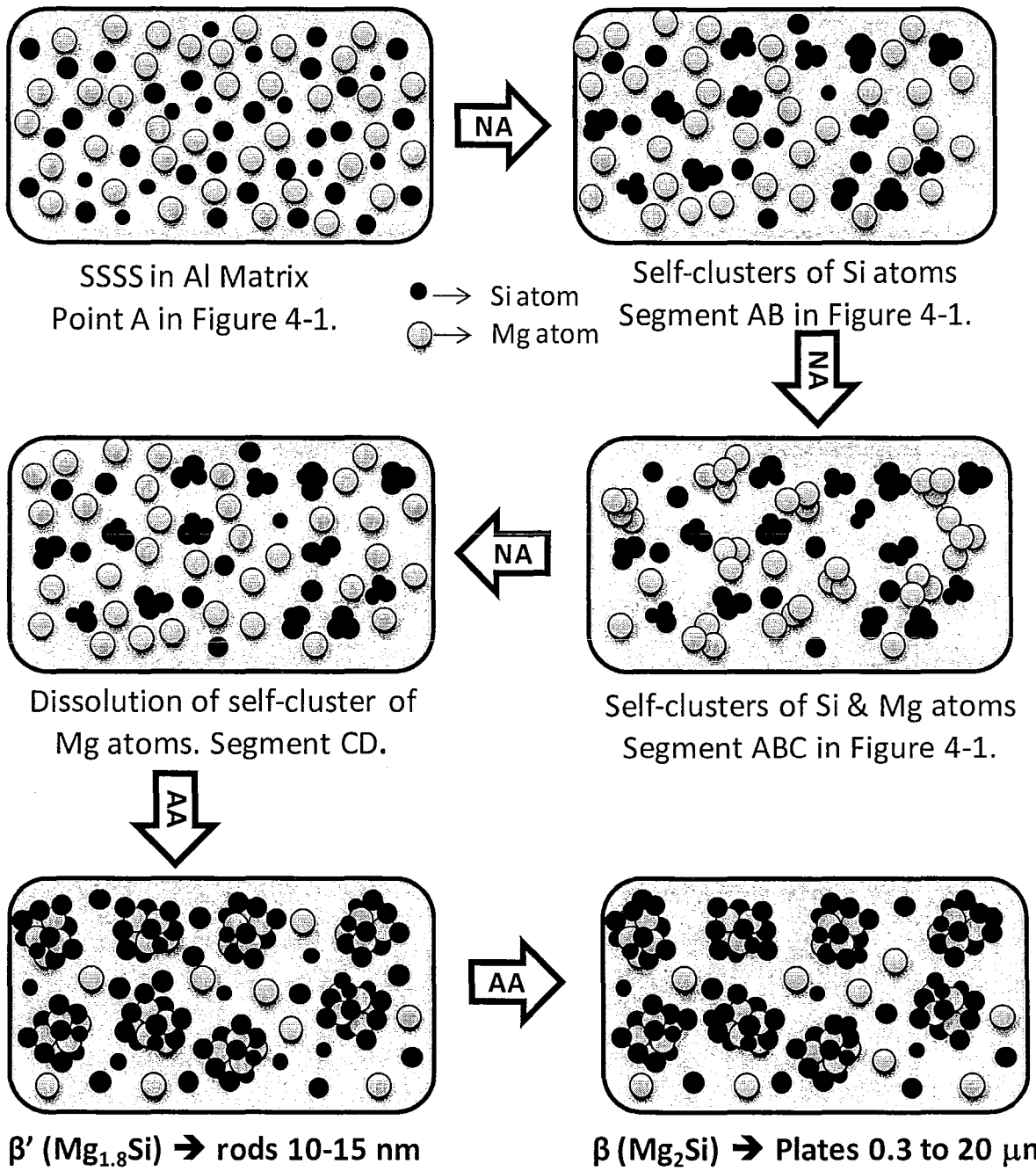

Figure 4-8. Schematic of a typical sequence for the precipitation reaction in the primary Al phase when the natural ageing (NA) is stopped during the reaction in Segment ABCD of Figure 4-1, and subsequently, artificial ageing (AA) is carried out.

When the natural ageing process is terminated after the formation of self-clusters of Mg atoms, the first stages of artificial ageing would be the dissolution of these Mg self-clusters to render the Mg atoms back into the solid solution of the Al matrix phase followed by diffusion of the Mg atoms in solid solution to the self-clusters of Si atoms to form the $\beta'(Mg_{1.8}Si)$ phase which would subsequently form the stable and terminal $\beta(Mg_2Si)$ phase. The dissolution of all the Mg self-clusters would result in the annihilation of vacancies in the primary Al matrix and the

resultant diffusion of the Mg atoms to join the Si self-clusters would be sluggish, resulting in a lesser volume fraction of the strengthening phases of β' and β during artificial ageing. This would be reflected by lower microhardness values for these alloys.

4.2.5. Duration of Natural Ageing is in Segment ABCDE

Figure 4-9 shows a schematic of a typical sequence of precipitation reaction when the duration of natural ageing is somewhere in the regions defined by segment DE in Figure 4-1; and subsequently, artificial ageing is carried out. The sequence of the precipitation reaction is given below:

SSSS → Self-clusters of Si and Mg atoms → Dissolution of Mg clusters → Formation of β'' (Mg_5Si_6) → *(Dissolution of β'')* → β' + B' + U1 + U2 → β (Stable Mg_2Si phase)

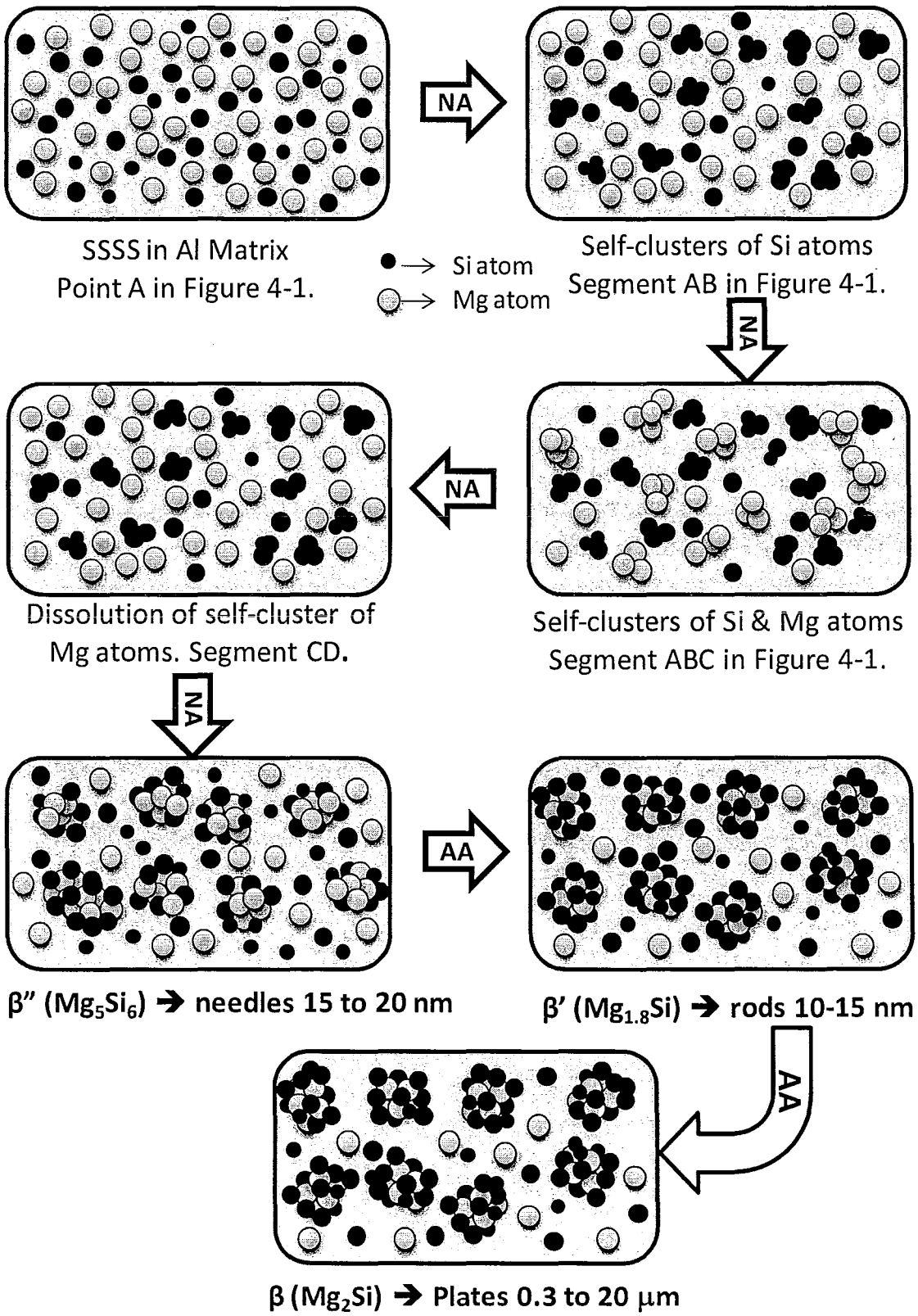

Figure 4-9. Schematic of a typical sequence for the precipitation reaction in the primary Al phase when the natural ageing (NA) is stopped during the reaction in Segment ABCDE of Figure 4-1, and subsequently, artificial ageing (AA) is carried out.

When the natural ageing is carried to beyond the formation of the β''(Mg_5Si_6) phase (co-cluster of Si and Mg atoms) which is the GP zone (GP-II), the first stages of the artificial ageing process would be the dissolution of some co-clusters of Si and Mg atoms and dissolution of the Mg self-clusters; thus, rendering the Mg and Si atoms back into the solid solution of the Al matrix phase. Subsequently, the solute atoms would diffuse and form the β'($Mg_{1.8}Si$) phase followed by the terminal and stable β(Mg_2Si) phase. The dissolution of the self-clusters of Mg and co-clusters and Mg and Si atoms would result in the annihilation of vacancies in the primary Al matrix and the resultant diffusion of the Mg atoms to join the Si self-clusters would be sluggish, resulting in a lesser volume fraction of the strengthening phases of β' and β during artificial ageing. This would be reflected by lower microhardness values for these alloys.

The significant contribution to the above-mentioned proposal in sections 4.1. and 4.2. for the sequence of precipitation reaction in the primary Al phase is in identifying the plausible reactions that take place during the natural ageing process at room temperature alone followed by the plausible reactions taking place in the artificial ageing process carried out after various levels of natural ageing at room temperature.

4.2.6. Experiment Results for Microhardness during Artificial Ageing

Figure 4-10 shows the typical micro-hardness data obtained from the primary Al phase matrix during artificial ageing following the natural ageing at room temperature for various durations. The data from the artificial ageing process is superimposed on the base curve marked "no AA" which represents the micro-hardness data for the natural ageing process and identical to the data in Figure 4-2 (a) for samples quenched in water at 80 °C. The uncertainties in the experiment data shown in Figure 4-10 is presented in Section 4.3. of this dissertation.

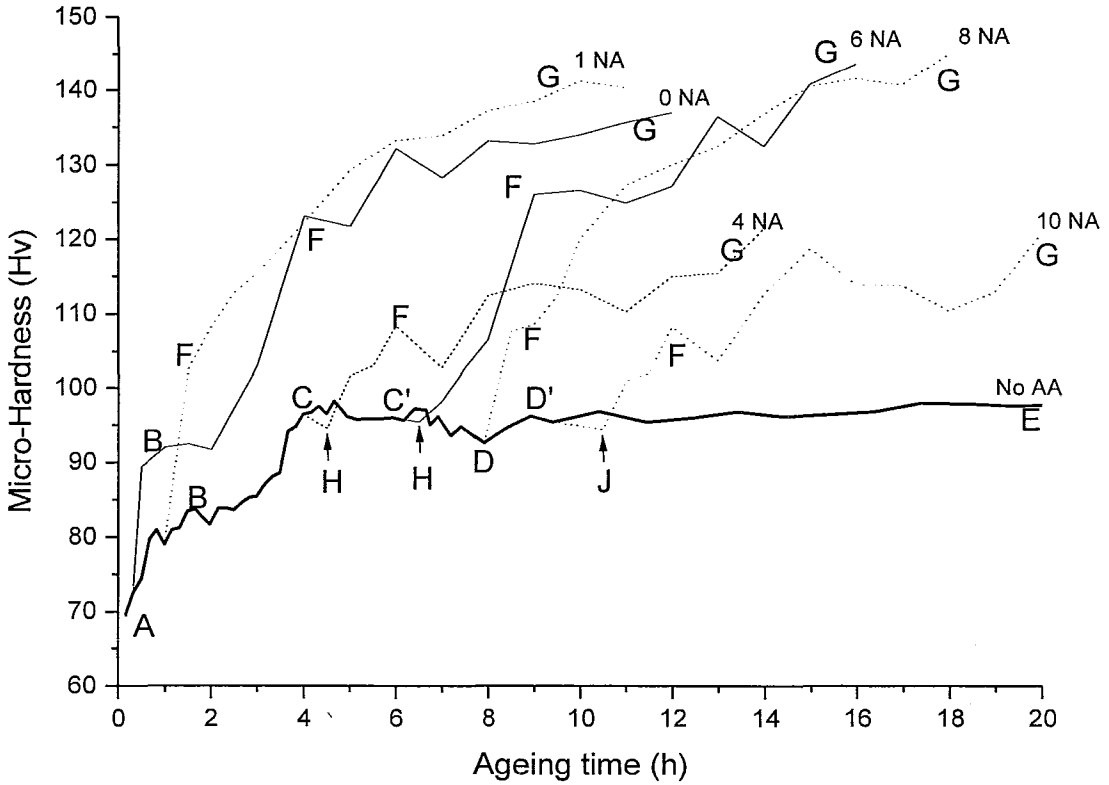

Figure 4-10. Typical micro-hardness data during artificial ageing at 155 °C following natural ageing at room temperature for various times for samples quenched in water at 80 °C after solution heat treatment. The notation "NA" and "AA" in the graph stand for "Natural Ageing" and "Artificial Ageing", respectively.

The uncertainty analysis for the experiment data presented in Figure 4-10 is carried out in the following sub-section 4.3.

4.2.7. Nomenclature in Figure 4-10

In Figure 4-10, the following are the nomenclature for the points shown at various stages of the reaction during the artificial ageing processes.

Point A	As quenched state after solution heat treatment wherein, the Si and Mg atoms are in the supersaturated solid solution of primary Al phase matrix.
Points B to E	As explained in section 4.1. .
Point C'	An intermediate point between Points C and D wherein a part of the Mg self-cluster would have disassociated and dissolved in the primary Al phase matrix.
Point D'	An intermediate point between Points D and E wherein a part of the β" (GP-II →

	Mg_5Si_6) GP-zones would have disassociated and dissolved in the primary Al phase matrix.
Point F	Time in artificial ageing when the formation of β' ($Mg_{1.8}Si$) is nearly complete.
Point G	Formation of β (Mg_2Si) is nearly complete and near completion of the artificial ageing process.
Point H	The dissociation of the Mg self-clusters is nearly complete during artificial ageing.
Point J	The dissociation of the β" (GP-II → Mg_5Si_6) co-clusters of Mg and Si is nearly complete during artificial ageing.

The critical observations in Figure 4-10 are presented below with relevant discussions.

4.2.8. Curve "No AA" in Figure 4-10

This is the reference base curve and the curve is the same as shown in Figure 4-2(a) for micro-hardness data obtained during natural ageing for samples quenched in water at 80 °C. The points A to E denoting the various stages of precipitation during natural ageing is shown in this curve and the reaction mechanism of these stages is presented in section 4.1. .

4.2.9. Curve "0NA" in Figure 4-10

Critical observations in this curve are the high rate of increase in the hardness value (Segment BFG) and a high peak harness value after completion at Point G. Further, there is a noticeable hump in the hardness curve as shown by Point B at around the 1 h time interval.

In this process, the Si and Mg atoms would both be in the super saturated solid solution and hence all the precipitation reactions would take place in the artificial ageing process at 155 °C. The initial hump at around 1 hour may be due to the self clustering of Si atoms (Segment AB) onto which the Mg atoms join to form the β' ($Mg_{1.8}Si$) (Segment BF) and subsequently the stable β (Mg_2Si) phase (Segment FG). The formation of the β" (GP-II → Mg_5Si_6) GP-zones may not occur in this process since the Mg atoms may not form co-clusters with Si but rather have the energetic to form the β' ($Mg_{1.8}Si$) directly. There is no evidence in the 0NA curve of Figure 4-10 to suggest any co-cluster formation and the rate of increase of hardness values coupled with the high peak hardness attained suggested against the formation of the co-clusters as well.

4.2.10. Curve "1NA" in Figure 4-10

Critical observations in this curve are the high rate of increase in hardness value (Segment BFG) and high peak hardness value after completion at Point G.

The Si self clusters would have formed in this sample during the natural ageing process (point A in Figure 4-2(a)) and most Mg atoms would be in solid solution and free to diffuse and join the

Si self clusters and form the β' ($Mg_{1.8}Si$) (Segment BF)shortly followed by the stable β (Mg_2Si) phase (Segment FG). Since, the vacancy concentration would be very high at the onset of artificial ageing and that most Mg atoms would be in solid solution, the kinetics of the reaction would be high and maximize the formation of the strengthening precipitates in a short duration as all displayed in the micro-hardness curve.

4.2.11. Curve "4NA" in Figure 4-10

The critical observations in this curve are the low rate of increase (Segment HFG) in hardness value and low peak hardness value after completion at Point G. Further, there is an initial decrease in hardness value as shown by segment CH in the curve.

Both the Si and Mg self-clusters would have formed during the natural ageing process as shown in Figure 4-2 (c). Hence, the first stages during artificial ageing would be the breakdown of the Mg clusters by the dissolution of Mg atoms in the primary Al phase matrix. This phenomenon leads to a decrease in the hardness value as shown by Segment CH in the "4NA" curve of Figure 4-10. Subsequently, the Mg atoms in the solid solution would diffuse and join the Si self-clusters to form β' ($Mg_{1.8}Si$) shortly followed by the stable β (Mg_2Si) phase. However, due to the extent of natural ageing and the use of vacancy concentration for the breakdown and dissolution of Mg atoms into solid solution, there is less vacancy concentration available for the formation of the β' ($Mg_{1.8}Si$) (Segment HF) and then the β (Mg_2Si) phase (Segment FG). This is shown by the low rate of increase in the Segment HFG and the low value of hardness at the completion (point G) of the ageing process.

4.2.12. Curve "6NA" in Figure 4-10

The critical observations of this curve are the high rate of increase (Segment HFG) in hardness and the high peak hardness value after completion at Point G. Further, there is a discernable decrease in hardness value at the onset of artificial ageing shown by Segment C'H in the curve.

At the onset of artificial ageing after 6 h of natural ageing, the primary Al phase matrix would have Si self-clusters and some Mg self-clusters with a part of the Mg atoms dissolved in the Al matrix. The stage of the precipitation reaction would be somewhere in the Segment CD of the natural ageing curve (0NA) and as explained in section 4.1. , hence, the starting point of the "6NA" curve is labeled C'. Subsequently, at the beginning of the artificial ageing process there would be a marginal decrease in the hardness value as shown by Segment C'D which signified the dissolution of the remaining Mg self-clusters into the Al matrix to form the solid solution. The Segment C'H in the "6NA" curve is shorter and has lesser gradient than the corresponding Segment CH in the "4NA" curve, because the amount of Mg dissolving in Al is lesser in "6NA" curve than the "4NA" curve. Further, there is a simultaneous diffusion and formation of β' ($Mg_{1.8}Si$) in the Segment C'H and continued in Segment HF as well, by the Mg atoms in solid solution of Al phase. Further, since, the vacancy concentration is still high in this artificial ageing process, there is enough energy and vacancies for the redistribution of the Si and Mg

atoms to fully form the β' ($Mg_{1.8}Si$) (Segment HF) shortly followed by the stable β (Mg_2Si) phase (Segment FG).

4.2.13. Curve "8NA" in Figure 4-10

The critical observations in this curve are the high rate of increase of hardness (Segment DFG) and the high peak hardness value at near completion shown by Point G.

At the onset of artificial ageing for this curve, nearly all Mg atoms would be dissolved into the solid solution of the primary Al phase matrix and at point D, the Mg atoms would begin to diffuse and join the Si self clusters to form the β' ($Mg_{1.8}Si$) (Segment DF) shortly followed by the stable β (Mg_2Si) phase (Segment FG). There would be enough vacancy concentration for the complete precipitation of the stable β (Mg_2Si) phase. However, the vacancy concentration during artificial ageing of "8NA" would be less than those in "0NA" and "1NA" curve processes.

4.2.14. Curve "10NA" in Figure 4-10

The critical observations of this curve are the low rate of increase (Segment JFG), the low peak hardness value attained at Point G and the decrease in the hardness in Segment D'J at the initial stages of artificial ageing process.

The primary Al phase matrix would contain some Si-self clusters, some Mg dissolved in the matrix and sufficient concentration of co-clusters of Mg and Si atoms as the β" (GP-II → Mg_5Si_6) GP-zones. At the beginning of the artificial ageing process shown by Segment D'J, the hardness decreases because the β" phase would breakdown and dissolve. The duration of Segment D'J is greater than the corresponding Segments CH and C'H in "4NA" and "6NA" curves because of the higher energies required and lower kinetics of the disassociation and dissolution of the β" GP zones into the Al matrix. Subsequently, the atoms redistribute and form β' ($Mg_{1.8}Si$) (Segment JF) followed by the stable β (Mg_2Si) phase (Segment FG). Since, the extent of natural ageing, initial dissolution and diffusion of the β" (GP-II → Mg_5Si_6) would have consumed sufficient vacancies, there would be a marked decrease in the vacancy concentration in the Al phase available for the precipitation of the β' ($Mg_{1.8}Si$) and β (Mg_2Si) phases. This is shown by the low rate of increase in the hardness (Segment JFG) and the low peak hardness value at Point G. The nature of the curve for "10NA" is similar in nature and hardness values to the curve for "4NA" and in both cases similar reaction mechanisms are taking place except that in "10NA" the initial dissolution is for β" GP-zones and in "4NA" it is the Mg self-clusters.

4.3. Uncertainty in Micro-Hardness Data

The mean of the data for the micro-hardness measurements during the natural ageing process is shown in Figure 4-11 (a) to (c) for samples quenched in water at 80 °C, water at room temperature (23 °C), and a mixture of anti-freeze and dry ice at -40 °C, respectively, immediately after solution heat treatment. It can be observed that the 95% confidence interval

for the mean values are quite small and follow the same trend as that of the mean. Figure 4-11 shows that the data for micro-hardness during the natural ageing process is quite reliable and the trend of the mean data could be used to confidently explain the mechanism of precipitation reaction in the primary Al phase during natural ageing. The mean data in Figure 4-11 is a reproduction of Figure 4-2. Figure 4-12 is a reproduction of the micro-hardness data obtained during the artificial ageing process for samples quenched in water at 80 °C along with the 95% confidence interval band on either side of the mean data curve. This figure also shows that the trend shown by the mean values is also repeated by the confidence interval band and that the data during artificial ageing process could also be confidently used to explain the mechanisms of precipitation reactions in the primary phase during this stage of heat treatment. The mean data in Figure 4-12 is a reproduction of that in Figure 4-10.

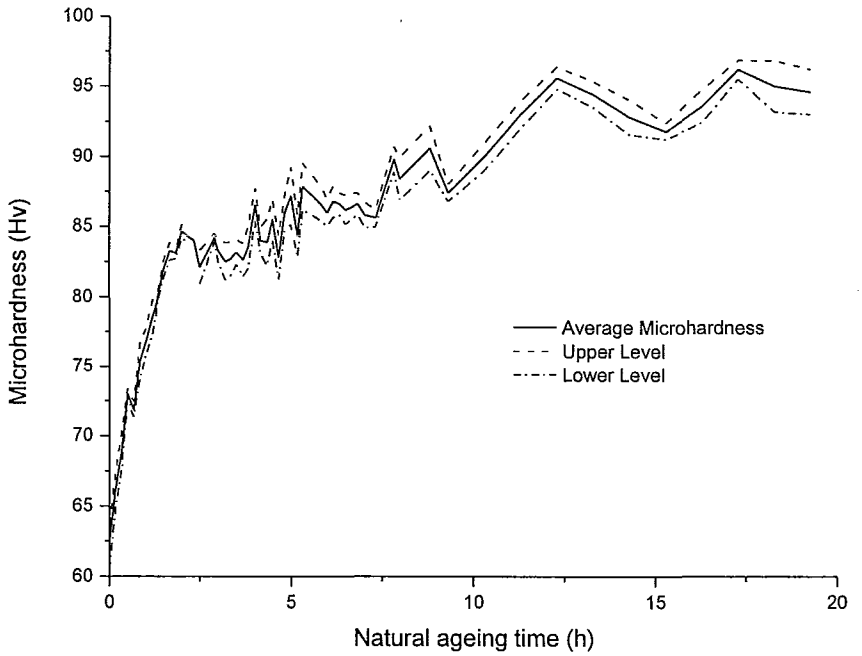

(a)

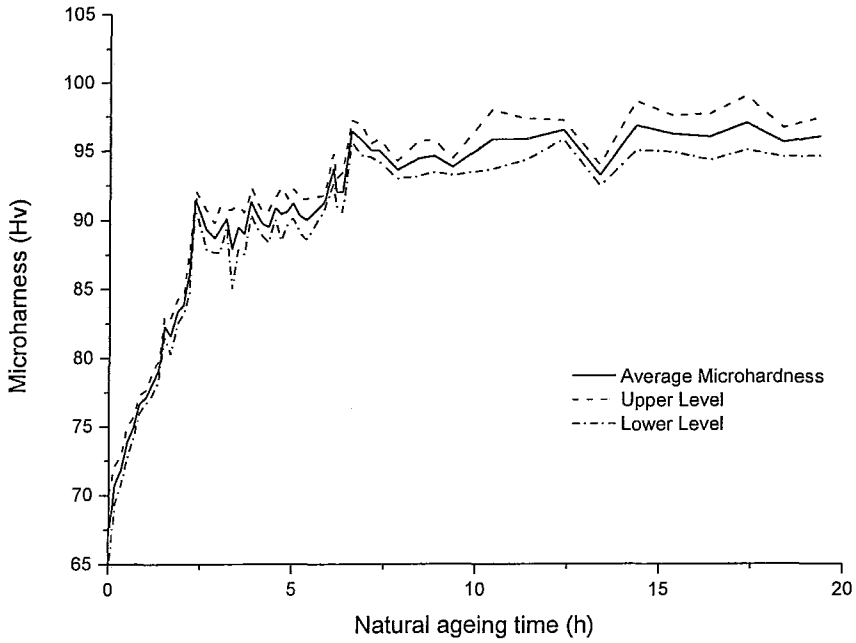

(b)

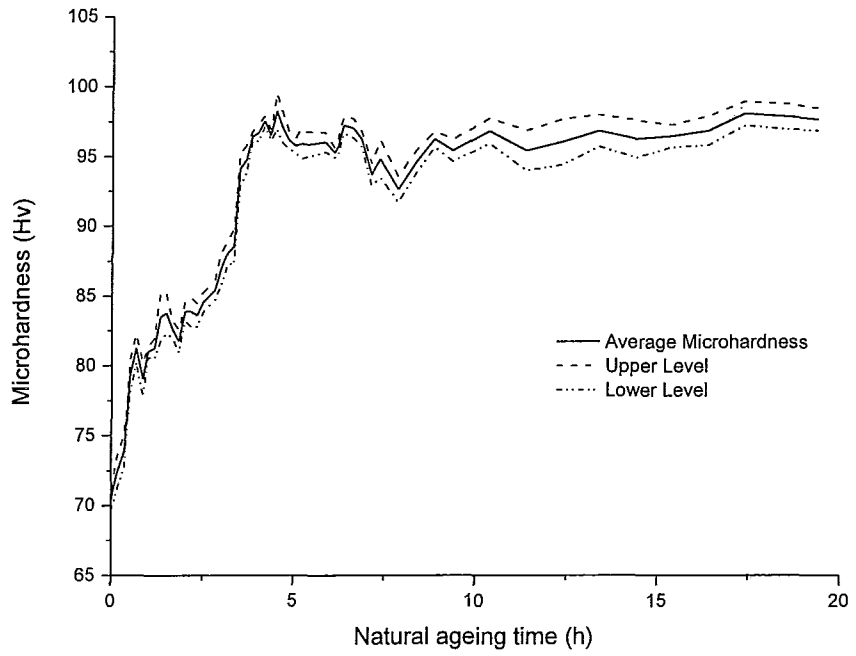

(c)

Figure 4-11. Micro-hardness data with 95% confidence interval during natural ageing at room temperature in samples quenched in (a) water at 80 °C, (b) water at room temperature (23 °C), (c) anti-freeze and dry ice at -40 °C, respectively, immediately after solution heat treatment.

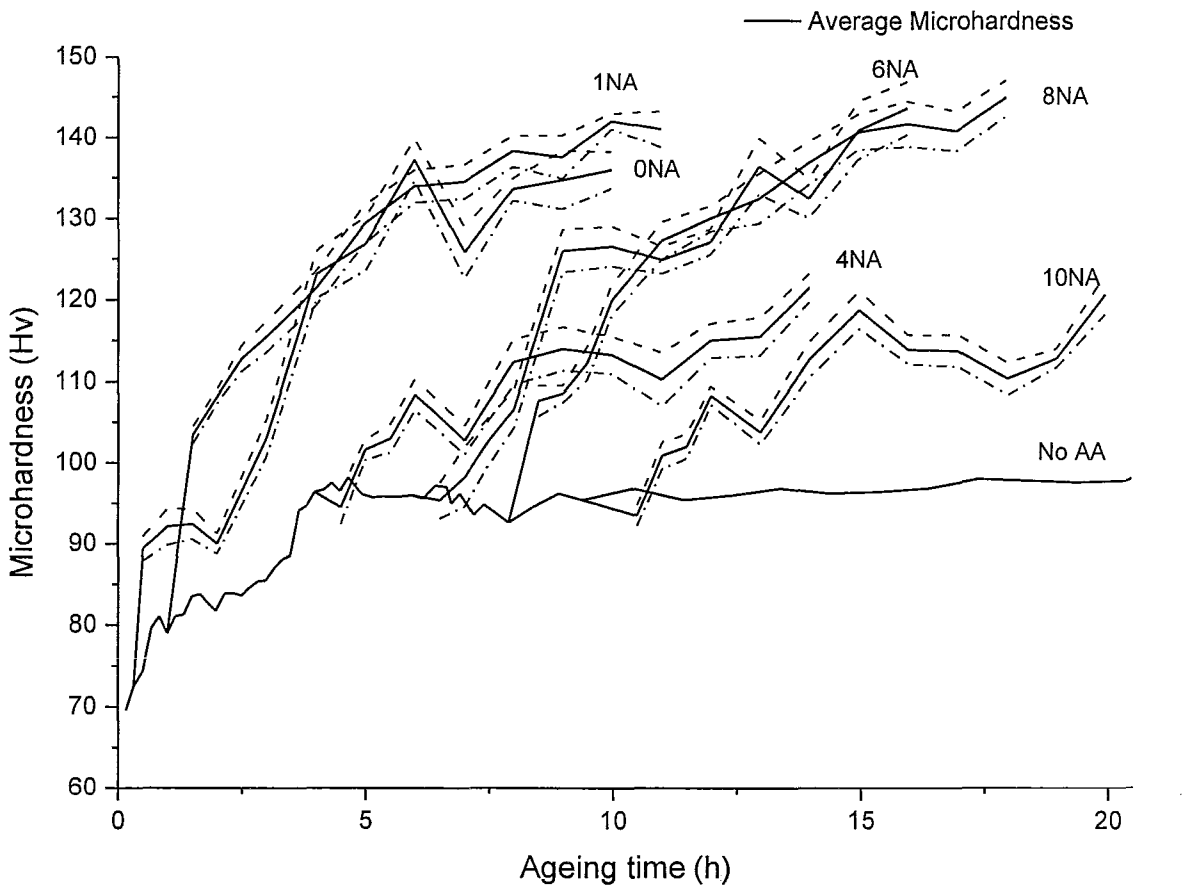

Figure 4-12. Micro-hardness data with 95% confidence interval during artificial ageing at 155 °C following natural ageing at room temperature for various times for samples quenched in water at 80 °C after solution heat treatment. The notation "NA" and "AA" in the graph stand for "Natural Ageing" and "Artificial Ageing", respectively.

4.4. TENSILE PROPERTIES

Mechanical properties were evaluated under uni-axial tensile loading of the test bars cast and heat treated as presented in Section 3.2. and Figure 2-3, respectively. Three properties were evaluated under the test conditions specified in Section 3.6. It is to be noted that the fracture at the end of the test was nearly at the middle of the gauge section of each sample showing the high integrity of the casting process and the reliability of the tensile test data.

Figure 4-13 show the typical mechanical properties (UTS, YS and %el for all the ageing conditions shown in Figure 2-3. The uncertainties in the tensile property data shown in Figure 4-13 is presented in Section 4.5. of this dissertation.

A quick glance at Figure 4-13 shows that there is a significant deviation in UTS, YS and %el for various natural ageing times at room temperature. This strengthens the argument that the natural ageing process at room temperature prior to the artificial ageing process has a significant impact on the resultant mechanical properties and performance of the cast component with A356.2 Al alloy.

It should be noted that the resultant precipitation reaction during the ageing treatment has a significant influence on the YS and %el and not so much on the UTS [42]. Hence, our discussion on the effect of the precipitation reaction on the tensile properties would be limited to the consideration of only the YS and %el and not the UTS. It must be further noted that the quenching of the tensile test bar samples after solution heat treatment was carried out in bundles of five samples to alleviate distortions due to the rapid cooling process. However, the cylindrical samples used to evaluate the micro-hardness measurements during natural and artificial ageing processes were quenched as single samples. Hence, there would be a lower vacancy concentration in the tensile test bar samples when compared to the smaller cylindrical samples leading to the proposition that the reactions stages shown in Figure 4-1 shall be delayed in the tensile bar samples. In Figure 4-13, NA and AA refer to "Natural Ageing" and "Artificial Ageing", respectively. Hence, a qualitative analysis and explanation could be obtained when the tensile test results are compared to the micro-hardness data in Figure 4-2 for natural ageing and Figure 4-10 for artificial ageing processes.

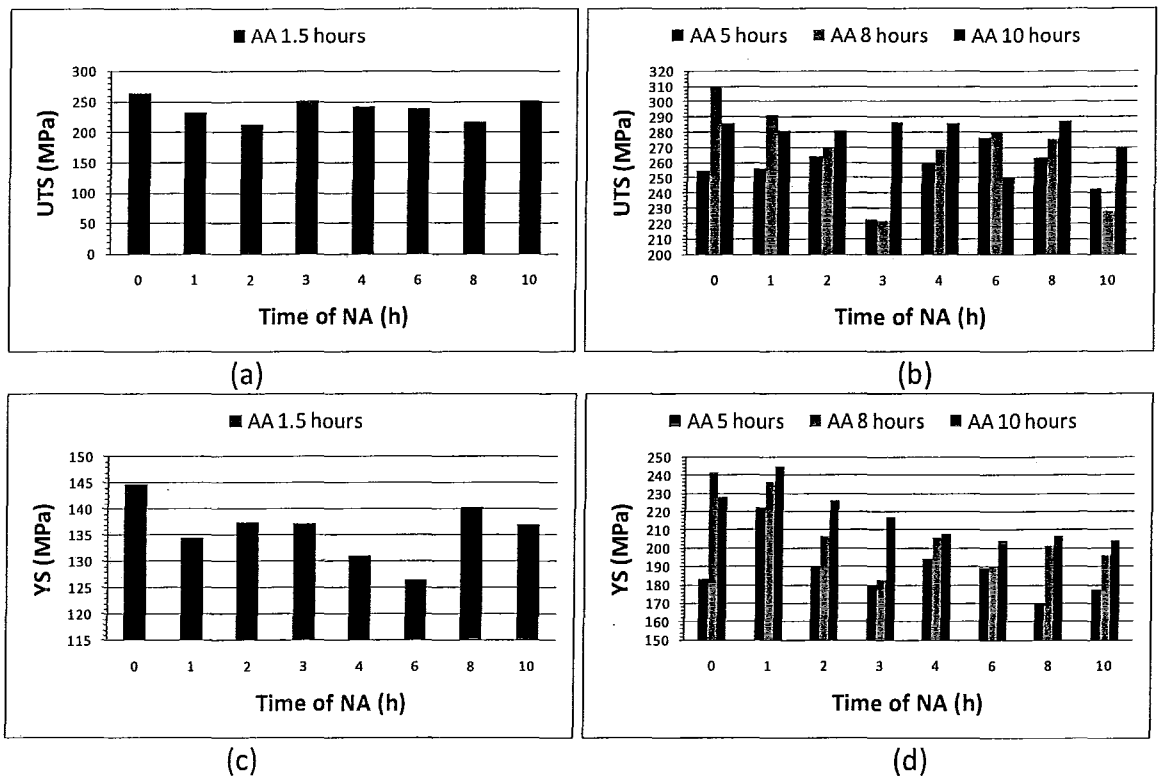

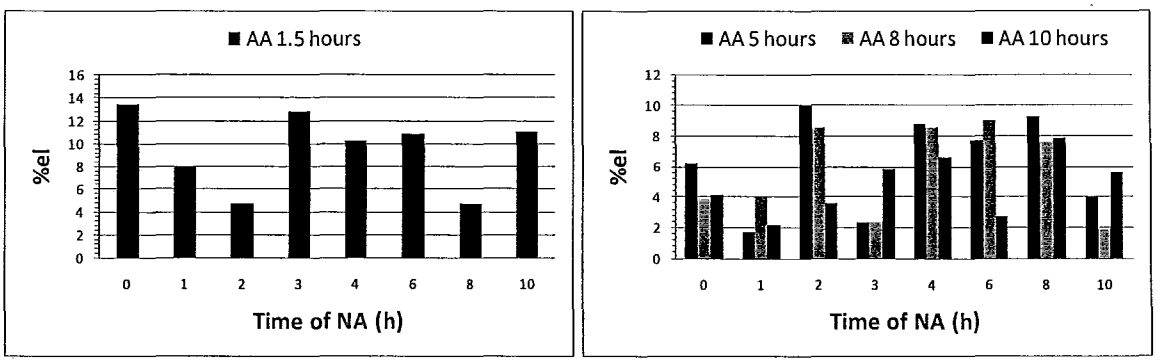

(e) (f)

Figure 4-13. Mechanical tensile properties of A356.2 under various heat treatment conditions shown in Figure 2-3. (a) to (f) show the Ultimate Tensile Strength (UTS), Yield Strength (YS) and Percent Elongation (%el) for the various ageing conditions.

4.4.1. Artificial Ageing Time of 1.5 h (Figure 4-13)

The YS remains high in the first three hours of NA and decreases at about 6 h and subsequently increases at about 8 to 10 h of NA. The high YS initially would be due to the high rate of increase of the micro-hardness value as result of the precipitation reaction proceeding from the Si self clusters to the β'-$Mg_{1.8}Si$ without the formation of the Mg self clusters and the co-clusters of Si and Mg atoms. At around 6 h of NA there would be the initial breakdown of the Mg self clusters which would retard the precipitation mechanism and hence, show low YS values during initial stages of AA. At a NA time greater than 8 h, the self clusters of Mg would have dissolved in the NA process itself and hence the AA would result in the formation of β'-$Mg_{1.8}Si$ precipitates during the initial stages of AA. Typically the %el follows a similar trend as the YS but in reverse where the value is lower at lower NA times and higher between 4 and 6 hours and lower again at 8 h NA for the same reasons as stated for the trend of YS.

4.4.2. Artificial Ageing Time of 5 h to 10 h (Figure 4-13)

During AA of 5 to 10 h for various times of NA, it can be observed that the YS is higher for lower times of NA such as 1 and 2 h and then gradually decreases for higher times and reaches a near constant value at about 4 h for the respective times of AA. The reasons presented in Section 4.4.1. in addition to the fact that the vacancy concentration would be higher for lower times of NA would result in an increased concentration and kinetics of the precipitation reaction for these times. Further, the %el show a low value at 1h showing that the extent of precipitation reaction is high at this condition and the %el is again low at 10 h of NA showing that this may correspond to the condition wherein the Mg self clusters had dissolved leading to an accelerated precipitation condition during the AA process.

There are various factors in addition to the micro-hardness measurements that would directly affect the YS and %el of these samples. Some of these would include, the density and distribution of the precipitates, the coherency between the precipitate and the primary Al

phase matrix, size and morphology of the precipitates. To evaluate the exact reasons for the significant fluctuations in the tensile properties as shown in Figure 4-13, a rigorous study in Transmission Electron Microscopy (TEM) coupled with other advanced characterization techniques would be mandatory and such a task was beyond the scope of this project.

Given the complexity of the precipitation mechanism and the various critical parameters affecting the YS and %el, the results obtained in this project have emphatically shown that there is a marked difference between the mechanical properties of the cast A356.2 under the T6 heat treatment condition with variations in the extent of natural ageing and the subsequent artificial ageing process. One of the quantified results in Figure 4-13 is that for the same T6 heat treatment process, when the time for NA is lower, the resultant properties of the casting shows high strength and low elongation and vice-versa. A typical application of A356.2 alloy in casting an engine block would require a high YS of about 240 MPa and a low %el of less than 2%; and this could be economically achieved by having less than one hour of NA at room temperature rather than the present practice of adding more Mg to the alloy to about 0.60 wt% and effecting a higher distribution and concentration of the final precipitates after the ageing process. Further, for a structural automotive application of the alloy such as a steering knuckle, cylinder heads and structural frames, a high %el of greater than 6% is required coupled with high YS of greater than 200 MPa; and this could be economically achieved by a NA process of about 2 h in room temperature.

4.5. Uncertainties in Tensile Property Data

Figure 4-14 to Figure 4-16 show the mean of the UTS, YS and %el data along with the95% confidence interval band around the mean, respectively, as a function of the natural ageing and artificial ageing times. In these figures, 'AA' refers to Artificial Ageing time in hours.

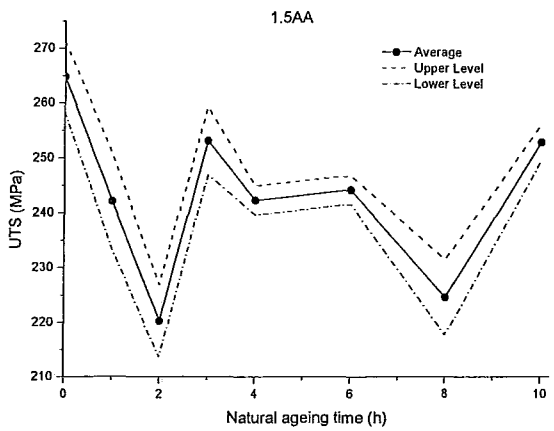

(a)

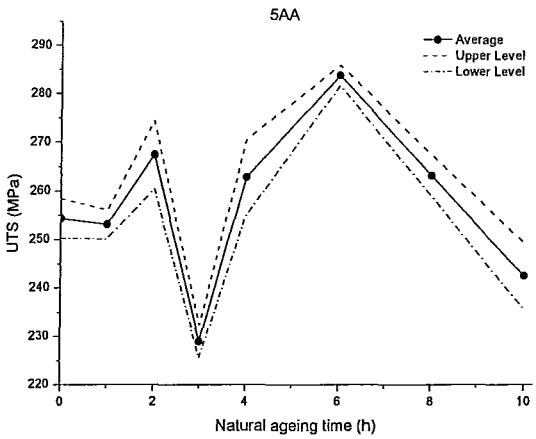

(b)

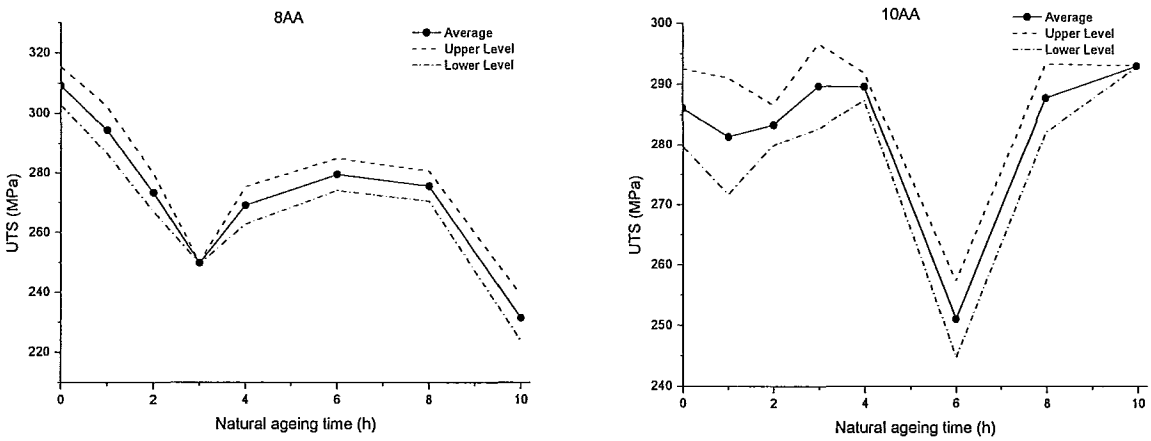

(c) (d)

Figure 4-14. Mean Ultimate Tensile Strength (UTS) as a function of natural ageing time along with the 95% confidence interval for (a) 1.5 h Artificial Ageing (AA) time, (b) 5 h AA time, (c) 8 h AA time and (d) 10 h AA time.

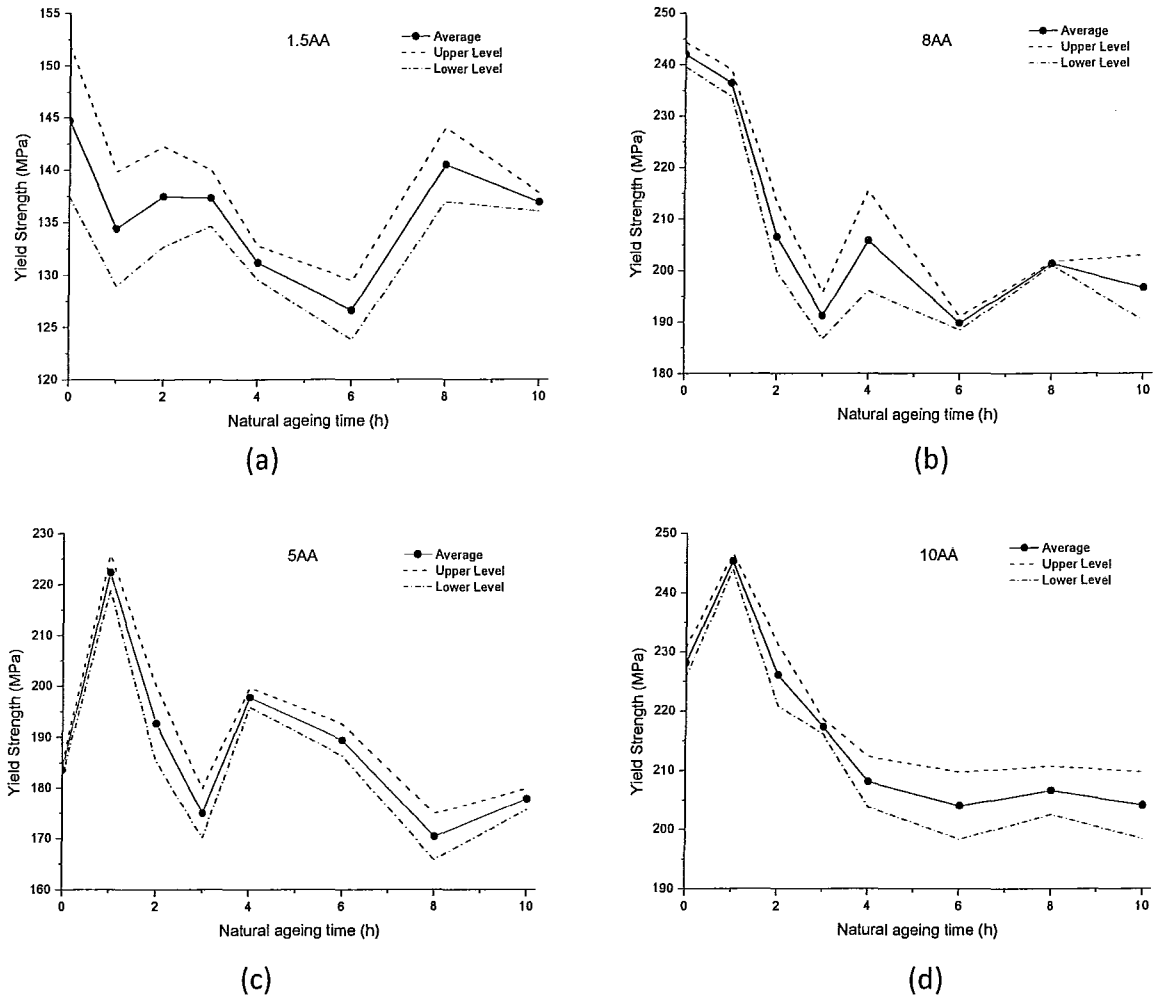

Figure 4-15. Mean Yield Strength (YS) as a function of natural ageing time along with the 95% confidence interval for (a) 1.5 h Artificial Ageing (AA) time, (b) 5 h AA time, (c) 8 h AA time and (d) 10 h AA time

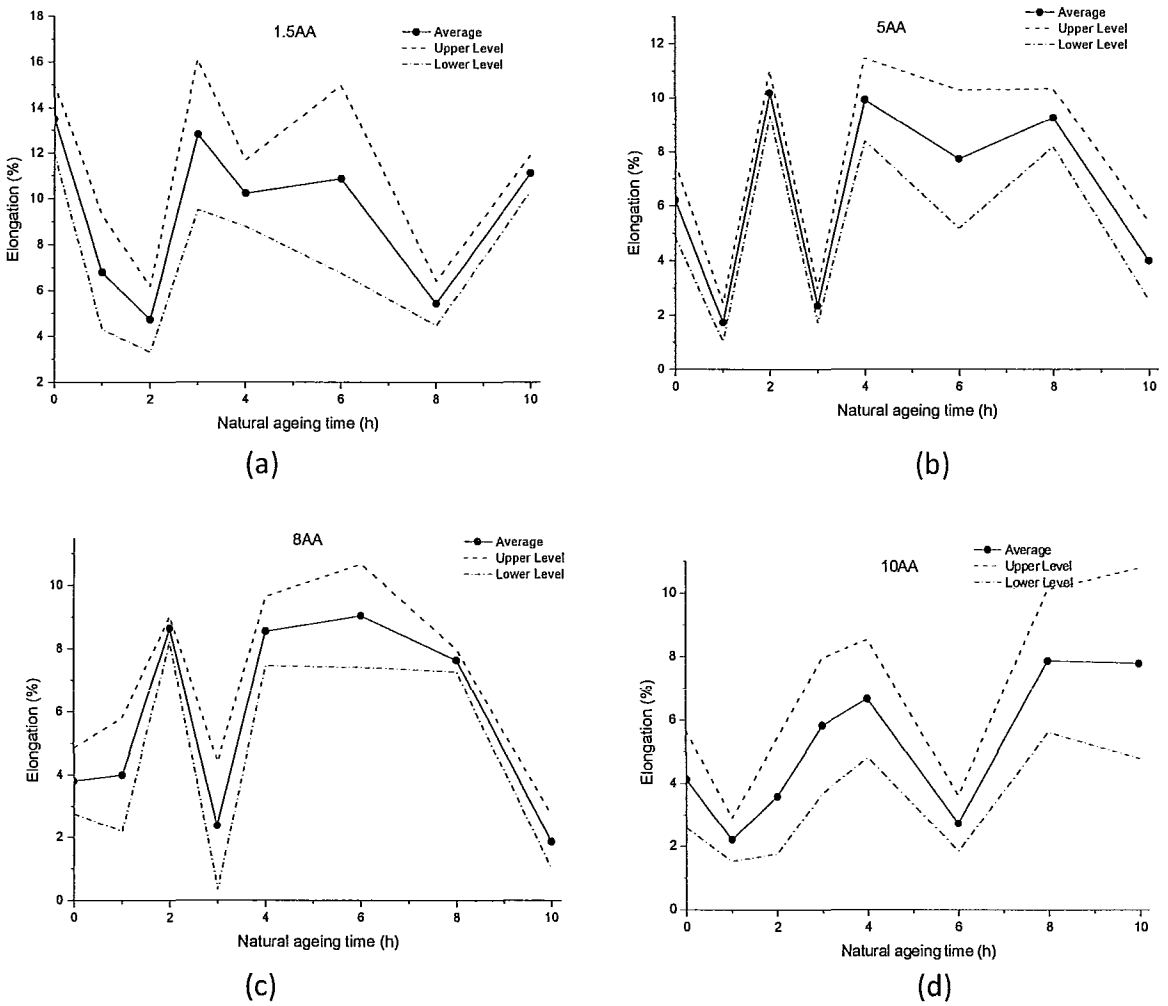

Figure 4-16. Mean Percent Elongation Rate (%el) as a function of natural ageing time along with the 95% confidence interval for (a) 1.5 h Artificial Ageing (AA) time, (b) 5 h AA time, (c) 8 h AA time and (d) 10 h AA time

In Figure 4-14 to Figure 4-16, all the three mechanical properties (UTS, YS and %el) show a distinctly discernable change in their trends with various levels of natural ageing process for each and every artificial ageing time. This emphasizes our conclusion that the various levels of natural ageing do significantly impact the tensile properties of this alloy. Further, Figure 4-15 (a) shows a large region of overlap in the confidence interval between 0 and 2 hours of natural ageing for the 1.5 h artificial ageing process. During this stage the Mg and Si atoms are mostly in the independent or self-cluster stages and very few would have formed defined phases. Hence, there would be a larger variation in the stress required for yield since the resistance offered to yield (the state of the solute atoms and precipitates in the primary phase) is not uniformly distributed. For higher times of artificial ageing, some form of defined co-cluster or precipitate would have formed in the primary Al matrix and hence, the resistance the yield

would be more uniform as reflected by the smaller variations in the mean data in Figure 4-15 (b) to (d).

Variation in the mean elongation percent depends of several factors such as the micro-porosity levels in the casting, and type, size and distribution of the precipitates in the Al matrix. The level of spread in the %el observed in Figure 4-16 is typical of those observed in a tensile data of casting samples.

CHAPTER 5 CONCLUSIONS

The following summarizes the salient conclusions and contributions from this project:

- The sequence of precipitation reactions during the ageing heat treatment of Al-Si-Mg alloy has been refined to identify the plausible reactions during the natural ageing process at room temperature and those in the artificial ageing process at a high temperature, specifically for the A356.2 Al casting alloy. Sections 4.1. and 4.2. presents a viable hypothesis to describe the stages of precipitation reaction in the natural ageing at room temperature and artificial ageing at high temperature, respectively.
- The mechanism of the precipitation reaction is strongly influenced by the rate of quenching subsequent to the solution heat treatment. Higher quenching rates would result in a higher vacancy concentration in the primary Al phase matrix and a higher kinetics of the precipitation reaction.
- The natural ageing process at room temperature subsequent to the solution heat treatment and quenching has a significant influence on the precipitation reaction sequence and kinetics during the artificial ageing process at high temperature. This is reflected in the mechanical tensile properties, specifically the yield strength and elongation of the cast component.
- The A356.2 alloy could be tailored to have a high strength (~235 MPa) and nominal elongation (~2%) as well as a nominal strength (~195 MPa) and high elongation (>8 %) by solely varying the extent of natural ageing at room temperature after solution heat treatment and quenching.
- Commercial T6 heat treatment specification, ASTM Standard B917/B917M 2008, must be refined and elaborated to include the specific effects of natural ageing coupled with the artificial ageing processes on the mechanical properties of the cast component.

CHAPTER 6 SUGGESTIONS FOR FUTURE WORK

The results of this project have provided emphatic evidence of the critical role played by the process of natural ageing at room temperature coupled with the artificial ageing on the resultant mechanical properties of the A356.2 cast component. The scope of the study was to merely provide evidence to support this argument and has successfully been carried out. Subsequently, there would have to be an elaborate research project to specifically identify the nature, morphology and distribution of the phases during the various stages of the precipitation reaction process. This could be carried out by extensive studies with advanced characterization techniques such as Differential Scanning Calorimeter (DSC), and Transmission Electron Microscopy (TEM) and its peripheral technologies. The primary Al phase matrix with the terminal precipitates of β (Mg_2Si) phases after the artificial ageing process subsequent to various duration of natural ageing could be analyzed to evaluate the nature, concentration and distribution of these precipitation phases and validate the hypothesis for the sequence of precipitation reaction.

Only the process of natural and artificial ageing has been studied in this project. The solution heat treatment time and temperature, and the effect of various quenching rates following the solution heat treatment would also have a significant effect on the precipitation mechanism during the ageing process. Further, only one Mg level in the A356.2 alloy was studied and the alloy specification suggests 0.3 to 0.45 wt% Mg. A study to quantify the role of Mg content in the alloy on the resultant precipitation reaction would also be important.

APPENDIX A DATA

The data in Figure 4-2, Figure 4-10 and Figure 4-13Figure 4-13 are presented in this Appendix.

Table A-1. Micro-hardness data for natural ageing process for samples quenched in a mixture of anti-freeze and dry ice maintained at -40 °C.

Time (h)	HV	95% Confidence Interval (±)	Time (h)	HV	95% Confidence Interval (±)
0.00	62.43	1.59	7.33	85.60	0.75
0.17	66.11	1.47	7.83	89.80	1.09
0.35	69.14	1.61	8.00	88.40	1.85
0.50	73.00	0.45	8.83	90.60	1.92
0.67	71.89	0.65	9.33	87.40	0.75
0.83	75.33	1.62	10.33	90.00	1.18
1.00	76.75	1.16	11.33	93.00	1.18
1.18	78.50	1.48	12.33	95.60	0.95
1.33	80.00	0.45	13.33	94.40	1.12
1.50	81.90	0.73	14.33	92.80	1.50
1.67	83.25	0.74	15.33	91.80	0.70
1.83	83.10	0.47	16.33	93.60	1.40
2.00	84.67	0.59	17.33	96.20	0.80
2.17	84.25	0.59	18.33	95.00	2.21
2.33	83.88	0.00	19.33	94.60	1.92
2.50	82.11	1.41	20.33	94.00	2.05
2.90	84.20	0.37	21.33	93.40	1.83
3.00	83.29	0.92	22.33	93.60	1.73
3.20	82.50	1.60	23.33	98.50	1.77
3.33	82.67	1.46	25.33	94.40	1.27
3.50	83.17	1.05	26.33	96.33	1.74
3.68	82.60	1.43	27.33	98.40	1.85
3.83	83.50	1.81	28.33	96.75	1.43
4.00	86.56	1.39	29.35	96.75	1.43
4.17	84.00	1.11	31.33	93.40	1.83
4.35	83.88	1.97	35.33	104.33	1.72
4.50	85.50	1.73	37.33	95.60	0.75
4.67	82.80	1.85	41.33	101.60	1.92
4.83	86.00	1.53	43.33	100.00	1.93
5.00	87.20	2.47	49.33	98.80	0.84
5.18	84.33	1.81	55.33	98.60	1.27
5.33	87.88	2.02	70.33	99.80	0.92
5.83	86.57	1.44	76.33	100.80	1.28
6.00	86.00	1.18	94.33	100.00	0.84
6.17	86.80	1.37	100.38	99.80	1.09
6.33	86.60	0.95	117.92	99.00	1.32
6.50	86.20	1.25	123.45	100.80	1.24
6.83	86.60	0.95	141.50	100.60	1.40
7.03	85.80	1.09	147.55	100.80	1.91

Table A-2. Micro-hardness data for natural ageing process for samples quenched in water at room temperature (23 °C).

Time (h)	HV	95% Confidence Interval (±)	Time (h)	HV	95% Confidence Interval (±)
0.00	67.00	1.74	7.33	95.00	1.02
0.17	70.78	1.66	7.83	93.60	0.75
0.33	71.78	1.24	8.40	94.40	1.52
0.50	73.88	1.37	8.83	94.60	1.40
0.67	74.86	0.89	9.33	93.80	0.70
0.83	76.63	0.77	10.42	95.80	2.60
1.02	77.14	0.58	11.33	95.80	1.81
1.17	78.00	0.92	12.33	96.50	0.84
1.35	79.13	0.94	13.33	93.20	0.92
1.50	82.29	0.93	14.33	96.80	2.16
1.67	81.57	1.59	15.33	96.20	1.61
1.85	83.43	1.06	16.33	96.00	2.05
2.02	83.86	0.75	17.33	97.00	2.37
2.17	86.13	1.81	18.33	95.60	1.27
2.33	91.50	0.70	19.33	96.00	1.67
2.63	89.30	1.73	20.33	96.60	1.73
2.85	88.70	1.26	21.33	101.20	1.61
3.00	89.30	1.97	22.33	102.80	1.37
3.18	90.10	0.75	23.33	104.40	1.52
3.33	87.90	3.44	25.33	96.60	1.12
3.50	89.50	1.93	26.33	99.40	1.73
3.67	89.00	1.81	27.33	100.40	1.52
3.85	91.33	1.14	28.33	100.00	1.18
4.02	90.33	1.14	29.33	98.20	1.71
4.17	89.71	1.05	32.33	96.00	1.67
4.33	89.50	1.37	35.33	98.60	1.40
4.52	90.86	1.02	38.33	99.40	1.27
4.68	90.40	2.30	41.33	100.00	0.59
4.85	90.60	1.08	43.33	100.00	1.32
5.00	91.20	1.28	50.40	101.80	1.09
5.18	90.30	1.45	54.40	100.20	0.70
5.37	90.00	1.77	71.48	100.20	0.70
5.83	91.20	0.70	78.33	100.80	0.70
6.08	93.67	1.28	95.33	101.00	2.21
6.17	92.00	1.18	104.57	102.60	0.95
6.33	92.00	1.77	119.77	104.40	1.52
6.58	96.40	0.95	128.83	102.60	0.95
6.83	95.80	1.37	143.68	104.80	1.09
7.12	95.00	0.59	151.33	104.40	1.73

Table A-3. Micro-hardness data for natural ageing process for samples quenched in water at 80 °C.

Time (h)	HV	95% Confidence Interval (±)	Time (h)	HV	95% Confidence Interval (±)
0.00	70.40	0.97	7.33	94.80	1.61
0.17	72.40	1.38	7.83	92.60	1.12
0.35	73.89	1.44	8.33	94.60	0.95
0.50	79.20	1.46	8.83	96.20	0.70
0.67	81.22	1.24	9.33	95.40	0.95
0.85	79.00	1.45	10.33	96.80	1.09
1.00	81.00	0.48	11.35	95.40	1.73
1.17	81.25	0.87	12.33	96.00	1.96
1.33	83.50	2.10	13.33	96.80	1.37
1.50	83.75	1.72	14.33	96.20	1.61
1.67	82.56	0.74	15.33	96.40	0.95
1.83	81.75	0.97	16.33	96.80	1.24
2.00	83.88	0.83	17.33	98.00	1.02
2.17	83.88	1.30	18.53	97.80	1.09
2.33	83.63	0.99	19.33	97.60	0.95
2.50	84.56	0.85	20.33	97.80	1.71
2.83	85.44	0.85	20.92	99.20	1.81
3.00	87.00	1.42	22.33	99.80	2.24
3.17	88.11	1.06	23.33	98.40	1.73
3.33	88.56	1.51	25.33	97.80	1.61
3.50	94.11	1.41	26.33	96.40	0.46
3.67	94.78	1.17	27.33	98.00	1.56
3.83	96.43	0.45	28.33	97.00	1.45
4.00	96.67	0.72	29.33	98.00	1.02
4.17	97.50	0.45	20.33	97.80	1.09
4.33	96.50	0.45	35.33	98.80	1.61
4.50	98.20	1.52	38.38	100.20	2.39
4.67	97.00	1.32	41.33	98.00	1.32
4.83	96.14	0.75	44.33	98.80	1.37
5.02	95.71	0.63	50.33	100.40	1.40
5.17	95.86	1.32	54.60	100.00	1.67
5.33	95.83	1.11	72.83	100.20	1.09
5.83	96.00	0.84	78.35	100.20	1.09
6.08	95.25	0.42	96.33	100.00	1.32
6.17	95.67	0.72	102.37	100.20	0.70
6.33	97.20	0.70	120.38	100.60	1.40
6.60	97.00	0.84	126.42	100.40	0.95
6.83	96.20	0.70	143.58	100.80	1.37
7.10	93.67	0.97	150.70	100.40	1.27

Table A-4. Micro-hardness data for the artificial ageing process after various times of natural ageing at room temperature.

AA Time (h)	0 NA		1 NA		2 NA		3 NA	
	HV	95% Confidence Interval (±)	HV	95% Confidence Interval (±)	HV	95% Confidence Interval (±)	HV	95% Confidence Interval (±)
0.5	89.38	1.50	103.43	1.06	99.13	1.30	104.13	1.92
1	92.14	2.21	108.25	0.87	101.71	2.03	105.38	0.77
1.5	92.43	1.86	112.88	1.58	109.25	1.77	108.00	1.90
2	90.00	1.26	115.50	1.90	108.00	2.19	114.00	2.37
3	103.13	2.34	121.43	2.15	103.14	3.59	122.00	3.16
4	123.13	2.95	129.38	2.36	107.75	2.94	127.13	1.92
5	126.86	3.29	134.00	1.99	108.57	2.45	127.63	3.95
6	137.25	2.56	134.57	2.10	111.63	2.00	127.75	2.44
7	125.88	3.18	138.29	1.91	111.88	2.16	135.63	1.48
8	133.63	1.41	137.57	2.64	116.29	4.06	132.75	2.75
9	134.75	3.57	142.00	0.97	118.75	2.75	137.13	2.51
10	136.00	2.24	141.00	2.21	119.38	1.94	136.13	1.70

AA Time (h)	4 NA		6 NA		8 NA		10 NA	
	HV	95% Confidence Interval (±)	HV	95% Confidence Interval (±)	HV	95% Confidence Interval (±)	HV	95% Confidence Interval (±)
0.5	94.50	2.05	95.38	2.19	107.63	1.89	93.50	1.26
1	101.63	1.26	98.25	3.68	108.50	1.01	100.88	1.64
1.5	103.00	1.73	102.75	2.96	112.25	2.04	102.00	1.48
2	108.38	1.89	106.50	2.28	120.00	1.84	108.25	1.16
3	102.75	1.77	126.00	2.64	127.25	2.31	103.75	1.47
4	112.38	2.79	126.57	2.45	130.00	1.55	112.75	2.18
5	114.00	2.64	124.88	1.70	132.50	3.11	118.71	2.30
6	113.25	2.27	127.13	1.58	136.88	2.66	113.88	1.76
7	110.25	3.30	136.50	3.44	140.63	2.19	113.75	1.94
8	115.00	2.10	132.50	2.44	141.63	2.79	110.38	2.00
9	115.50	2.32	140.88	3.56	140.75	2.44	112.88	1.13
10	121.50	1.73	143.63	3.31	144.88	2.26	120.63	2.36

Table A-5. Mechanical properties of uni-axial tensile loading tests for various ageing conditions. NA and AA represent "Natural Ageing" and "Artificial Ageing", respectively.

NA	UTS (MPa)	95% Confidence Interval (±)	Yield Strength (MPa)	95% Confidence Interval (±)	Elongation (%)	95% Confidence Interval (±)
As-cast	188.10	4.02	90.72	1.84	8.53	0.27
As-quench	224.37	5.35	102.81	3.02	17.32	1.43
			AA → 1.5 h			
0NA	264.76	6.43	144.70	7.20	13.51	1.54
1NA	242.10	8.63	134.44	5.44	6.80	2.49
2NA	220.25	6.59	137.45	4.79	4.74	1.43
3NA	253.10	6.13	137.32	2.67	12.81	3.29
4NA	242.30	2.68	131.16	1.62	10.23	1.45
6NA	244.18	2.62	126.63	2.83	10.86	4.11
8NA	224.54	6.88	140.50	3.54	5.43	0.96
10NA	252.73	3.24	136.92	0.87	11.11	0.79
			AA → 5 h			
0NA	254.32	4.08	183.59	1.25	6.21	1.36
1NA	253.12	2.93	222.33	3.48	1.74	0.71
2NA	267.41	6.94	192.65	7.28	10.19	0.84
3NA	228.98	3.38	174.90	4.92	2.35	0.62
4NA	262.78	7.73	197.77	1.90	9.93	1.53
6NA	283.72	2.14	189.33	3.10	7.74	2.56
8NA	263.13	4.24	170.30	4.54	9.28	1.08
10NA	242.48	6.85	177.75	2.09	4.00	1.44
			AA → 8 h			
0NA	309.20	6.27	241.95	2.37	3.80	1.05
1NA	294.45	8.03	236.37	2.55	4.00	1.80
2NA	273.30	6.36	206.52	6.71	8.63	0.41
3NA	249.75	0.19	191.20	4.55	2.37	2.04
4NA	268.99	6.25	205.76	9.69	8.55	1.10
6NA	279.38	5.41	189.75	1.31	9.04	1.63
8NA	275.51	5.04	201.31	0.33	7.63	0.36
10NA	231.34	7.66	196.61	6.33	1.86	0.86
			AA → 10 h			
0NA	286.07	6.44	228.14	2.51	4.13	1.55
1NA	281.36	9.68	245.25	1.35	2.21	0.69
2NA	283.32	3.35	226.06	5.24	3.59	1.83
3NA	289.68	6.98	217.29	1.25	5.83	2.12
4NA	289.59	2.26	208.06	4.26	6.67	1.86
6NA	251.04	6.32	203.98	5.69	2.73	0.89
8NA	287.72	5.58	206.55	4.11	7.86	2.24
10NA	292.97	0.18	204.05	5.67	7.79	2.99

APPENDIX B REFERENCES

1 J. L. Jorstad, W.M. Rasmussen and D.L. Zalensas, "Aluminum cast technology, 2nd Edition", *American Foundry Society*, Des Plaines, IL, USA (2001), 35-53.

2 ASTM Standard B917/B917M 2008: "standard practice for heat treatment of aluminum-alloy castings for all purpose", *ASTM,* (2008).

3 D.S. Thompson, B.S. Subramanya and S.A. Levy, "Quench rate effects in Aluminum-Zinc-Magnesium-Copper alloys", *Metallurgical Transactions*, 2 (1971), 1149-1160.

4 G.A. Edwards, K. Stiller, G.L. Dunlop and M.J. Couper, "The precipitation sequence in Al-Mg-Si alloys", *Acta Materalia , 46* (11) (1998), 3893-3904.

5 F. Ernst, "Precipitation hardening of Al-Si-Mg alloys", *Materials Laboratory III*, EMSE-290, http://dmseg5.case.edu/Groups/Ernst/Courses/EMSE-290-S06/Pages/instructions/Exp1.pdf. (2008), 1-29.

6 Kovács, J. Lendvai and E. Nagy, "Mechanism of clustering in supersaturated solid solution Al-Mg2Si alloy", *Acta Metallurgica,* 20 (1972), 975-983.

7 M. Jeyakumar, M. Hamed, S. Shankar, "Heat treatment of A356.2 aluminum alloy: effect of quench rate and natural aging", *TMS 2009 138th Annual Meeting and Exhibition,* San Francisco, CA (2009), 87-95.

8 N. Maruyama, R. Uemori, N. Hashimoto, M. Saga and M. Kikuchi, "Effect of silicon addition on the composition and structure of fine scales precipitates in Al-Mg-Si alloys", *Scripta Materialia,* 36 (1) (1997), 89-93.

9 J.R. Davis, "ASM Specialty Handbook: Aluminum and aluminum alloys", *ASM International*, Material Park, Ohio, USA (1993).

10 FactSage Thermodynamic Databank System, www.factsage.com.

11 L. Bäckerud, G. Chai and J. Tamminen, "Solidification charactersistics of aluminum alloys", *Foundry Alloys*, AFS-Skanaluminium, 2 (1990), 71-84.

12 S. Shankar, Y W Riddle and M. M. Makhlouf, "Nucleation mechanism of eutectic phase in aluminum-silicon hypoeutectic alloys", *Acta Meterialia*, 52 (2004), 4447-4460.

13 L. Heusler and W. Schneider, "Recent investigations of influence of P on Na and Sr modifiction of Al-Si alloys", *AFS Trans,* 97(1997), 915-921.

14 Y.H. Cho, H.C. Lee, K.H. Oh and A.K. Dahle, "Effect of strontium and phosphorous on eutectic Al-Si nucleation and formation of β-Al5FeSi in Hypoeutectic Al-Si foundry alloys", *Metallurgical and Materials Transaction A*, 39 (2008), 2435-2448.

15 G. Sigworth, "The modifications of Al-Si casting alloys: Important practical and theoretical aspects", International Journal of Metalcasting, 2 (2) (2008), 19-42.

16 P.D. Hess and E.V. Blackmun, "Strontium as modifying agent for hypoeutectic aluminum-silincon alloys. *AFS Trans,* 84 (1975), 87-90.

17 B. Closset and J.E. Gruzleski, "Mechanical properties of A356.0 alloys modified with pure strontium", *AFS Trans,* 90 (1982), 453-464.

18 J. L. Jorstad, "Applications of 390 Alloy: An update", *AFS,* (1984), 573-578.

19 J.B. Andrews and M.V.C Seneviratne, "A new highly wear-resistant aluminum-silicon casting alloy for automotive engine block applications", *AFS Trans,* 92 (1984), 209-216.

20 M. Mulazimoglu, "Electrical conductivity studies of cast Al-Si and Al-Si-Mg alloys", *Ph.D. Thesis, McGill University*, Montreal, Canada (1988).

21 D. Apelian, S. Shivkumar and G. Sigworth, "Fundamental aspects of heat treatment of cast Al-Si-Mg alloys", *AFS Trans,97* (1989), 727-742.

22 S. Shivkumar, S. Ricci, J.C. Keller and D. Apelian, "Influence of solution treatment on tensile properties of cast aluminum alloys", *Journal of Heat Treating , 8* (1) (1990), 63-70.

23 S. Shivkumar, C. Keller and D. Apelian, "Aging behavior in cast Al-Si-Mg alloys", *AFS Trans,* 179 (1990), 905-911.

24 L.F. Modolfo, "Aluminum alloys: sructure and properties", Butterworth & Co., London, UK (1976).

25 P. Ouellet and F.H. Samuel, "Effect of Mg on the ageing behavior of Al-Si-Cu 319 type aluminum casting alloys", *Journal of Materials Sciences*, 34 (1999), 4671-4697.

26 D.S. Thompson, B.S. Subramanya and S.A. Levy, "Quench rate effects in Aluminum-Zinc-Magnesium-Copper alloys", *Metallurgical Transactions ,* 2 (1971), 1149-1160.

27 J.W. Martin, "*Precipitation hardening* (2nd ed.)", *Butterworth-Heinemann*, Oxford, UK(1998).

28 J.T. Staley, "Quench factor analysis of aluminum alloys", *Material Science and Technology ,* 3 (1987), 923-935.

29 C.E. Bates, "Quench optimization for aluminum alloys", *AFS Trans,* American Foundry Society, 93-25 (1994), 1045-1054.

30 D.L. Zhang, "Precipitation of excess silicon during heat treatment of casting Al-7wt%Si-0.4wt%Mg alloy", *Materials Science Froum,* 217-222 (1996), 1-6.

31 Kovács, J. Lendvai and E. Nagy, "Mechanism of clustering in supersaturated solid solution Al-Mg2Si alloy", *Acta Metallurgica ,* 20 (1972), 975-983.

32 T. Gladman, "Grain size control", *Woodhead Publishers Ltd.* Cambridge, UK (2004).

33 Y. Nakayama, T. Takaai and D. Jin, "Precipitation behaviors of β-phase and changes in mechanical properties of Al-Mg system alloys", *Material Science Forum*, 217-222 (1996), 1269-1274.

34 Gaber, M.A. Gaffar, M.S. Mostafa and E.F. Abo Zeid, "Precipitation kinetics of Al-1.2Mg2Si-0.35 Si and Al-1.07Mg2Si-0.33Cu alloys", *Journal of Alloys and Compounds*, 429 (2007), 167-175.

35 P. Donnadieu and A. Proult, "Cluster-based models for the crystal structure of the hardening precipitates of Al-Mg-Si alloys", *Material Science Forum*, 217-222 (1996), 719-724.

36 C.D. Marioara, S.J. Anderson, J. Jansen and H.W. Zandbergen, " The influence of temperature and storage time at RT on nucleation of the β" phase in a 6082 Al-Mg-Si alloy", *Atca Materialia*, 51 (2003), 789-796.

37 S.J. Anderson, H.W Zandbergen. C.Traeholt. U. Tundal and O.Reiso, "The crystal structure of the β" phase in Al-Mg-Si alloy", Acta Materialia, 46 (2003), 3283-3298.

38 R. Visser, M.A. van Huis et al., "The crystal structure of the β' phase in Al-Mg-Si alloys", *Acta Materialia*, 55 (2007), 3815-3823.

39 W.F. Miao and D. E. Laughlin, "A differential scanning calorimetry study of aluminum alloy 6111 with different pre-aging treatments", *Journal of Materials Science Letters* , 19 (2000), 201-203.

40 M. Murayama, K. Hono, M. Saga and K. Kikuchi, "Atom probe studies on the early stages of precipitation of Al-Mg-Si alloys", *Material Science & Engineering* , A250 (1998), 127-132.

41 M. Murayama and K. Hono, "Pre-precipitate clusters and precipitation process in Al-Mg-Si alloys", *Acta Materialia , 47* (5) (1999), 1537-1548.

42 H. Seyedrezai, "Early Stages of Ageing in Al-Mg-Si Alloys", *M. Sc thesis, McMaster University*, Hamilton, Canada (2007).

43 W.F. Miao and D.E. Laughlin D.E, "Effects of Cu content and preageing on precipitation characteristics in aluminum alloy 6022", Metallurgical and Materials Transactions A, 31A (2000), 361-371.

44 I. Dutta and S.M. Allen, "A Calorimetric Study of Precipitation in Commercial Aluminum Alloy-6061", *Journal of Materials Science Letters*, 10 (6) (1991), 323-326

45 G.E. Dieter, "*Mechanical Metallurgy* (3rd ed.)", *McGraw-Hill Book Co.*, New York, USA (1986).

46 P. A. Rometsch and G. B. Schaffer, "An age hardening model for Al-7Si-Mg casting alloys", *Materials Science and Engineering , A325 (2002)*, 424-434.

47 C.H. Caceres, C.J. Griffiths, L.M. Hogan and Q.G. Wang, "Hypoeutectic Al-Si-Mg foundry alloys", *Materials Forum*, 21 (1997), 27-43.

48 I.J. Polmear, "Metallurgy of the light metals (3rd ed.)", Light Alloys, Arnold, London, UK (1995), 26.

49 H. Möller, G. Govender and W.E. Stumpf, " Optimization of the T6 heat treatment of rheocast alloy A356", *8th Annual International Conference on Transportation Weight Reduction*, Pilanesburg, South Africa, (2007), 19-38.